الجـــــــــــــــــــمـهـوريـــــة الجـــــــــــــزائـريـة الديمـــــــقـراطيـة الـشـــــــــعبيـة

PEOPLE'S DEMOCRATIC REPUBLIC OF ALGERIA

وزارة التـــــــــــــــــــــــــعـليـم العـــــــالي والبـــــــــحث العـــــلـمـــي

Ministry of Higher Education and Scientific Research

جـــــــــــــامعة أبي بكـــر بـلـقـايد – تـلمســـــــــــــان –

University of Abou Bekr Belkaid – Tlemcen –
Faculty of Technology

THESIS

Presented to obtain of the degree of **Doctorate**, **3rd Cycle**

In: Mechanical engineering

Specialty: Energetics

By: Embarek Noureddine

Subject

Experimental analysis of a new thermal energy storage system for air conditioning

Publicly defended on 16 June 2026, in front of the jury composed of:

Mr. SAIM RACHID	Pr.	Univ. Tlemcen	President
Mr. GUELLIL HOCINE	MCA.	Univ. Tlemcen	Supervisor
Mr. KORTI. A. NABIL	Pr.	Univ. Tlemcen	Co-supervisor
Mr. BENZENINE HAMIDOU	Pr.	Univ. Ain Temouchent	Examiner
Mr. SELADJI CHAKIB	Pr.	Univ. Tlemcen	Examiner

Academic year: 2025 - 2026

Acknowledgments

First and foremost, I express my deepest gratitude to Allah Almighty, who guided me and granted me the strength, patience, and perseverance to successfully complete this work. Without His blessings, this achievement would not have been possible.

I would like to extend my sincere appreciation to my supervisors, Dr. Guellil Hocine and Professor Abdel Ilah Nabil korti, for their continuous guidance, insightful advice, and unwavering support throughout this research. Their expertise, encouragement, and dedication played a fundamental role in shaping this thesis and ensuring the successful completion of this work.

I am also profoundly grateful to the members of the examination committee Professor Saim Rachid, Professor Benzenine Hamidou and Professor Seladji Chakib for accepting to evaluate this thesis. Their time, thoughtful remarks, and constructive feedback have greatly contributed to improving the quality and clarity of this research.

My sincere thanks also go to Mr. Ibrahim Soulimieh for his valuable assistance, technical support, and continuous efforts throughout this study.

Finally, I dedicate special thanks to my parents and my brothers for their constant encouragement, and unwavering belief in me. Their sacrifices and support have been the foundation of my academic journey. To my family and friends, I am deeply thankful for your understanding, patience, and comforting presence during challenging moments. This work is the result of the support, guidance, and encouragement of many people, and I am truly grateful to all who contributed, directly or indirectly, to its completion.

Dedication

To Allah Almighty, for His endless blessings and guidance.

To my beloved parents, whose unconditional love, sacrifices, and constant prayers have been the foundation of my success.

And to my dear friends, for their encouragement, support, and companionship throughout this journey.

Embarek noureddine

Abstract

Maintaining a stable air temperature over prolonged periods in space heating and drying applications using solar air heaters remains a significant challenge, particularly under variable solar irradiance conditions. This thesis presents a comprehensive experimental investigation of a hybrid double-pass solar air heater integrated with a latent heat thermal storage unit, with the aim of developing a reliable and efficient system capable of all-weather operation for space heating and drying applications. To ensure a holistic evaluation of the proposed system, a multi criteria assessment methodology that included energy, exergy, economic, and environmental analyses was used. The experimental study was systematically conducted in three consecutive phases. In the first phase, parametric and dimensional analyses were performed on a baseline double-pass solar air heater to investigate the influence of air gap variation on thermal and exergetic performance, showing that increasing the upper air channel height considerably improved system performance, with a maximum thermal efficiency of 66.4% achieved at a 12 cm air gap configuration, while smaller gaps led in higher irreversibility and increased exergy destruction. The second phase focused on the integration of an auxiliary electric heater and a latent heat thermal storage unit using paraffin wax to improve thermal stability and extend operating hours. This configuration enabled a stable outlet temperature of 54±1.25 °C, prolonged system operation after sunset, and reduced electrical energy consumption. At an air mass flow rate of 0.024 kg/s, the system achieved average thermal and exergetic efficiencies of 72.3% and 3.5%, respectively. The third phase addressed further performance optimization through the integration of wavy fins and the evaluation of auxiliary heater positioning. A fin inclination angle of 45° enhanced thermal efficiency by 13.8% compared to a flat absorber, while positioning the auxiliary heater at the outlet section improved temperature regulation, minimized fluctuations, and reduced electrical energy consumption by 4.23%. Overall, the findings demonstrate that using both latent heat thermal storage and heat transfer enhancement techniques significantly improves energy efficiency, thermal stability, sustainability, and practical applicability of hybrid solar air heaters, making the proposed system a promising and sustainable solution for agricultural drying and space heating applications.

Keywords: Double pass solar air heater; Latent heat thermal storage unit; Thermal efficiency; PCM; Exergy; Payback period.

الملخص

يعدّ الحفاظ على درجة حرارة هواء مستقرة وثابتة لفترات تشغيل طويلة في تطبيقات التدفئة والتجفيف باستخدام سخانات الهواء الشمسية تحديًا كبيرًا، لا سيما في ظل تقلبات الإشعاع الشمسي. تقدم هذه الأطروحة دراسة تجريبية شاملة لسخان هواء شمسي هجين مزدوج المرور مدمج مع وحدة تخزين حراري كامن، بهدف تطوير نظام موثوق وعالي الكفاءة قادر على التشغيل في مختلف الظروف المناخية لتطبيقات التدفئة والتجفيف. ولضمان تقييم شامل للنظام المقترح، تم اعتماد منهجية تقييم متعددة المعايير شملت التحليل الطاقي، والإكسرجي، والاقتصادي، والبيئي. بحيث نُفذت الدراسة التجريبية بشكل منهجي عبر ثلاث مراحل متتالية. في المرحلة الأولى، أُجريت تحليلات تشغيلية وبُعدية على سخان هواء شمسي مزدوج المرور أساسي لدراسة تأثير تغير الفجوة الهوائية على الأداءين الحراري والإكسرجي، حيث أظهرت النتائج أن زيادة ارتفاع القناة الهوائية العلوية تُحسن أداء النظام بشكل ملحوظ، مع تحقيق كفاءة حرارية قصوى بلغت 66.4%عند فجوة هوائية مقدارها 12 سم، في حين أدت الفجوات الأصغر إلى زيادة اللاانعكاسية وارتفاع تدمير الإكسرجي. فيما ركزت المرحلة الثانية على دمج سخان كهربائي مساعد ووحدة تخزين حراري كامن باستخدام شمع البارافين بهدف تحسين الاستقرار الحراري وتمديد ساعات التشغيل. وقد مكّن هذا التكوين من تحقيق درجة حرارة الهواء عند المخرج الى درجة حرارة مستقرة بلغت 54±1.25 درجة مئوية، مع إطالة فترة تشغيل النظام بعد غروب الشمس وتقليل استهلاك الطاقة الكهربائية. وعند معدل تدفق كتلي للهواء قدره 0.024 كغ في الثانية، حقق النظام متوسط كفاءة حرارية وإكسرجية بلغ 72.3% و3.5% على التوالي. أما المرحلة الثالثة فقد تناولت تحسين الأداء بشكل إضافي من خلال دمج زعانف متموجة وأيضا دراسة الموقع الأمثل للسخان الكهربائي المساعد. وقد أدى استخدام زعانف بزاوية ميل قدرها 45° إلى تحسين الكفاءة الحرارية بنسبة 13.8% مقارنة بالسطح الماص المستوي، في حين ساهم وضع السخان المساعد عند مخرج الهواء في تحسين تنظيم درجة الحرارة، وتقليل التذبذبات الحرارية، وخفض استهلاك الطاقة الكهربائية بنسبة 4.23.%. وبصفة عامة، تُظهر النتائج أن الدمج بين التخزين الحراري الكامن وتقنيات تعزيز انتقال الحرارة يُحسن بشكل كبير من الكفاءة الطاقية، والاستقرار الحراري، والاستدامة، وقابلية التطبيق العملي لسخانات الهواء الشمسية الهجينة، مما يجعل النظام المقترح حلاً واعدًا ومستدامًا لتطبيقات التجفيف الزراعي والتدفئة.

كلمات مفتاحية: سخان هواء شمسي مزدوج المرور؛ وحدة التخزين الحراري بالحرارة الكامنة؛ الكفاءة الحرارية؛ مادة متغيرة الطور؛(الطاقة المتاحة)؛ فترة الاسترداد.

Résumé

Le maintien d'une température d'air stable sur de longues durées dans les applications de chauffage des locaux et de séchage à l'aide des capteurs solaires à air demeure un défi majeur, notamment en raison des fluctuations de l'irradiation solaire. Cette thèse présente une investigation expérimentale approfondie d'un capteur solaire à air hybride à double passage intégrant une unité de stockage thermique latent, dans le but de développer un système fiable et performant, capable de fonctionner sous des conditions climatiques variables pour des applications de chauffage et de séchage. Afin d'assurer une évaluation globale et cohérente du système proposé, une méthodologie d'analyse multicritère a été adoptée, incluant des analyses énergétique, exergétique, économique et environnementale. L'étude expérimentale a été menée de manière systématique en trois phases successives. La première phase a porté sur des analyses paramétriques et dimensionnelles d'un capteur solaire à air à double passage de référence, visant à étudier l'influence de la variation de l'espace d'air sur les performances thermiques et exergétiques. Les résultats ont montré que l'augmentation de la hauteur du canal d'air supérieur améliore significativement les performances du système, avec un rendement thermique maximal de 66,4 % obtenu pour une configuration d'espace d'air de 12 cm, tandis que des espaces d'air plus réduits ont entraîné une augmentation des irréversibilités et de la destruction d'exergie. La deuxième phase s'est concentrée sur l'intégration d'un chauffage électrique auxiliaire et d'une unité de stockage thermique latent utilisant de la paraffine, dans le but d'améliorer la stabilité thermique et de prolonger la durée de fonctionnement du système. Cette configuration a permis d'obtenir une température de sortie stable de 54 ± 1,25 °C, de prolonger le fonctionnement du capteur après le coucher du soleil et de réduire la consommation d'énergie électrique. Pour un débit massique d'air de 0,024 kg/s, le système a atteint des rendements thermique et exergétique moyens de 72,3 % et 3,5 %, respectivement. La troisième phase a porté sur l'optimisation supplémentaire des performances par l'intégration d'ailettes ondulées et l'évaluation de la position optimale du chauffage auxiliaire. Une inclinaison des ailettes de 45° a permis d'augmenter le rendement thermique de 13,8 % par rapport à un absorbeur plan, tandis que le positionnement du chauffage auxiliaire au niveau de la sortie a amélioré la régulation de la température, réduit les fluctuations thermiques et diminué la consommation d'énergie électrique de 4,23 %. Dans l'ensemble, les résultats démontrent que la combinaison du stockage thermique latent et des techniques d'amélioration du transfert de chaleur permet d'améliorer de manière significative l'efficacité énergétique, la stabilité ther-

mique, la durabilité et l'applicabilité pratique des capteurs solaires à air hybrides. Le système proposé constitue ainsi une solution prometteuse et durable pour les applications de séchage agricole et de chauffage des locaux.

Mots-clés : Chauffe-air solaire à double passage ; Unité de stockage thermique à chaleur latente ; Rendement thermique **;** MCP ; Exergie ; Période de retour sur investissement.

Table of Contents

General introduction 1
Chapter I: Literature review 6
I.1 Introduction 7
I.2 Double pass and multi pass solar air heaters 7
I.3 Heat transfer enhancement techniques in SAHs 10
I.4 Thermal storage integration in SAHs 15
I.5 Hybrid SAH configurations incorporating auxiliary heating and thermal storage 23
I.6 Discussion and research gaps 28
Chapter II: Experimental procedures 30
II.1 Introduction 31
II.2 Phase 1: Selection of the optimal air gap for DPSAH 31
II.2.1 Experimental procedures followed in the first phase 31
II.3 Phase 2: Integration of the LHTSU into the HDPSAH 33
II.3.1 Experimental procedures followed in the second phase 36
II.4 Phase 3: Integration of the novel wavy fin design and evaluation of auxiliary heater position effects 38
II.4.1 Experimental procedures followed in the third phase 40
II.5 Experimental measurements and uncertainty evaluation 43
II.5.1 Thermocouple calibration procedure and measurement performance evaluation 45
II.6 Data analysis 48
II.6.1 Analysis of energy performance 48
II.6.2 Analysis of exergy performance 49
II.6.3 Environmental impact analysis 50
II.6.4 Economic feasibility analysis 51
II.7 Summary of experimental methodology 53
Chapter III: Results and discussion 54
III.1 Introduction 55
III.2 Effect of air gap variations on DPSAH Performance 55
III.3 Effect of LHTSU integration on the thermal stability of the HDPSAH 58
III.3.1 Environmental and economic assessment 66
III.4 Effect of wavy-fin Inclination and auxiliary heater position on HDPSAH Performance 68
III.4.1 Indoor analysis: effect of wavy-fin inclination 68
III.4.2 Outdoor analysis: effect of auxiliary heater position 71
III.5 Conclusion 80

General Conclusion 81
References 84

List of figures

Figure I.1. Schematic view of double pass SAH..... 8
Figure I.2. Schematic view of the DPSAH with transverse fins 9
Figure I.3. Geometrical arrangements of the examined SAH configurations: (a) PFVSAH, (b) TFVSAH, and (c) combined-SAH 10
Figure I.4. Experimental setup of the SPSAH with triangular-fin absorber configurations ... 11
Figure I.5. Schematic representation of different fin configurations in the DPSAH 12
Figure I.6. Schematic of the curved DPSAH with varying relative absorber-plate positions (y/H) 13
Figure I.7. Schematic representation of the V-baffle block with staggered perforation arrays. 14
Figure I.8. Schematic of the DPSAH integrated with lava rock in the second channel..... 16
Figure I.9. Schematic representation of a SAH with a heat pipe vacuum tube collector..... 17
Figure I.10. Pictorial view of the DPSAH with encapsulated PCM tubes..... 19
Figure I.11. Test section of the PVT-DPSAH..... 19
Figure I.12. Schematic representation of the SPSAH with embedded paraffin-wax PCM fins 20
Figure I.13. Schematic of the DPSAH with flat absorber plate and spherically encapsulated PCM balls 21
Figure I.14. Schematic representation and photographs of the finned heat exchanger TSU .. 21
Figure I.15. Photograph and schematic of DPSAH integrated with infrared film. 25
Figure I.16. Schematic of electric and biogas hybrid-mode solar dryers..... 25
Figure I.17. Pictorial view of the HSED with PV panel 26
Figure I.18. Experimental configuration of the recycled HSAH 27
Figure I.19. Experimental setup used by Hassan et al. 28
Figure I.20. Schematic representation of the solar electric dryer applied to SED, ISED, and ISEDS techniques..... 28
Figure II.1. Schematic representation of the DPSAH structure. 32
Figure II.2. Schematic representation of the DPSAH structure, (b) sectional view 33
Figure II.3. Photograph of the auxiliary finned electric heater. 34
Figure II.4. Velocity-field visualization in the YZ plane for different DPSAH configurations developed by Elakrout et al. 34
Figure II.5. (a) Heat exchanger, (b) Paraffin wax shown in solid and liquid states. 35
Figure II.6. (a) Schematic representation of the HDPSAH, (b) Sectional view 36
Figure II.7. Experimental setup of the HDSAH. 37
Figure II.8. Schematic of the control unit. 38
Figure II.9. Illustrative design of the wavy-fin arrangement 39
Figure II.10. Schematic view of the HDPSAH with fins. 39
Figure II.11. Overview of the experimental steps conducted during phase 3. 40
Figure II.12. (a-b) Illustration of fin arrangements at different inclination angles (30°, 45°, and 60°) 41

Figure II.13. Laboratory setup 41
Figure II.14. Experimental setup for outdoor testing..... 42
Figure II.15. LabVIEW Interface with block diagram..... 45
Figure II.16. Photograph of the calibration setup: (a) reference sensor; (b) experimental test bench. 46
Figure II.17. Experimental methodology flowchart..... 53
Figure III.1. Temperature evolution of the absorber and outlet temperatures for 3, 6, 9, and 12 cm Configurations 56
Figure III.2. Comparison of (a) thermal efficiencies for the 3, 6, 9, and 12 cm configurations and (b) useful heat gain 57
Figure III.3. Comparison of exergy efficiency for various DPSAH configurations..... 58
Figure III.4. Variation of ambient temperature and solar irradiance over time. 59
Figure III.5. Impact of incident solar radiation on auxiliary electrical power usage..... 60
Figure III.6. Temporal temperature variations of the HDPSAH components. 61
Figure III.7. Temperature difference evaluation upstream and downstream of the LHTSU. 62
Figure III.8. Relative contribution of solar and electrical energy to the total system energy. 63
Figure III.9. Combined impact of solar energy input and auxiliary heater temperature on thermal efficiency. 64
Figure III.10. Variation of exergy gain and destruction and their impact on exergetic efficiency over time..... 65
Figure III.11. Evaluation of sustainability indicators for the system. 66
Figure III.12. Comparison of temperature difference for different configurations. 70
Figure III.13. Comparison of thermal efficiency for different configurations 71
Figure III.14. Temporal variation of ambient temperature and solar irradiance. 72
Figure III.15. (a) Operating profile of the auxiliary heater under variable solar irradiance; (b) distribution of energy contributions for the two configurations..... 74
Figure III.16. Evolution of absorber and outlet air temperatures for two configurations..... 75
Figure III.17. Comparison of the temperature differences. 76
Figure III.18. Comparison of PCM temperature evolution under different configurations. .. 77
Figure III.19. Temporal variation of top heat losses..... 78
Figure III.20. Variation of thermal efficiency during the operating period..... 79

List of tables

Table I.1. Heat transfer improvement approaches in SAH designs 14
Table I.2. Comparative summary of LHTSUs integration in SAHs. 22
Table II.1. Thermophysical properties of paraffin wax 35
Table II.2. Instruments used for measurements 43
Table III.1. Distribution of embodied energy among HDPSAH materials..... 67
Table III.2. Variation of CO_2 emissions with operational lifespan. 67
Table III.3. Economic assessment of the HDPSAH system. 68
Table III.4. Variation of air gap spacing with inclination angle. 69
Table III.5. Comparison between the present study and previously reported works. 79
Table III.6. Accuracy characteristics of the experimental equipment. 80

Nomenclature

A	Surface (m^{-2})
AMC	Annual maintenance cost (DZD)
ASV	The annual salvage value (DZD)
Ce	Annual cost of electrical energy (DZD)
C_p	Specific heat (J kg^{-1} K^{-1})
CRF	Capital Recovery Factor (-)
EEF	Electric energy fraction (%)
E_{el}	Electrical energy (kWh)
EPBT	Energy payback time (years)
E_s	Solar thermal energy (kWh)
E_{ts}	Thermal storage energy (kWh)
$\dot{E}x$	Exergy (W)
FAC	The First Annual Cost (DZD)
I	Irradiation (W m^{-2})
IP	Improvement potential (W)
$\dot{m}$	Mass flow rate (kg s^{-1})
P	Power (W)
PBP	Payback period (years)
Q_u	Useful heat (W)
R	Resistance (ohm)
SEF	Solar energy fraction (%)
SFF	Sinking fund factor (-)
SI	Sustainability index (-)
t	Time (hour)
TAC	Total annual cost (DZD)
TSF	Thermal storage fraction (%)
U	Voltage (V)

Greek letters

η	Efficiency
ψ	Rational exergy management mode efficiency

Subscript

amb	Ambient
CO_2	Carbon dioxide
dest	Destruction
el	Electric
ex	Exergy
f	Fluid
in	Inlet
out	Outlet
s	Solar
th	Thermal

Abbreviations

DPSAH	Double-pass solar air heater
DZD	Algerian dinar
HDPSAH	Hybrid Double-pass solar air heater
HSAH	Hybrid solar air heater
LHS	Latent heat storage
PCM	Phase change material
RCRP	Relative CO_2 reduction potential
SAH	Solar air heater
SHS	Sensible heat storage
TSU	Thermal Storage Unit

General introduction

General introduction

The sustained growth in global energy demand has become one of the most pressing challenges of the modern era. Rapid population expansion, intensified industrialization, and increasing geopolitical instability have placed unprecedented pressure on conventional energy systems. As a result, the extraction, processing, and transportation of fossil fuels have become increasingly complex, costly, and environmentally burdensome. In parallel, the accelerating consumption of natural energy resources has raised serious concerns regarding long term energy security, while exacerbating environmental problems such as climate change, greenhouse gas emissions, and ozone layer depletion [1].

In this situation, the transition toward sustainable and resilient energy systems has become a strategic priority for both the scientific community and decision-makers worldwide. Particular emphasis has been placed on renewable energy technologies and advanced thermal energy management solutions as viable pathways to mitigate environmental impacts while ensuring a reliable energy supply [2]. Among the available renewable resources, solar energy stands out due to its abundance and wide geographical availability. It is estimated that the Earth receives approximately 174 000 TW of solar radiation from the sun [3]. This immense and continuously available resource positions solar energy as a cornerstone for the development of clean, sustainable, and long-term energy solutions. Which has consequently stimulated the development of a wide range of advanced solar technologies, including photovoltaic applications, concentrating solar power systems, and solar thermal collectors. Among these technologies, solar thermal collectors are regarded as one of the most practical and efficient means of harnessing solar energy [4], operating on a simple and robust principle, absorb incident solar radiation and convert it into useful thermal energy. Due to their operational simplic-

ity, reliability, and cost effectiveness, solar thermal collectors have been widely adopted in various applications, such as domestic water heating, solar distillation, agricultural and textile drying, solar cooking, and space heating to ensure indoor thermal comfort in buildings.

Solar air heaters (SAHs) represent one of the simplest and most practical configurations within solar thermal collector technologies. This Type of collectors is distinguished by its straightforward design, low manufacturing cost, and reliable operation, as it does not encounter typical issues associated with liquid-based systems, such as freezing, boiling, leakage, or corrosion [5]. These characteristics make SAHs particularly attractive for applications that require robust, low maintenance, and cost-effective thermal energy systems. Despite these advantages, conventional SAHs generally exhibit relatively limited thermal performance. This drawback is mainly attributed to the inherently low thermal conductivity of air and its weak convective heat transfer coefficient, which constrain effective heat exchange between the absorber surface and the airflow. Consequently, a considerable fraction of the absorbed solar energy is not efficiently transferred to the working fluid, leading to reduced thermal efficiency. To overcome the inherent performance limitations of conventional SAHs, extensive research efforts have been devoted to the development of various enhancement techniques aimed at improving heat transfer efficiency. A major focus has been placed on absorber surface modification, as it plays a central role in thermal energy exchange. Common approaches include increasing the effective absorber surface area through the adding of fins, baffles, ribs, and other flow-disturbing elements, as well as introducing surface roughness to promote turbulence and enhance convective heat transfer. In addition, optimization of the airflow configuration has been widely investigated, particularly through the adoption of double-pass and multi-pass designs, which increase air residence time and improve thermal interaction between the absorber and the working fluid.

As a result of these combined strategies, several advanced SAH configurations reported in the literature have achieved thermal efficiency levels ranging from approximately 70% to 80%, depending on the operating conditions and design parameters. However, in practice, the primary limitation hindering the widespread application of SAHs is not their relatively low thermal performance, but rather their complete dependence on solar radiation as the sole energy source. This dependence significantly limits their ability to supply sufficient thermal energy under cloudy conditions or during sunset periods. Such kind of inconsistency represents a major challenge for applications that require continuous heat delivery throughout the day, particularly processes such as agricultural drying, where stable and uninterrupted thermal input is essential. In response to this limitation, a considerable body of research has focused on enhancing the operational reliability of SAHs through the integration of thermal energy storage units (TSU). In recent years, two main storage approaches have been extensively investigated: sensible heat thermal energy storage, typically using materials such as rocks, gravel, or sand, and latent heat thermal energy storage, which commonly employs phase change materials (PCMs) such as paraffin wax. The incorporation of these TSUs enables the operating duration of SAHs to be extended by approximately 20 to 30% beyond sunshine hours [6]. In parallel, other studies have focused on the integration of auxiliary heating systems powered by electrical energy or conventional energy sources to ensure continuous heat supply throughout the day. Although the operation of auxiliary heaters inevitably leads to additional energy consumption and increased operating costs, their incorporation has been shown to be effective in compensating for the intermittency of solar radiation.

A review of the existing literature on the development of SAHs and hybrid solar air heater HSAH systems indicates that auxiliary heating devices are most commonly installed either at the outlet of the solar collector or in direct thermal contact with the absorber surface. While these configurations are frequently adopted to ensure continuous heat delivery, limited

attention has been devoted to systematically evaluating how the position of the auxiliary heater influences collector performance, outlet air temperature, and the overall thermal behavior of the system. In particular, the impact of heater placement on temperature fluctuations and thermal stability remains insufficiently explored. In response to this research gap, the present thesis focuses on achieving stable and well-regulated outlet air temperatures in a hybrid double-pass solar air heater (HDPSAH) through the integration of an auxiliary electric resistance heater equipped with fins. A particular focus is directed towards examing the impact of of auxiliary heater positioning on the system's thermal response and electrical energy consumption. Furthermore, to enhance thermal regulation and extend the system operation, a latent heat storage unit (LHSU) in the form of a heat exchanger loaded with PCM is incorporated, using paraffin wax. The proposed system is subsequently evaluated through comprehensive energy and exergy analyses, in addition to environmental and economic assessments. Accordingly, this thesis is structred as follows:

Chapter 1 provides a comprehensive review of the existing literature on SAHs, hybrid configurations, thermal energy storage techniques, and performance enhancement strategies, with particular emphasis on double pass systems and PCMs.

Chapter 2 describes the experimental setup, instrumentation, measurement procedures, and uncertainty analysis employed in this study.

Chapter 3 presents the experimental results and discussion, structured into three main phases:

- Parametric and dimensional analysis focusing on the effect of air gap variation under controlled laboratory conditions.
- Evaluation of the integration of a LHTSU and auxiliary electric heating on system performance

- Optimization of the HDPSAH through the incorporation of wavy fins and investigation of fin inclination angle and auxiliary heater positioning.

Finally, the thesis is concluded with a general conclusion and outlines recommendations for future research.

Chapter I: Literature review

I.1 Introduction

Solar air heaters (SAHs) represent one of the simplest and most practical devices for harnessing solar energy [4], operating as heat exchangers by converting solar radiation into useful thermal energy [7], with simple and low construction costs compared to other technologies. However, the SAH's performance remains constrained by the low thermal conductivity of air, poor heat transfer coefficient, limited heat transfer area [8], and the strong dependence on solar variability. To overcome these challenges, extensive research efforts have been conducted, including increasing the absorber surface area, integrating baffles, fins, ribs, and vortex generators, optimizing the number of air passes, integrating thermal storage units based on sensible or latent heat, and incorporating auxiliary heaters powered by conventional or renewable energy sources.

I.2 Double pass and multi pass solar air heaters

The single pass solar air heater (SPSAH) represents the simplest and most conventional design of SAHs, in which the air flows through a single channel located either above or below the absorber plate. However, this design is characterized by relatively low thermal performance due to the limited heat transfer area and considerable heat losses to the surroundings. In contrast, double and multi-pass SAHs allow the air stream to flow through two or more channels arranged either in parallel or counterflow. These configurations substantially reduce both top and bottom heat losses to the environment and increase the effective heat-transfer area, thereby improving the overall thermal performance [9], as illustrated in Figure I.1.

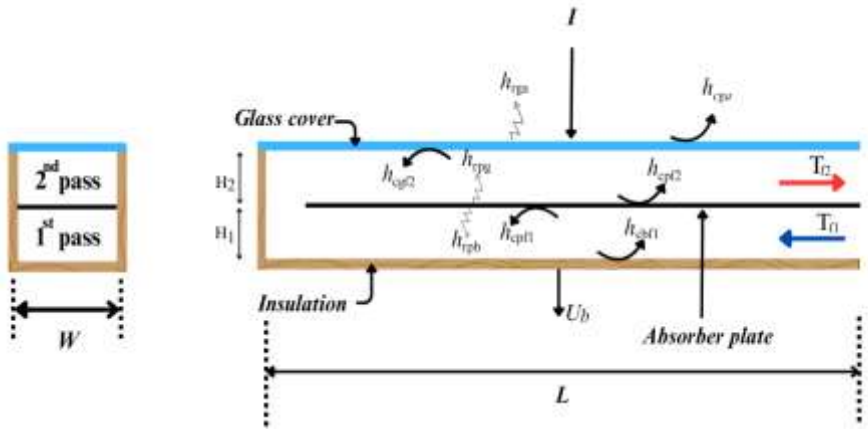


Figure I.1. *Schematic view of double pass SAH*

Wijeysundera et al. [10] conducted a combined analytical and experimental study to compare the performance of a conventional SPSAH with a double pass solar air heater (DPSAH). The study involved developing detailed heat transfer models for two-pass flow arrangements and validating these models using both previously published data and new outdoor experiments conducted according to ASHRAE testing procedures. The findings demonstrated that the DPSAH is 10-15% more efficient than the SPSAH, primarily due to reduced top and bottom heat losses and enhanced heat transfer between the absorber and the airflow.

Mahmood et al. [11] experimentally compared the thermal performance of an SPSAH with a DPSAH equipped with 16 layers of steel wire mesh as the absorber material, and systematically installed four transverse fins to force air to follow a longer flow path, as shown in Figure I.2. The study also examined the effect of varying the lower channel height in the DPSAH configuration. The results showed that the DPSAH consistently outperformed the SPSAH, achieving a maximum thermal efficiency of 62.5% compared with 55% for the SPSAH. The temperature difference across the collector increased as the mass flow rate diminished. Additionally, the results indicated that reducing the lower channel height further enhanced the thermal performance. However, the DPSAH exhibited a slightly higher pressure drop due to the presence of the porous medium and the extended flow path.

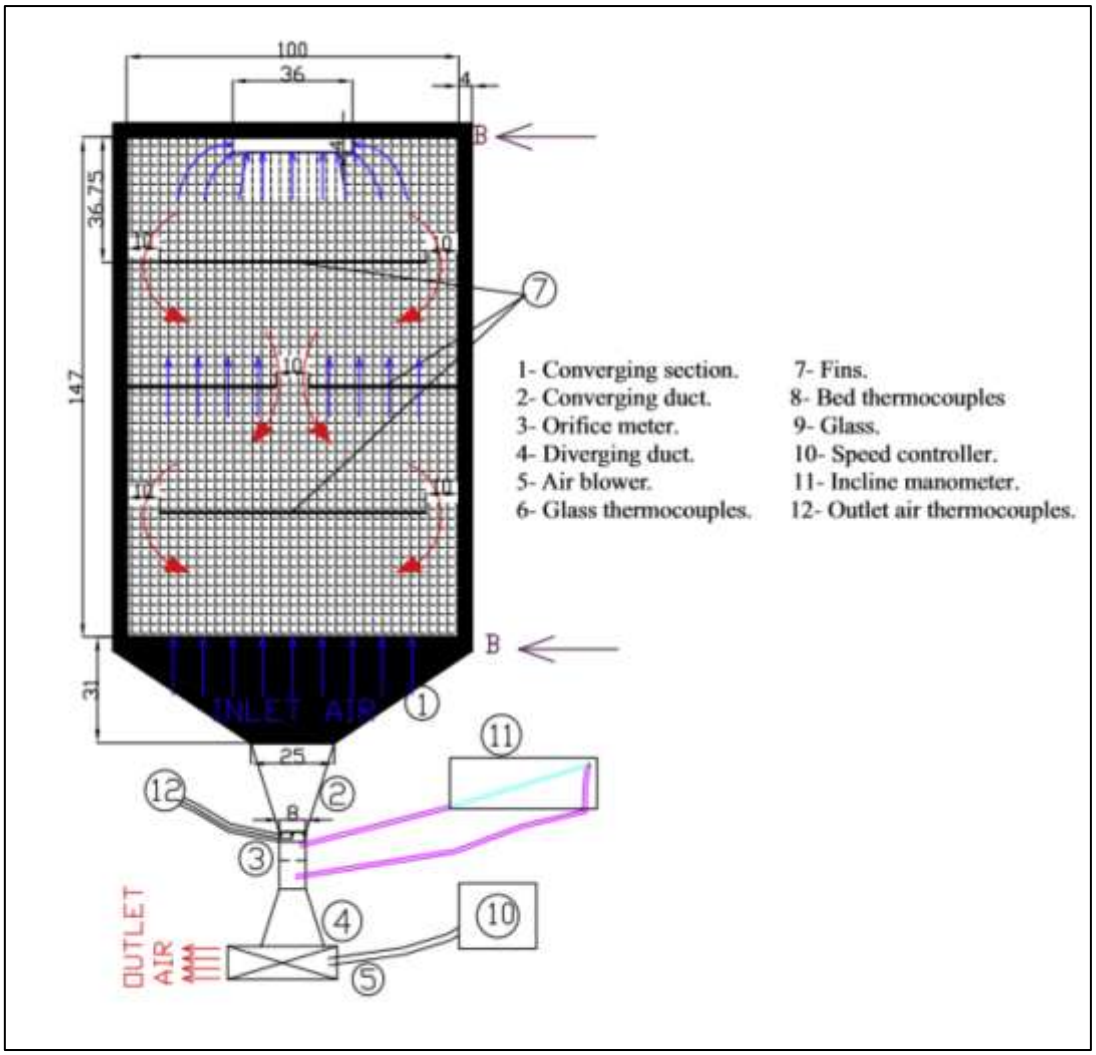


Figure I.2. *Schematic view of the DPSAH with transverse fins [11]*

Abdulmejeed et al. [12] experimentally and numerically demonstrated that the number of air passes and the flow arrangement in SAHs have a considerable effect on thermal losses and overall performance. The study examined the thermal and flow characteristics of three types of SAHs: the parallel flow V-grooved SAH (PFVSAH), the triple flow V-grooved SAH (TFVSAH), and a combined-SAH configuration under various climatic conditions, as presented in Figure I.3, showing that the combined-SAH achieved the highest performance, outperforming both the PFVSAH and TFVSAH with a maximum temperature difference of 29.1°C. The PFVSAH recorded the lowest outlet temperatures among the three configura-

tions, while numerical analysis indicated that the TFVSAH exhibited more complex flow patterns, including significant vortices generated by 180° flow deviations.

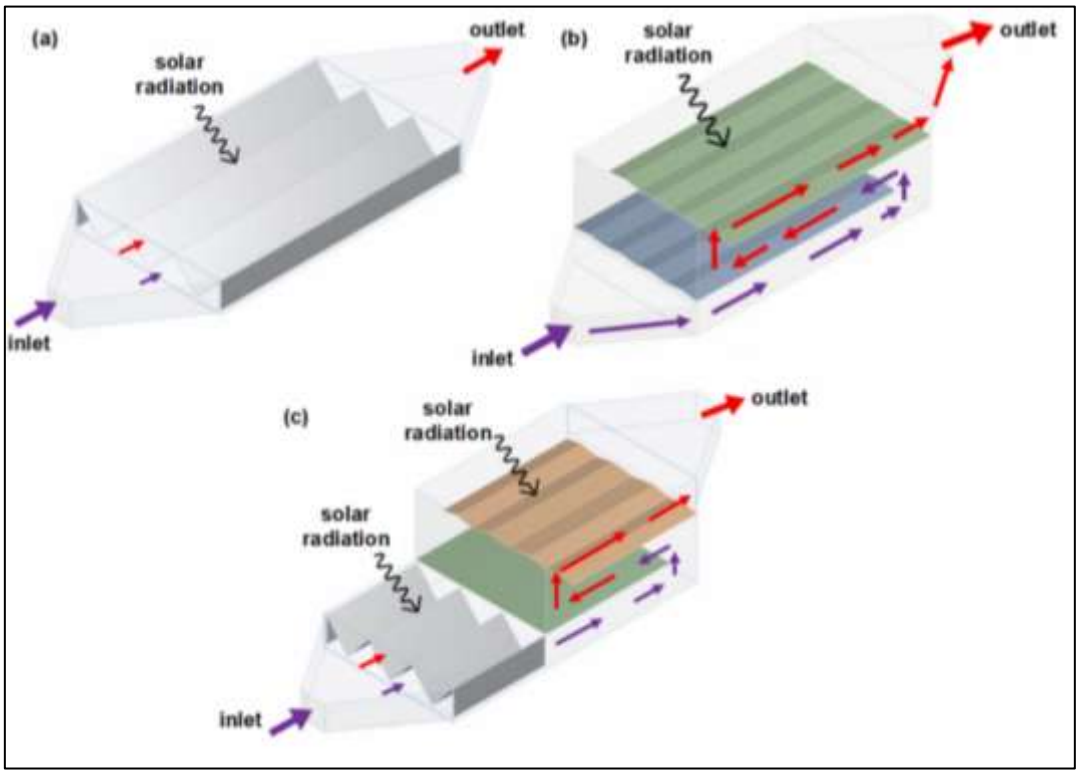


Figure I.3. *Geometrical arrangements of the examined SAH configurations: (a) PFVSAH, (b) TFVSAH, and (c) combined-SAH [12]*

I.3 Heat transfer enhancement techniques in SAHs

To enhance the convective heat transfer between the absorber and the airflow, many researchers have focused on increasing the absorber surface area through the utilization of trapezoidal and corrugated surfaces, as well as employing ribs, packed beds, fins, baffles, vortex generators, and artificially roughened surfaces. These techniques aim to create turbulence and disrupt the laminar boundary layer, which is considered the primary cause of the high thermal resistance to heat transfer.

Albdoor et al. [3] experimentally evaluated a modified SPSAH incorporating a new design of triangular fins arranged in different configurations and compared it with a conventional flat-plate SPSAH, as illustrated in Figure I.4. The experiments were conducted under real outdoor

conditions during the winter season, with air mass flow rates ranging from 0.02 to 0.1 kg/s. The findings showed that, for all mass flow rates, the finned absorbers produced a higher temperature rise than the flat absorber. The highest thermal efficiency, 86.4%, was achieved by the inclined staggered double-triangular-fin configuration, accompanied by an exergetic efficiency of 1.5%. However, the finned designs exhibited an increased pressure drop, which was identified as a limitation of the system.



Figure I.4. *Experimental setup of the SPSAH with triangular-fin absorber configurations [3]*

Borah et al. [13] experimentally investigated an SPSAH in which the flat absorber plate was integrated with square obstacles fitted with threaded pin fins, and compared it with a conventional flat-plate SPSAH using a comprehensive 4E analysis (energy, exergy, exergoeconomic, and enviroeconomic). This design aimed to enhance heat transfer while keeping hydraulic losses within reasonable limits. The modified SPSAH showed an increase in the outlet air temperature of about 9%, raised the useful heat gain and energy efficiency by up to 28.8%

and 23.6%, respectively, and improved exergy efficiency by approximately 30% compared to the conventional configuration.

Elakrout et al. [14] evaluated the effect of three distinct fin configurations : parallel, vertical, and opposed, integrated into the upper channel of a DPSAH as shown in Figure I.5, over mass flow rates ranging from 0.0036 to 0.0183 kg/s. The results reveal that parallel fins enhance thermal efficiency, particularly at lower mass flow rates, while vertical and opposed fins lead to increased pressure drops without a corresponding temperature rise.

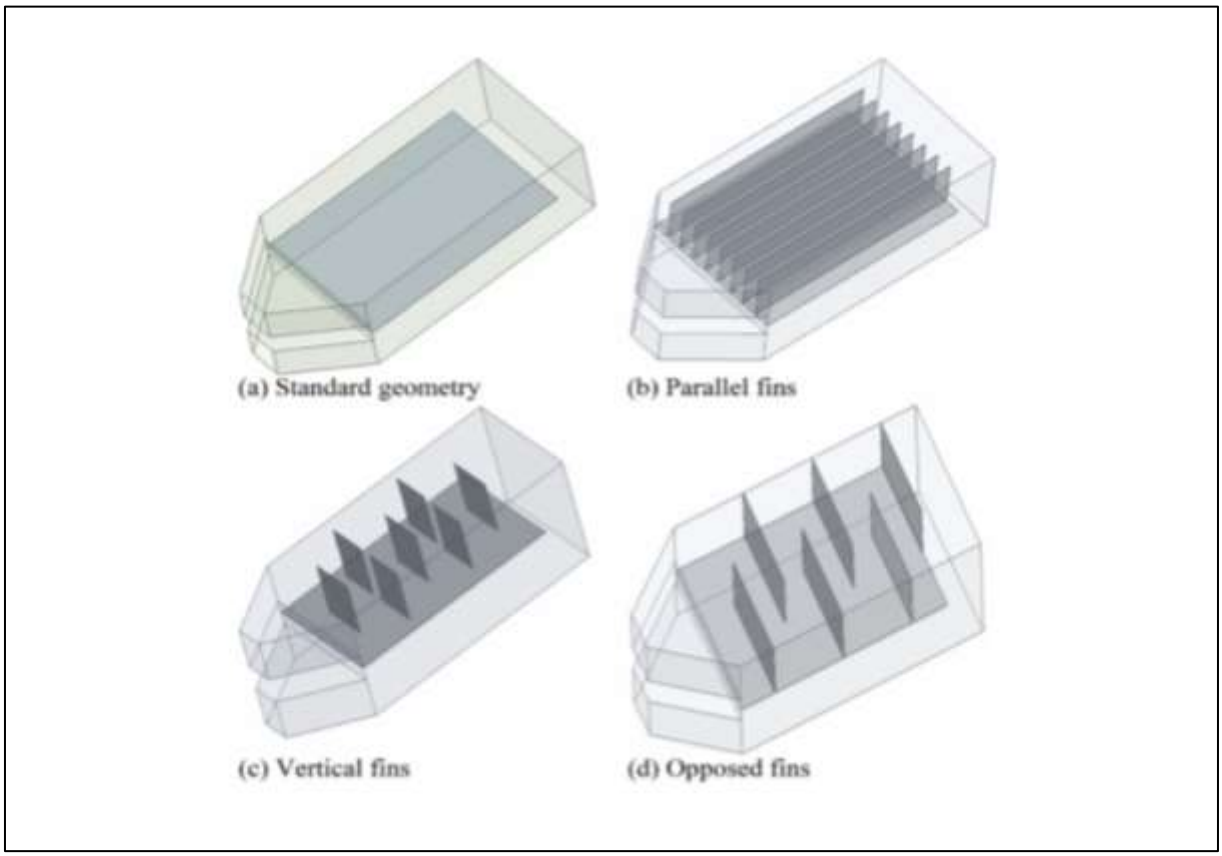


Figure I.5. *Schematic representation of different fin configurations in the DPSAH [14]*

Kumar et al. [15] optimized the performance of a curved DPSAH by integrating circular and semi-circular ribs and by varying the relative positions of the absorber plates, as shown in Figure I.6. The study revealed that asymmetric semi-circular ribs performed better than symmetric circular ribs, due to the enhanced formation of vortices. Additionally, positioning the absorber plate at the mid-height of the collector increased the outlet temperature by approximately 5 °C.

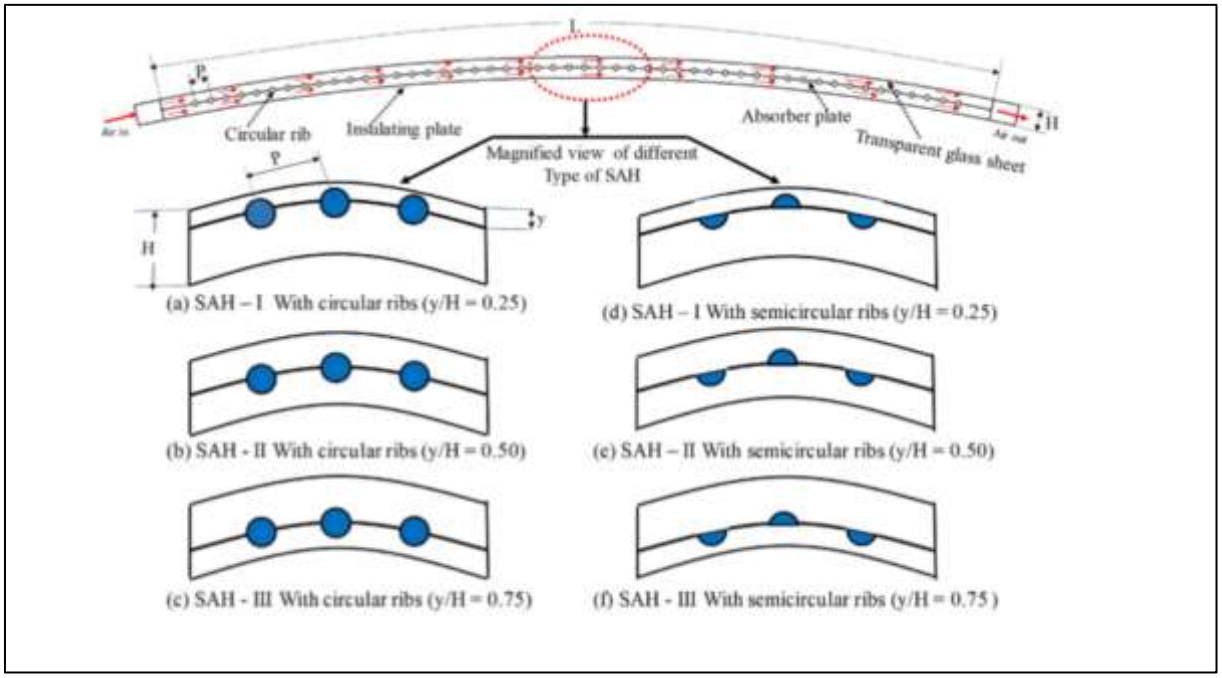


Figure I.6. *Schematic of the curved DPSAH with varying relative absorber-plate positions (y/H) [15]*

Pandey and Kumar [16] investigated the improvement of an SPAH by equipping the absorber plate with novel V-baffle blocks featuring staggered racetrack-shaped perforations (Figure I.7). The indoor experimental findings indicated that the V-down baffles with e/H = 0.7 and p/e = 2 provided the highest heat-transfer enhancement, with Nu/Nus = 4.559 and f/fs = 39.07 relative to the smooth duct. Furthermore, the V-down configuration with e/H = 0.5 and p/e = 4 at Re =13 021 yielded the maximum thermohydraulic performance factor of 1.435. However, the study was limited to indoor testing under a constant-flux configuration and considered only a specific range of Reynolds numbers and geometric factors.

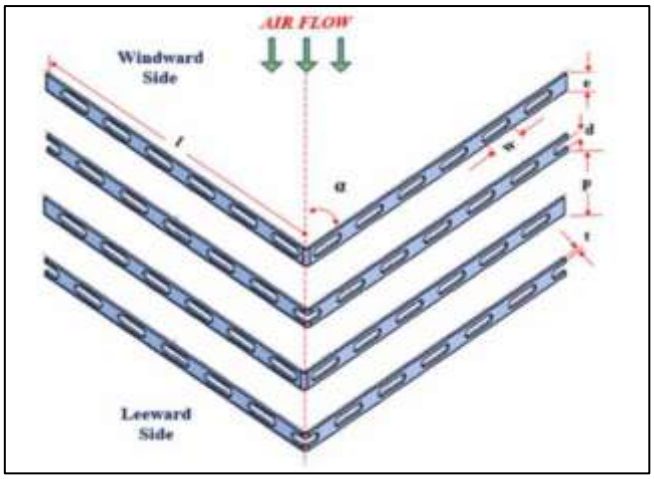
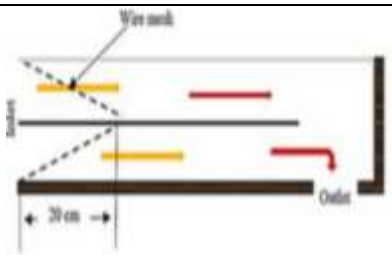
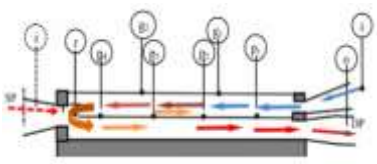
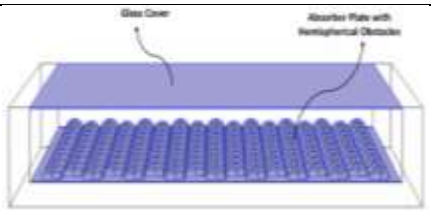
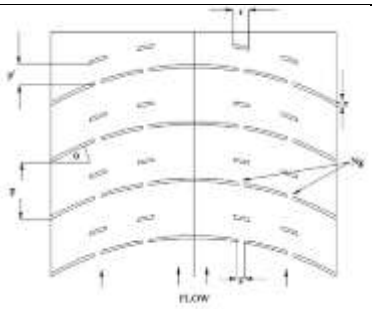
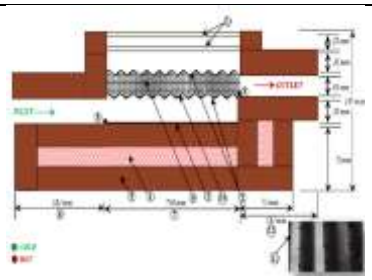
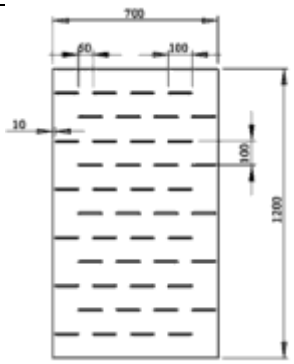


Figure I.7. *Schematic representation of the V-baffle block with staggered perforation arrays [16].*

As shown in Table I.1, most enhancement techniques are dependent on increasing the effective heat transfer area or promoting turbulence near the absorber surface. Although these methods consistently improve thermal performance, they often introduce additional pressure losses, highlighting the need for optimization between heat-transfer enhancement and hydraulic penalty.

Table I.1. *Heat transfer improvement approaches in SAH designs*

Enhancement technique	SAH design	Key findings	Ref.
Stainless-steel wire mesh wrapped around the absorber with three lengths: 20, 40, and 60 cm		The longest mesh (60 cm) at 0.045 kg/s yielded the highest temperature difference and daily efficiency of 76%.	[17]
Tubular absorber with and without packed aluminum-fiber porous material		Tubular absorber with porous material in double-pass mode achieved the best performance: higher exergy efficiency, lower top losses, shorter energy payback time, and lower cost per kWh.	[18]

Hollow obstacles on the absorber surface (conical, cylindrical, spherical,hemispherical,pyramidal,cubical)		Vertical cylindrical obstacles delivered the best performance: 69% higher daily thermal efficiency and up to 168.7% increase in relative CO_2 reduction potential.	[19]
Discrete arc-pattern ribs combined with staggered elements on the absorber plate		The modified absorber enhanced heat transfer and friction factor, achieving a peak thermohydraulic performance of 1.86, thermal and effective efficiencies of 59.5% and 57.6%, respectively	[20]
Circular jet impingement in a laterally corrugated wavy channel; porous wire-mesh bed.		Design-1 achieved the highest performance due to strong jet-induced mixing and recirculation,with thermal/thermohydraulic efficiencies of 94-96% and 84-85% for 40 holes. Design-2 (98% porosity) showed lower efficiencies.	[21]
Closed-cell aluminum-foam porous baffles (6 mm and 10 mm), arranged sequentially or staggered		All baffled designs outperformed the smooth SAH. Energy and exergy efficiencies ranged from 39-78% and 22-55%. The 6 mm staggered configuration achieved the highest efficiencies	[22]

I.4 Thermal storage integration in SAHs

To extend the operation of SAHs after sunset and ensure stable performance under cloudy weather conditions, many researchers have focused on integrating thermal storage units (TSUs), either through sensible heat storage (SHS) materials such as sand, rocks, water, concrete, or through latent heat storage (LHS) using phase change materials (PCMs). These

storage units enable excess thermal energy to be captured during peak solar periods and released when required, thereby improving the system reliability.

Din et al. [23] demonstrated that incorporating lava rock as a thermal storage medium in a DPSAH (Figure I.8) substantially improves its insulation characteristics and increases its thermal efficiency, achieving values of up to 76.41% compared with 65.02% for the system without lava rock. Additionally, charging and discharging tests showed that the lava rock can store heat up to 87 °C and release it for 70 to 120 min after the heat source is switched off. In a similar study, Algarni et al. [24] conducted an experimental investigation on three modified SAH configurations in which brick powder, graphite powder, and desert sand were encapsulated in small cylindrical containers. The systems were evaluated under both natural and forced convection regimes and compared with a conventional SAH. The findings showed that the collector using graphite powder delivered the best thermal performance, reaching an efficiency of 37.62% and a peak outlet air temperature of 41.2 °C. In general, all modified models performed significantly better than the conventional SAH, particularly in terms of heat transfer rates and thermal efficiency.

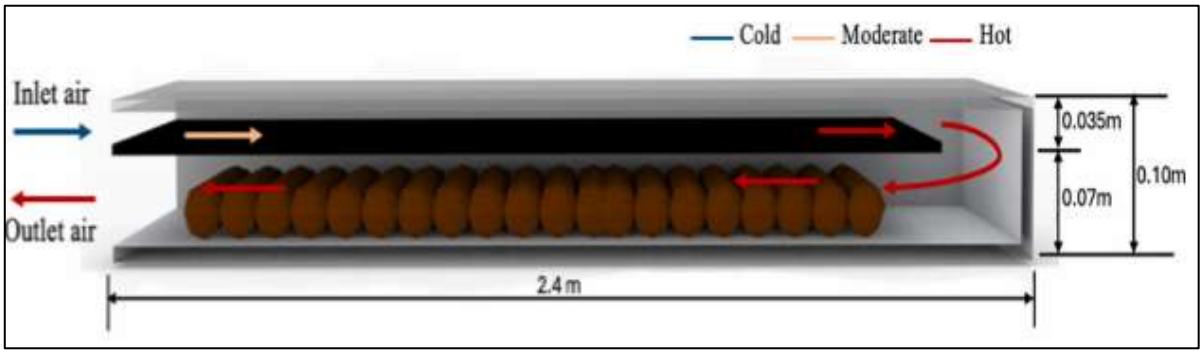


Figure I.8. *Schematic of the DPSAH integrated with lava rock in the second channel [23]*

Sachdeva et al. [25] carried out an experimental study on a novel SAH featuring a heat pipe vacuum tube collector coupled with two types of finned tube heat exchangers (four-row and eight-row) as shown in Figure I.9, using Therminol-55 as both the heat transfer fluid and sen-

sible heat storage medium under varying air flow rates. The results indicated that the eight-row heat exchanger provided superior air heating performance due to its increased length and larger heat transfer area, achieving an outlet air temperature of 89.4 °C and a maximum temperature rise of 55.4 °C at an air flow rate of 100 kg/h. Additionally, in terms of cost savings, the proposed system resulted in a monthly savings of $65.65 and a payback period of 12.4 months. The system also contributed to significantly lower CO_2 emissions.

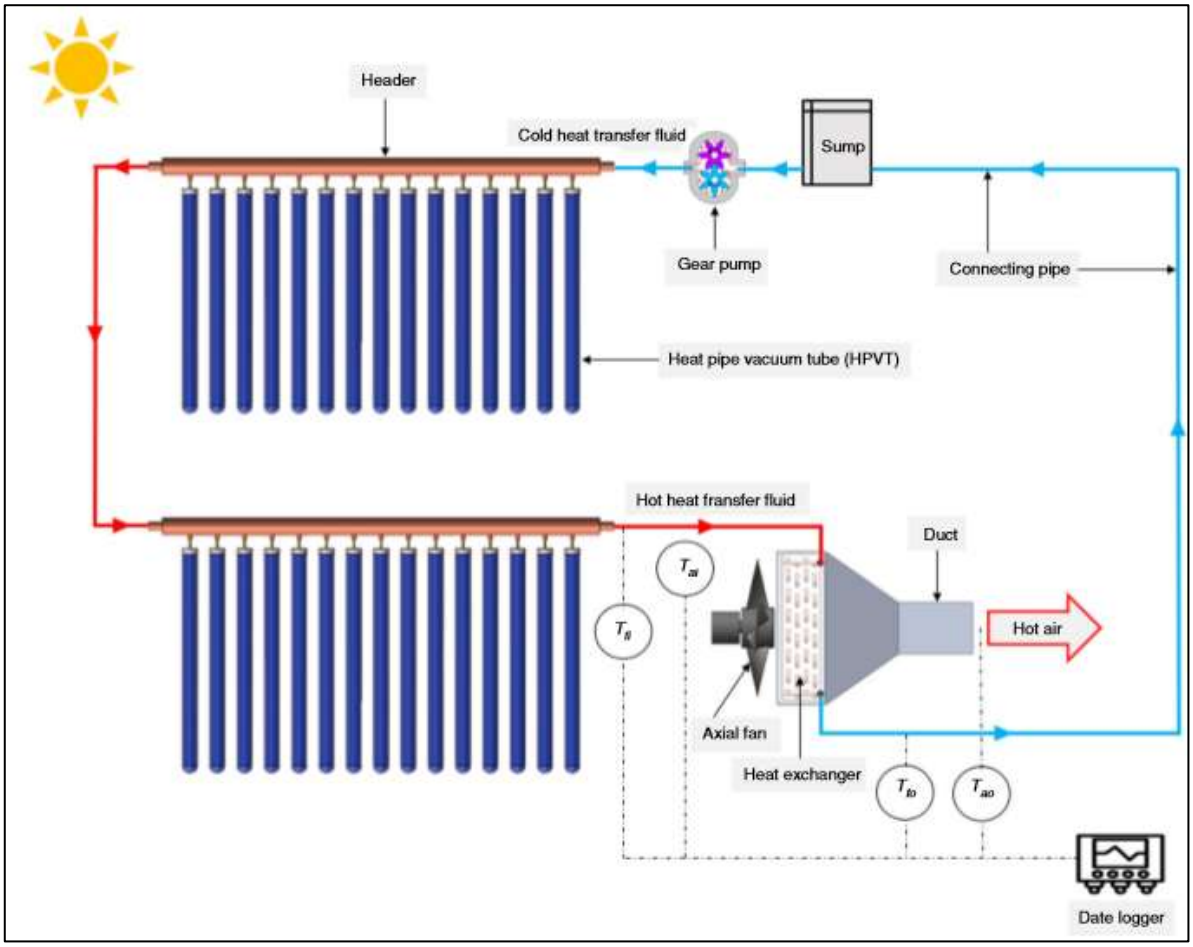


Figure I.9. *Schematic representation of a SAH with a heat pipe vacuum tube [25]*

Recently, many studies have shifted toward integrating LHS systems, primarily because of their higher energy density and ability to store heat isothermally, wherein LHS materials can store approximately 5 to 14 times more heat than an equivalent volume of sensible

SHS materials [26]. Kumar et al. [27] carried out an extensive experimental investigation on a forced-convection SAH enhanced with PCM, using paraffin wax embedded within three different absorber designs : pin-fin, circular-tube, and triangular-tube plates. The inclusion of PCM in these configurations resulted in an increase of 2 to 6 °C in outlet air temperature, while thermohydraulic efficiency improved by 3 to 40% and exergy efficiency by 2 to 20% compared with a conventional flat absorber plate.

Vengadesan et al. [8] experimentally examined a modified DPSAH equipped with PCM tubes filled with paraffin wax and arranged in a staggered, inclined zigzag configuration to intensify airflow mixing and extend the duration of heat release, as presented in Figure I.10. The integration of PCM markedly improved the system's thermal performance compared with the conventional design, with the modified collector achieving a maximum outlet temperature of 65 °C and a temperature rise of 29.5 °C, in contrast to 58 °C and 23.8 °C for the conventional configuration. Additionally, the modified DPSAH exhibited a higher thermal efficiency of 77.7% compared with 62.5% for the conventional system, along with a 252% increase in the convective heat transfer coefficient and reduced overall thermal losses. However, the study also reported certain limitations, notably the increased pressure drop, which requires greater blower power.

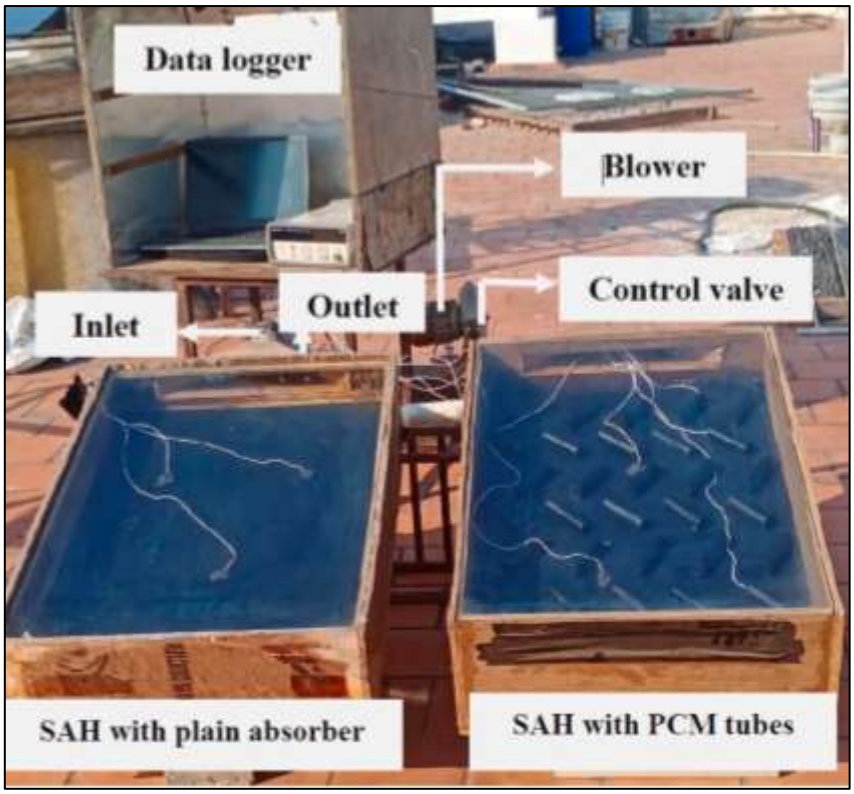


Figure I.10. *Pictorial view of the DPSAH with encapsulated PCM tubes [8]*

In another study, Din [28] reported that integrating cylindrical PCM capsules into a photovoltaic–thermal DPSAH (PVT-DPSAH) significantly boosts both its thermal and electrical outputs, as illustrated in Figure I.11. The presence of PCM enhanced the system's thermal efficiency by 31.45%. Moreover, the PCM cylinders provided passive cooling to the photovoltaic surface, thereby lowering its operating temperature and improving electrical performance.

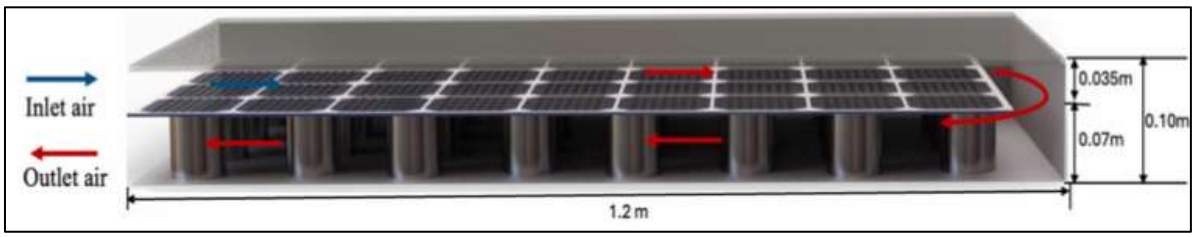


Figure I.11. *Test section of the PVT-DPSAH [28]*

Brahma et al. [29] focused on the effect of three types of PCM (acetamide, stearic acid, and paraffin wax) on the performance of a SAH, where the thermal storage unit was implemented as a cavity positioned beneath the absorber plate. The experimental results showed that paraf-

fin wax exhibited the highest performance, followed by stearic acid and acetamide. The research further pointed out a few operational challenges, such as the need to optimize the PCM container gap and poor thermal conductivity of the PCMs. Balakrishnan et al. [30] integrated rectangular metallic fins packed with Paraffin wax along the absorber surface of an SPSAH and arranged them in several configurations to enhance heat transfer performance while simultaneously providing short-term thermal storage, as depected in Figure I.12. Experimental results showed that the fin-PCM modules promoted strong flow mixing, leading to a notable increase in the convective heat-transfer coefficient, reaching 20.4 W/m²·K, and a corresponding rise in the Nusselt number to 5.3, while the encapsulated PCM provided additional thermal energy during the discharge period.

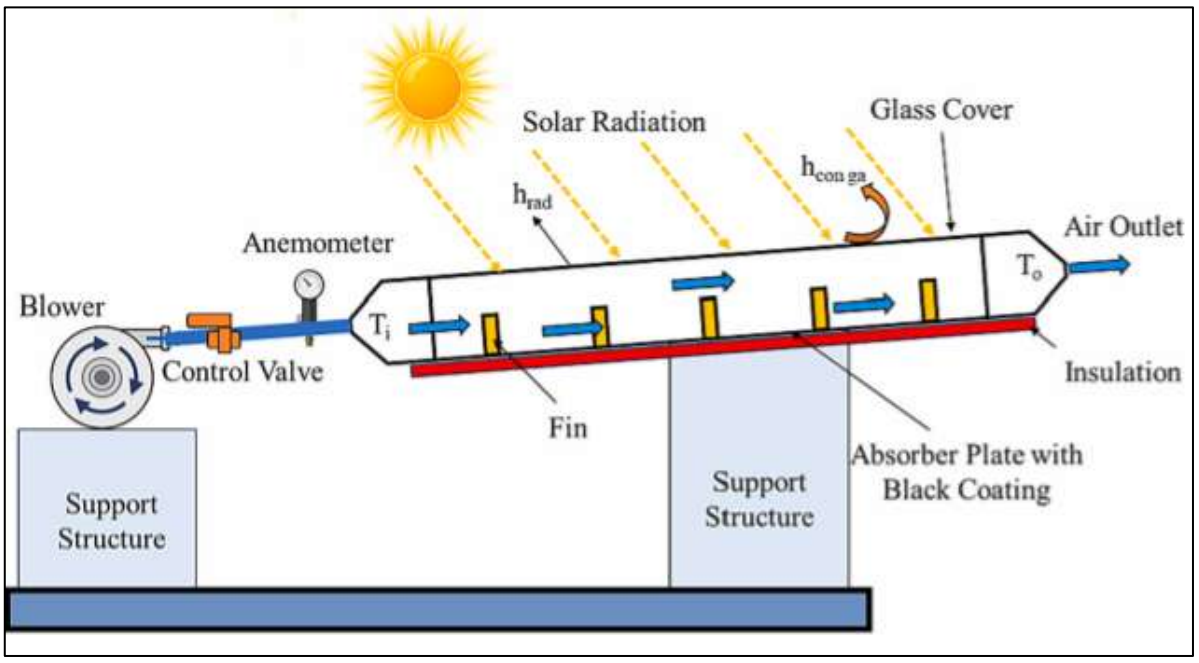


Figure I.12. *Schematic representation of the SPSAH with embedded paraffin-wax PCM fins [30]*

Sudhakar and Cheralathan [31] experimentally investigated a DPSAH integrated with spherically encapsulated PCM mounted in perforations on the absorber plate (Figure I.13), where the spherical capsules simultaneously act as turbulence promoters and latent heat storage units. Under outdoor operation at a constant mass flow rate of 0.009 kg/s, the modified

DPSAH increased the outlet air temperature and provided effective thermal storage, maintaining the outlet temperature in the range of about 45–55 °C for up to 2 h after sunset.

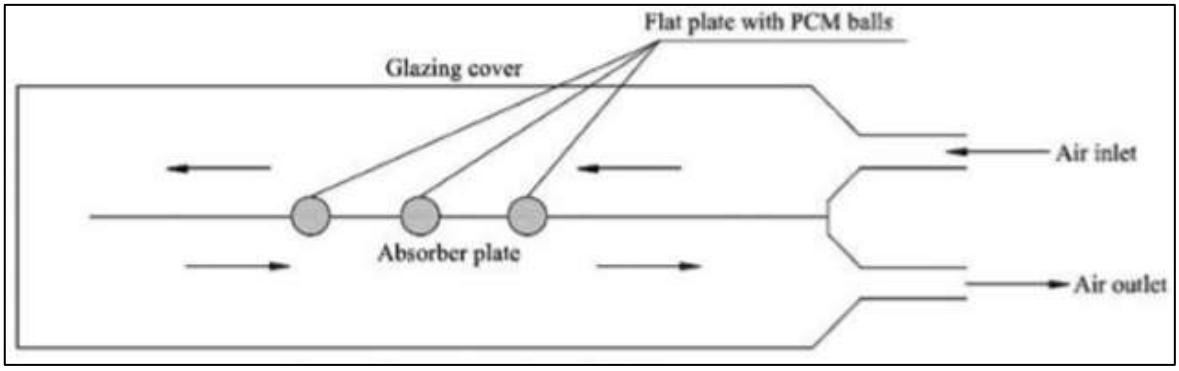


Figure I.13. *Schematic of the DPSAH with flat absorber plate and spherically encapsulated PCM balls [31]*

Dheyab et al. [32] developed a novel SAH configuration in which the traditional absorber plate was replaced with a finned heat exchanger that functioned simultaneously as the absorber and the thermal storage unit within a closed-loop DPSAH, as presented in Figure I.14. The heat exchanger was filled with 50 kg of PCM, using two different materials (RT42 and RT50) for comparison. The experiments showed that the system performed particularly well with RT42, achieving a peak discharge efficiency of 93.9%, while RT50 resulted in a slightly lower value of 88.1%.

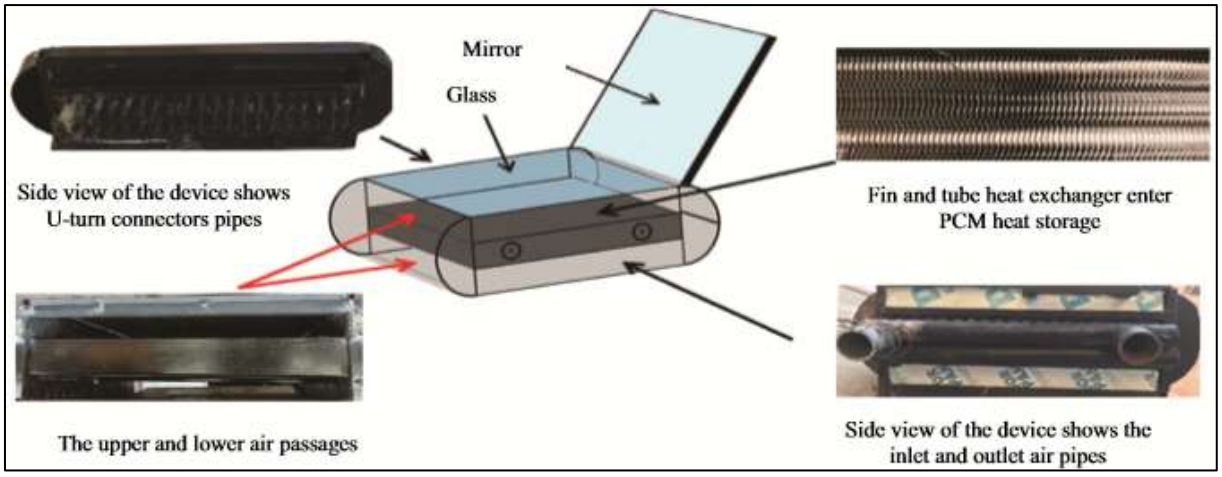
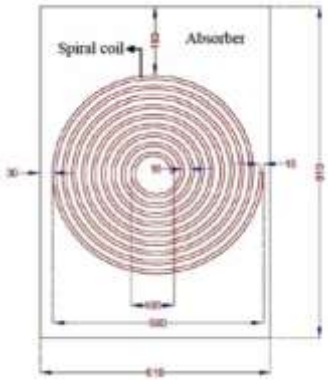
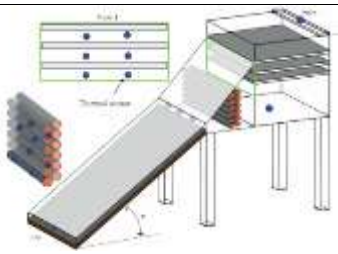
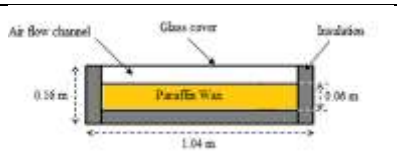
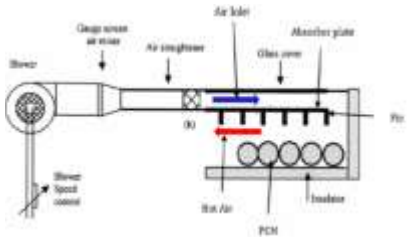


Figure I.14. *Schematic representation and photographs of the finned heat exchanger TSU[32]*

Additionally, Table I.2 provides a comparative summary of selected studies that have integrated latent heat thermal storage units (LHTSUs) into SAHs. The table highlights developments in TSU optimization, proposed new designs, and modifications, including the integration of new shapes and fin models in conjunction with TSUs. It also summarizes investigations comparing different types of PCM and their effects on system performance.

Table I.2. *Comparative summary of LHTSUs integration in SAHs.*

TSU Shape	SAH design	Key findings	Ref.
Spherical capsules filled with composite PCMs (graphite + paraffin wax, graphite + coconut oil)		SAH with graphite+paraffin wax achieved the highest thermal efficiency (78.8%) versus 74.3% for graphite+coconut oil, both systems provided discharge periods exceeding 6 hours, demonstrating strong thermal storage capability.	[33]
Spiral coil absorber filled with paraffin-wax PCM		SAH with the paraffin wax filled in spiral coil achieved the highest thermal efficiency (29.86%) and a peak outlet temperature of 59 °C at 0.0076 kg/s, offering improved short-term energy storage and enhanced CO_2 mitigation compared with the other tested configurations.	[34]
Cylindrical PCM tubes used as TSU		Integration of PCM tubes reduced drying time by 33% compared with open-sun drying, improved thermal stability, and better preserved product quality, including higher vitamin C retention in dried orange slices.	[35]
Rectangular aluminium cavity filled with 60 kg of paraffin wax		PCM reached 56 °C at melting and up to 75 to 90 °C at full charge,70% of absorbed power stored at noon, delivered nearly constant night-time	[36]

		heat flux, outlet air temperature remained 3to 7 °C higher and stable at 34 to 35 °C throughout the night	
Packed bed of spherical capsules filled with paraffin wax		The system stored up to 45 % of incident solar energy during the day, delivered a nearly uniform heat flux for 11 h at night, maintaining outlet air 17°C after sunset. Daily energy efficiency of 32to 45 %, daily exergy efficiency: 22 %. Compared with a commercial flat plate SAH	[37]
Cylindrical PCM capsules (40 units) arranged along the bottom plate of the collector.		Numerical results showed that combining fins and PCM gave the highest outlet temperature and energy efficiency. At 1000 W/m² and 0.09 kg/s, energy efficiency reached 66.5 % (fins+PCM) vs 64.6 % (fins only), 59.1 % (PCM only), and 60.7 % (conventional). Exergy efficiency improved up to 48 % relative to conventional DPSAH	[38]

I.5 Hybrid SAH configurations incorporating auxiliary heating and thermal storage

Although the integration of TSUs can effectively extend the operating period of SAHs without additional energy consumption, thereby maintaining a fully renewable mode of operation, the extra discharge duration typically achieved remains relatively limited. In most reported systems, the incorporation of latent or sensible storage increases operating hours by only 20 to 30% beyond periods of available solar radiation [6], which is often insufficient for applications requiring long and continuous operation, such as agricultural drying or space heating. This limitation has motivated researchers and practitioners to incorporate auxiliary heaters into SAH systems, powered by electricity or by conventional energy sources such as

natural gas or biomass. Such configurations are commonly referred to as hybrid SAHs (HSAHs).

Koşan [39] examined a DPSAH configuration in which an infrared heating film was installed in the lower air channel to ensure that the outlet temperature remained above 45 °C for sustainable drying applications (Figure I.15), specifically for grape pomace, even under varying levels of solar radiation. The hybrid system achieved thermal efficiencies between 45.63% and 76.4%, with energy supplied 69% by solar radiation and 31% by electric power. Heydari [40] conducted experimental tests on a hybrid spiral SAH under low solar radiation, with the heating element located at the collector's outlet. The results indicated that the spiral flow channel significantly improves heat transfer between the absorber and the airflow, achieving energy efficiency between 34.1 % and 58.5 %.



Figure I.15. *Photograph and schematic of DPSAH integrated with infrared film [39].*

Kalita et al. [6] investigated the performance of two hybrid-mode solar dryers incorporating different auxiliary heating systems: one powered by electricity and the other by biogas, as shown in Figure I.16. The study focused on comparing drying time, thermal performance, and overall energy consumption between the two configurations. The results revealed that the biogas assisted dryer achieved approximately 6 % higher efficiency than the electrically powered system. However, reduced biogas availability during winter constrains the system's performance and limits its sustainability in colder months.

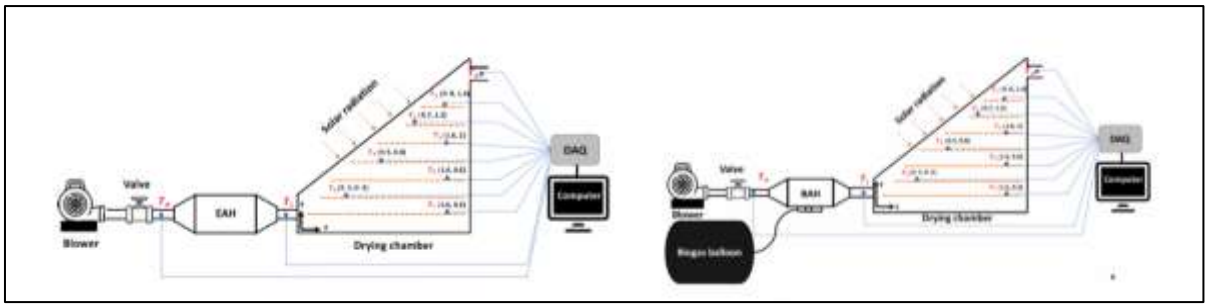


Figure I.16. *Schematic of electric and biogas hybrid-mode solar dryers [6]*

Nwakuba et al. [41] performed an experimental analysis of a HSAH in which an electric resistance wire was installed near the outlet to serve as an auxiliary heat source Figure I.17. The results indicated that the collector achieved thermal efficiencies between 15.67% and 38.17%. Additionally, the auxiliary electric heater supplied roughly 43.76% of the overall energy input, highlighting its substantial role in maintaining the desired temperature when solar radiation was insufficient.

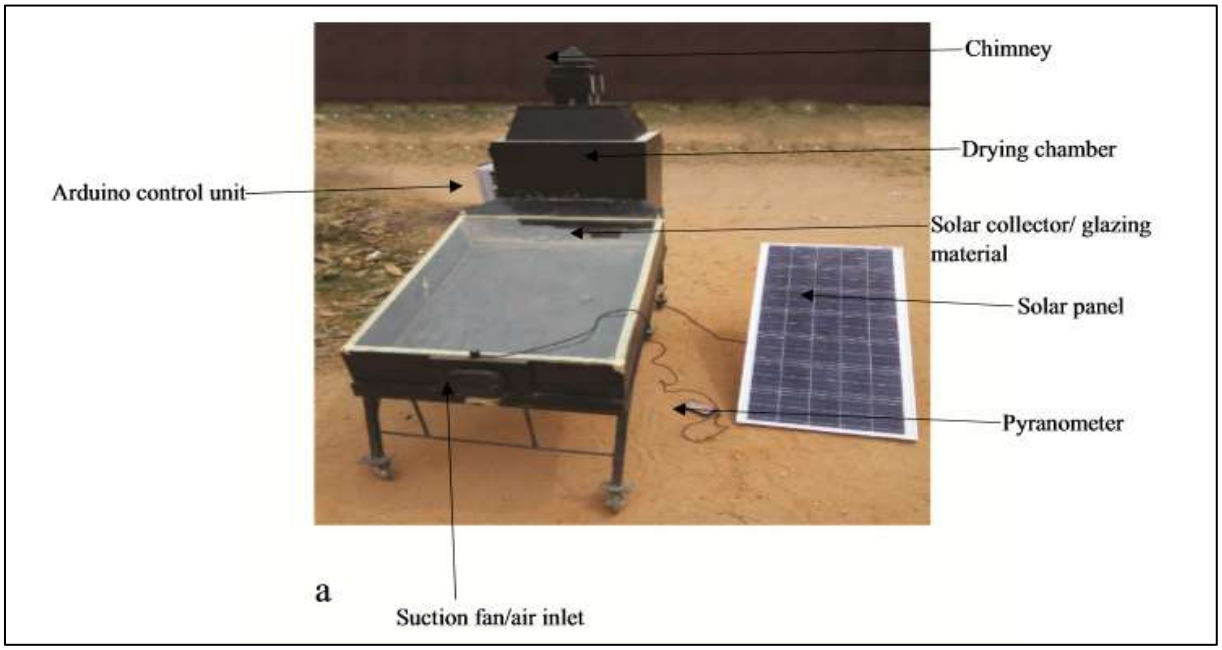


Figure I.17. *Pictorial view of the HSED with PV panel [41]*

To minimize the high energy consumption of the auxiliary heater during operation, which directly impacts the operating cost, integrating a TSU as a renewable energy source

with hybrid HSAHs is an effective strategy, demonstrating the optimization of SAH performance while simultaneously reducing operational costs, as discussed in the following studies:

Singh et al. [42] carried out experimental tests on a recycled HSAH incorporating a TSU in the form of a wavy PCM container (Figure I.18), along with an auxiliary electric heater to ensure stable thermal output during intermittent solar radiation. The system attained a peak thermal efficiency of 52% and successfully maintained the outlet air temperature above 40 °C.

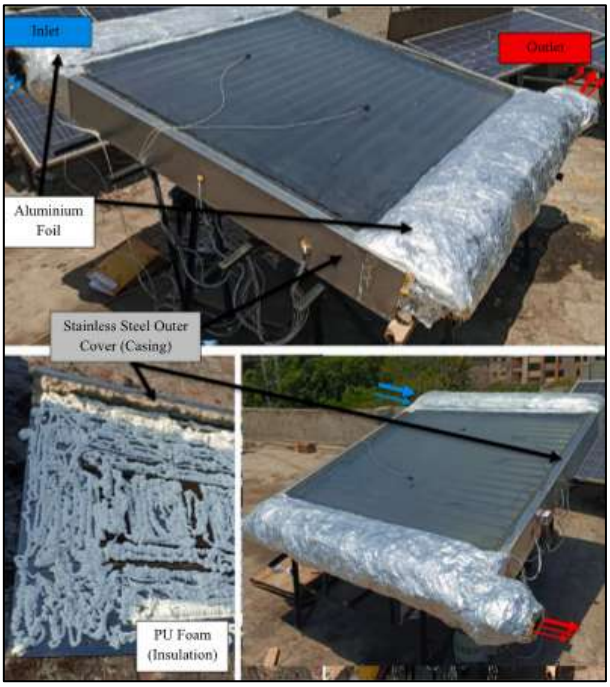


Figure I.18. *Experimental configuration of the recycled HSAH [42]*

Hassan et al.[43] conducted both experimental and thermodynamic analyses of a hybrid V-groove DPSAH coupled with a drying chamber and a TSU, as shown in Figure I.19. The system achieved a thermal efficiency of 88.8% at a mass flow rate of 0.051 kg/s, reducing specific energy consumption by 53.8% compared to conventional electric dryers, demonstrating its economic viability with an energy payback period of 0.78 years.

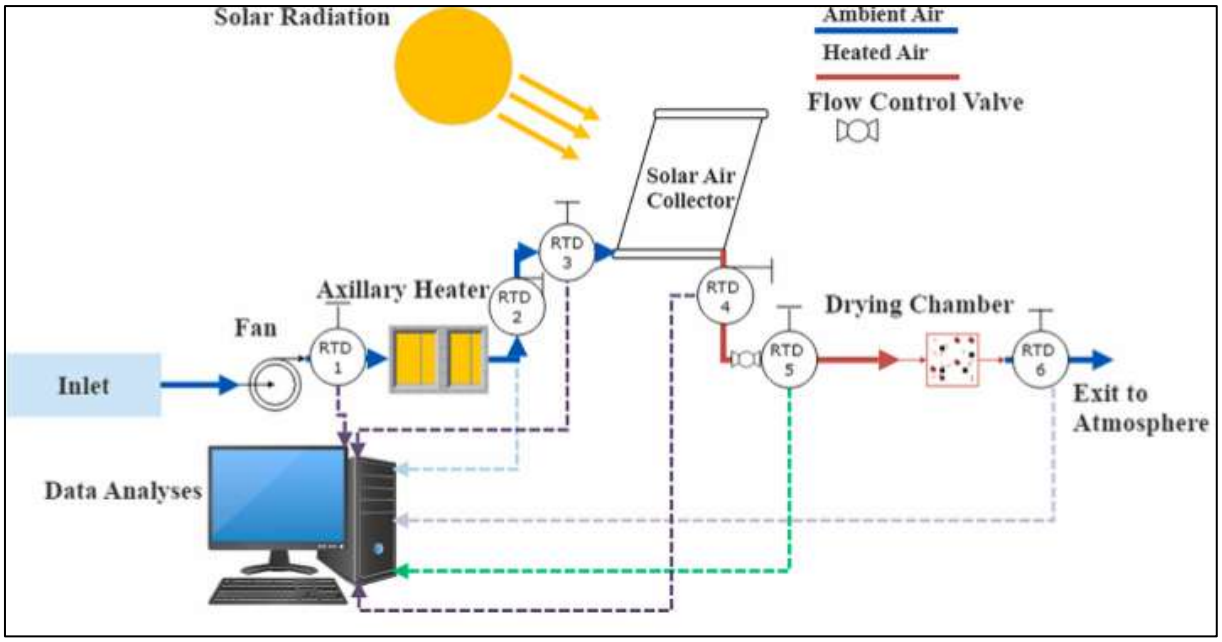


***Figure I.19**. Experimental setup used by Hassan et al. [43]*

Habibi et al. [44] carried out a comparative analysis of three solar dryer configurations: solar electric drying (SED), intermittent solar electric drying (ISED), and intermittent solar electric drying with a sensible heat storage medium (ISEDS), as illustrated in Figure I.20. The study evaluated the systems in terms of thermal performance and product quality. The results indicated that the ISEDS system reduced drying time by approximately 2 h compared to ISED while maintaining product quality. Furthermore, it demonstrated a short payback period of 0.70 years and annual cost savings of 16,203.7 CNY. Exergy efficiency and sustainability index metrics also favored intermittent drying, with ISEDS exhibiting the highest overall performance.

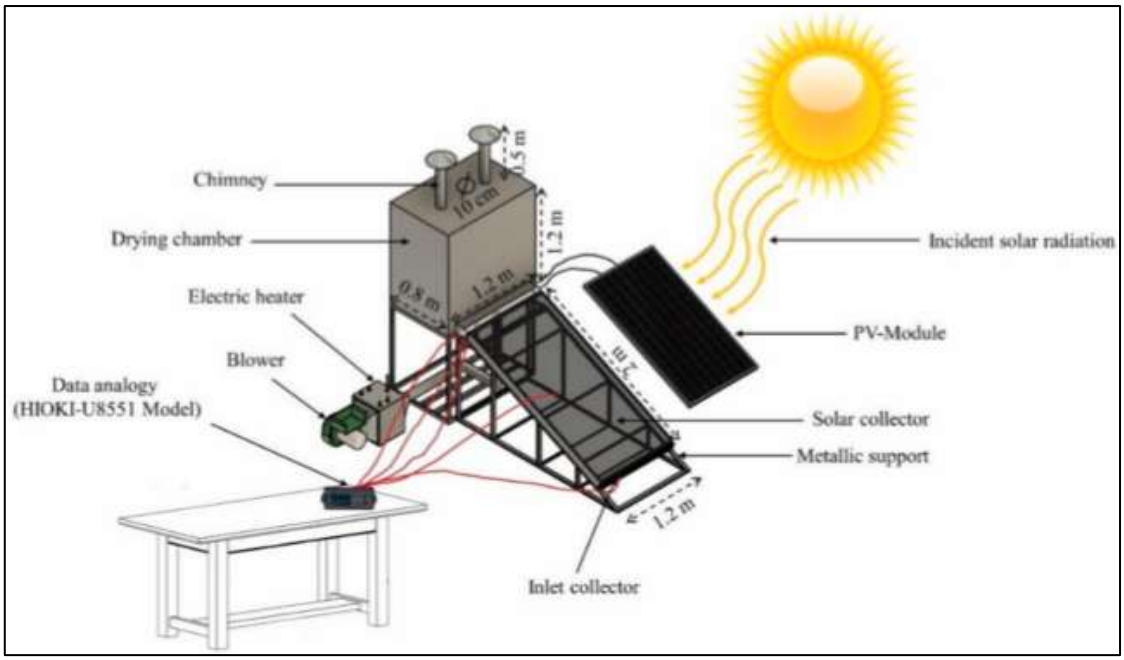


Figure I.20. *Schematic representation of the solar electric dryer applied to SED, ISED, and ISEDS techniques [44]*

I.6 Discussion and research gaps

From the literature reviewed, it is evident that the enhancement of SAHs and HSAHs has been widely pursued through multiple approaches, including the use of extended surfaces, modified absorber geometries, various types of baffles and fins, and the integration of different thermal storage materials and auxiliary heaters. Most existing studies have focused primarily on improving thermal performance, either by comparing modified designs with conventional systems or by examining the influence of operating parameters on the same configuration. However, several research gaps remain.

First, only limited attention has been given to the optimization of fundamental design parameters, such as the selection of air gap distances between the absorber and the glass cover or between the absorber and the bottom plate, despite their critical influence on thermal losses and overall performance. These parameters are essential for practitioners and system designers, yet systematic guidelines are largely absent from the literature.

Second, there is a lack of clear strategies for ensuring fully renewable and sustainable operation, particularly in HSAHs that continue to rely on auxiliary heaters powered by conventional energy sources.

Third, further investigation is required to establish effective techniques for controlling and regulating outlet-air temperature, especially in applications where temperature stability is crucial, such as agricultural drying and space heating, where fluctuations can significantly affect product quality or thermal comfort.

Finally, although the individual roles of fins, PCMs, and auxiliary heaters have been well documented, there remains a notable shortage of research that examines the system-level interactions among these components when integrated into an HSAH. Understanding these interactions is essential for developing optimized, high-performance, and reliable solar air heating systems.

Chapter II: Experimental procedures

II.1 Introduction

To address the research gaps identified in the previous chapter, the present experimental study focuses on the development of a novel hybrid DPSAH (HDPSAH) integrating a latent heat thermal storage unit (LHTSU), intended for space heating and drying applications. Wherein the experimental investigation was structured into three successive phases. The first phase aimed to analyze the influence of varying the air gap distance on the thermal performance of the DPSAH and to determine the optimal configuration to serve as a baseline for subsequent enhancements. The second phase examined the effect of incorporating the LHTSU on temperature regulation and thermal stabilization of the HDPSAH under real operating conditions. Finally, the third phase investigated additional performance improvements through the integration of newly designed wavy fins and the evaluation of the most effective position for the auxiliary heater to ensure optimal energy utilization.

II.2 Phase 1: Selection of the optimal air gap for DPSAH

As an initial experimental step, the study focused on a parametric evaluation aimed specifically at determining the optimal distance (air gap) between the absorber plate and the glass cover of the baseline DPSAH, based on both thermal and exergetic performance criteria, where this phase of the work was conducted in collaboration with a Master's student as part of their thesis work [45].

II.2.1 Experimental procedures followed in the first phase

The DPSAH used in this study consists of two air passages, in which air is drawn from the lower channel using an electric fan controlled by a DC power controller, with part of the heat recovered in this channel before the air exits through the upper passage as hot air. The collector was fabricated from a rectangular duct made of 19 mm-thick plywood, with overall dimensions of 1335 mm × 636 mm × 180 mm. The upper surface was covered with 6 mm

thick ordinary glass, while a flat absorber plate made of a 1.6 mm thick sheet, coated and painted black, was installed, as presented in Figure II.1.

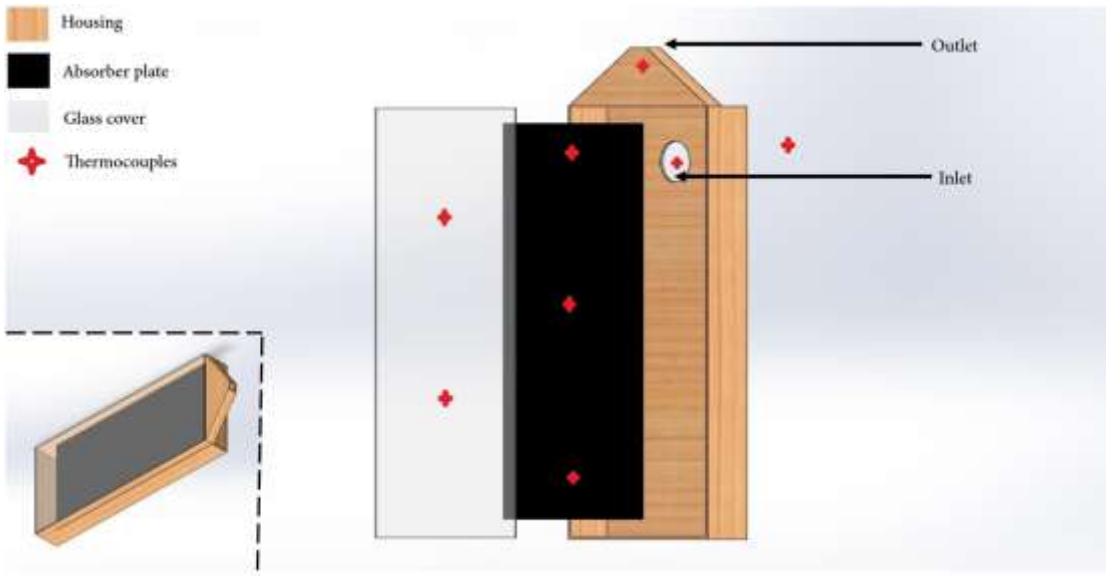
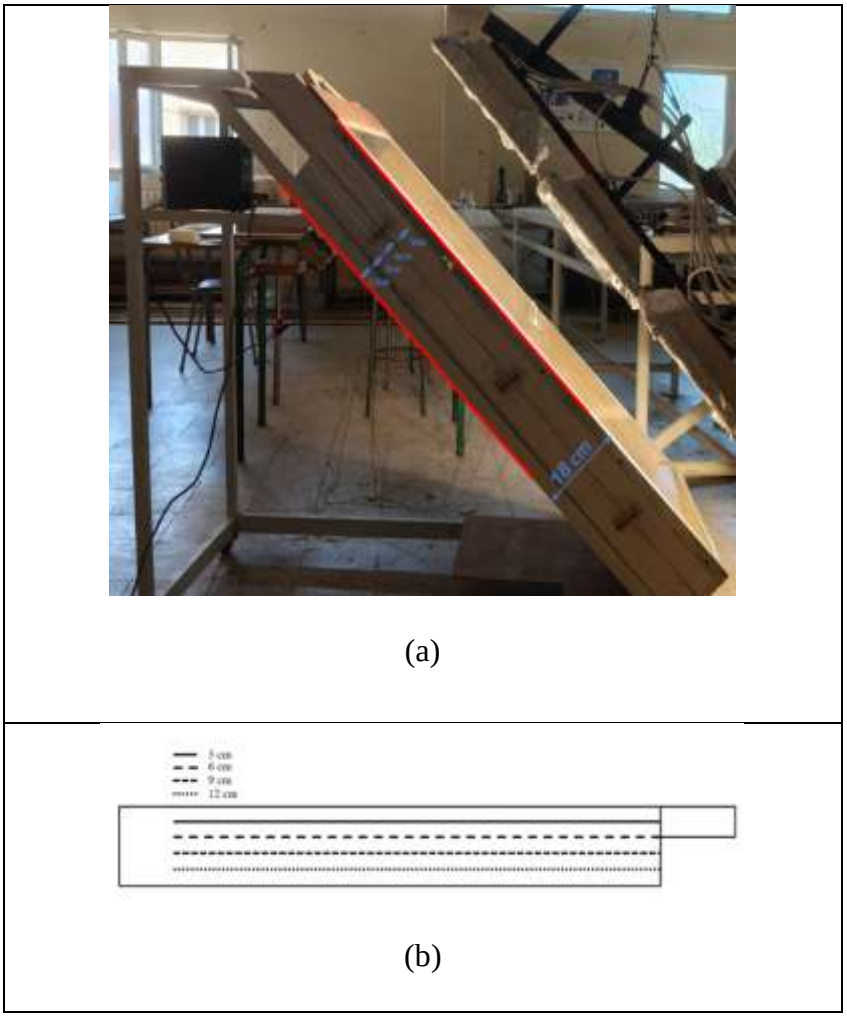


Figure II.1. *Schematic representation of the DPSAH structure.*

To select the optimal configuration, the gap between the absorber and the glass cover was adjusted to 3, 6, 9, and 12 cm, with tests conducted under controlled laboratory conditions using an artificial solar simulator equipped with 12 halogen lamps, each rated at 100 W, mounted perpendicularly at a distance of 300 mm from the glass cover, which effectively simulated solar radiation, as depicted in Figure II.2 (a-b). The radiation was adjusted to approximately 270 W/m², with the average airflow rate maintained at 0.006 kg/s, while temperature data from the thermocouples were recorded every 2 seconds using a data acquisition unit (DAQ9174) connected to LabVIEW software. For clarity and visualization, the experiments were concluded once all measured temperatures, including the inlet and outlet air, absorber, and glass, reached a steady state.



(a)

(b)

Figure II.2. *Schematic representation of the DPSAH structure, (b) sectional view*

II.3 Phase 2: Integration of the LHTSU into the HDPSAH

After completing the indoor experiments and identifying the optimal configuration, the second phase involved further development of the HDPSAH with the objective of achieving stable and well-regulated outlet air temperature, this was accomplished by integrating an auxiliary electric resistance heater equipped with fins (finned heater), consisting of two heating elements fitted with 35 aluminum fins with a maximum power of 756 W, as illustrated in Figure II.3. The auxiliary heater was strategically installed at the airflow U-turn based on fluid dynamic principles, indicating that this region is characterized by recirculation zones and vortex formation, as reported by the numerical study of Elakrout et al. [14] (Figure II.4), which promotes enhanced air mixing and improves convective heat transfer.



Figure II.3. Photograph of the auxiliary finned electric heater.

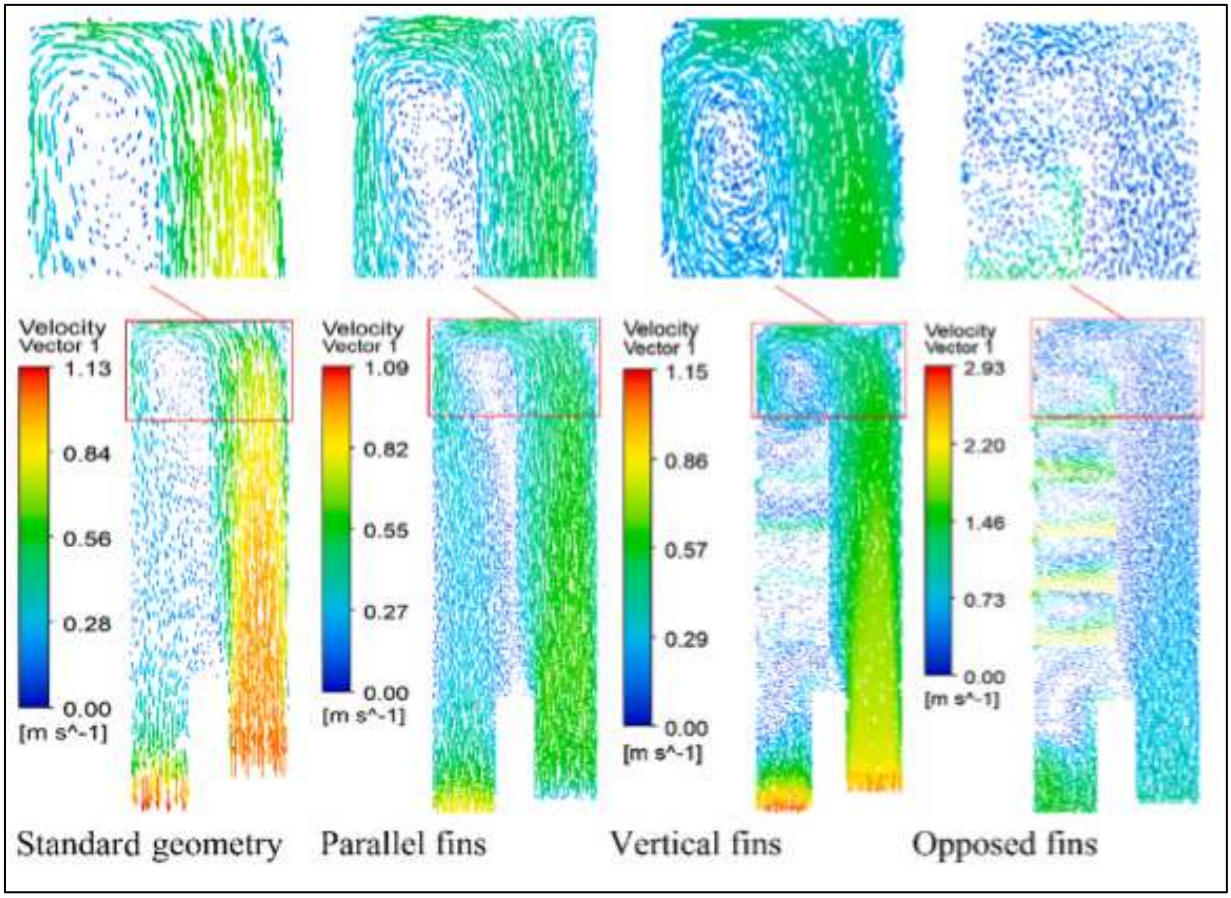


Figure II.4. *Velocity-field visualization in the YZ plane for different DPSAH configurations developed by Elakrout et al. [14]*

To further enhance thermal regulation, an LHTSU was incorporated in the form of a heat exchanger filled with paraffin wax (0.730 kg) and placed in the outlet section of the collector (Figure II.5). This part of the system was also insulated with a 20 mm layer of glass wool to minimize thermal losses. Paraffin wax was selected as the PCM in this study due to

its appropriate melting temperature of 55.68 °C, which matches the target operational temperature range of the system. The thermophysical properties of the paraffin wax used are summarized in Table II.1, while a schematic representation of the developed HDPSAH is presented in Figure II.6.

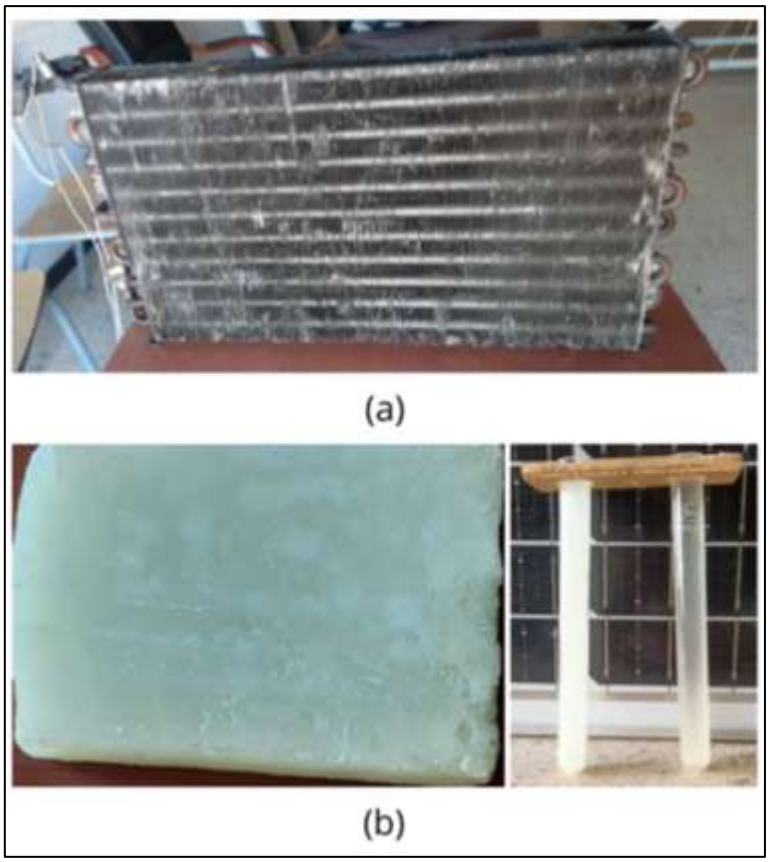
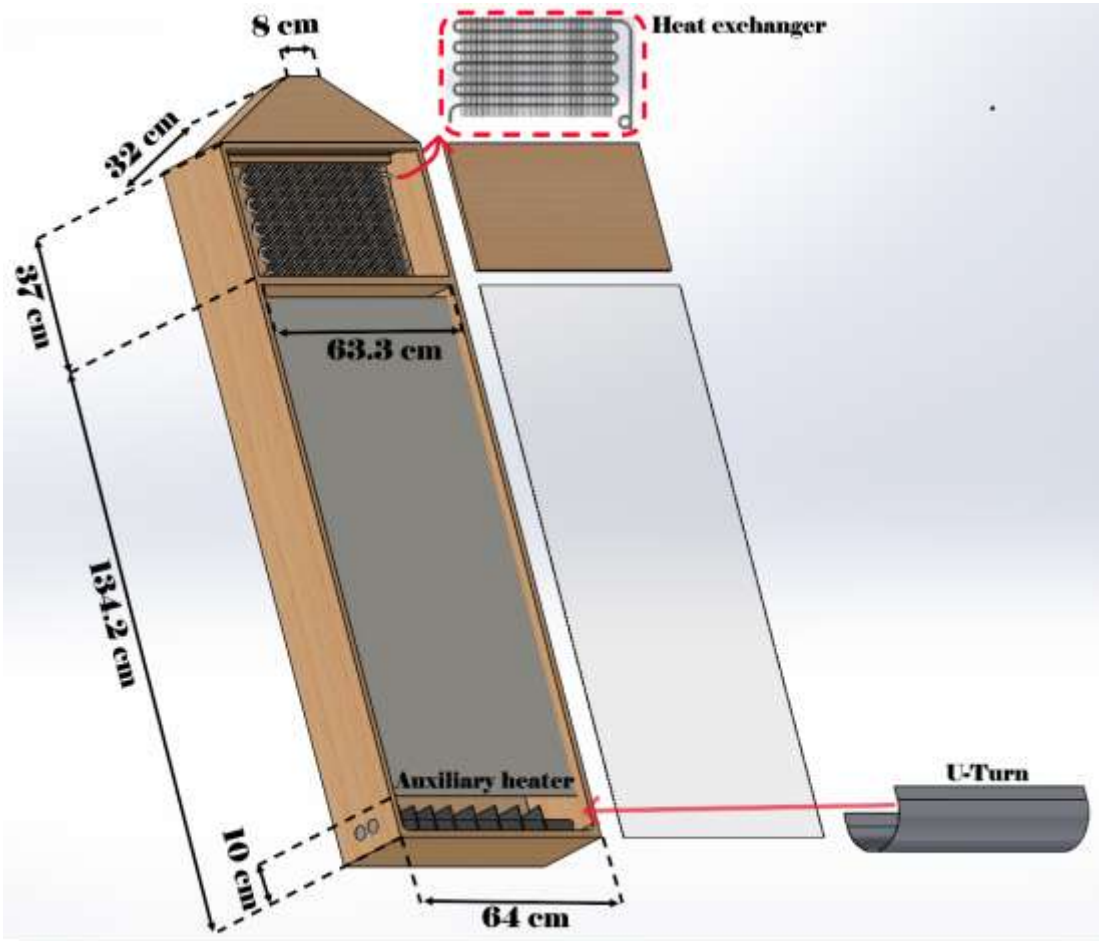


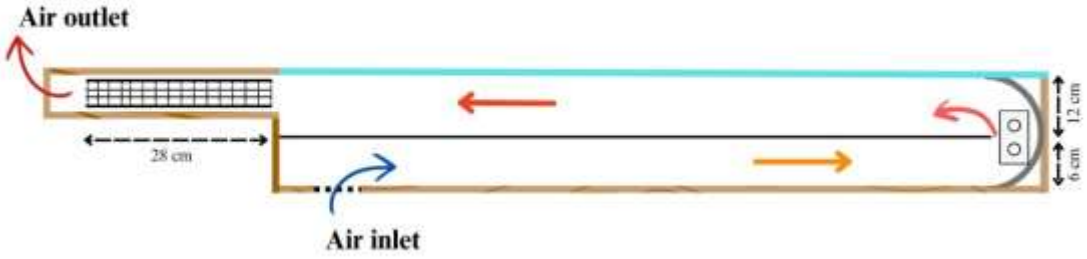
Figure II.5. *(a) Heat exchanger, (b) Paraffin wax shown in solid and liquid states.*

Table II.1. *Thermophysical properties of paraffin wax [35]*

Parameter	Value
Melting temperature	55.68 °C
Latent heat	98185.80 J/ kg
Specific heat capacity	2341.66 J/kg K
Thermal conductivity	0.40 W/ m K
Density	919.73 kg/ m



(a)



(b)

Figure II.6. *(a) Schematic representation of the HDPSAH, (b) Sectional view*

II.3.1 Experimental procedures followed in the second phase

To ensure a stable and regulated outlet air temperature of 55 °C under varying climatic conditions, experimental tests were conducted over three consecutive days at the experimental field of the University of Tlemcen, Algeria (34.920533° N, 1.301264° W) during the autumn

season. These repeated tests were performed to verify the system's reliability and reproducibility, with data from November 24, 2024, selected for detailed analysis. The target temperature of 55 °C was chosen as it lies within the recommended range of 50–60 °C for drying and low temperature heating applications [46,47], thereby ensuring efficient operation while preventing thermal degradation of the product. The collector was positioned facing south to maximize solar exposure and tilted at an angle of 45°, corresponding to the local latitude (34.92 ° N) plus 10°, which is suitable for winter and late autumn operation [48] (Figure II.7).



***Figure II.7**. Experimental setup of the HDSAH.*

Meanwhile, the electric finned heater was controlled by a thermostat set at 55 °C, with its temperature sensor installed immediately upstream of the TSU to maintain precise temperature regulation. As illustrated in Figure II.8, the auxiliary heater was automatically activated whenever the measured temperature fell below 55 °C and deactivated when the temperature exceeded this set point, thus ensuring complete charging of the PCM. The experimental procedure was carried out daily from 09:00 h, with the electric heater switched off at 17:00 h, and the overall experiment concluding at 18:30 h.

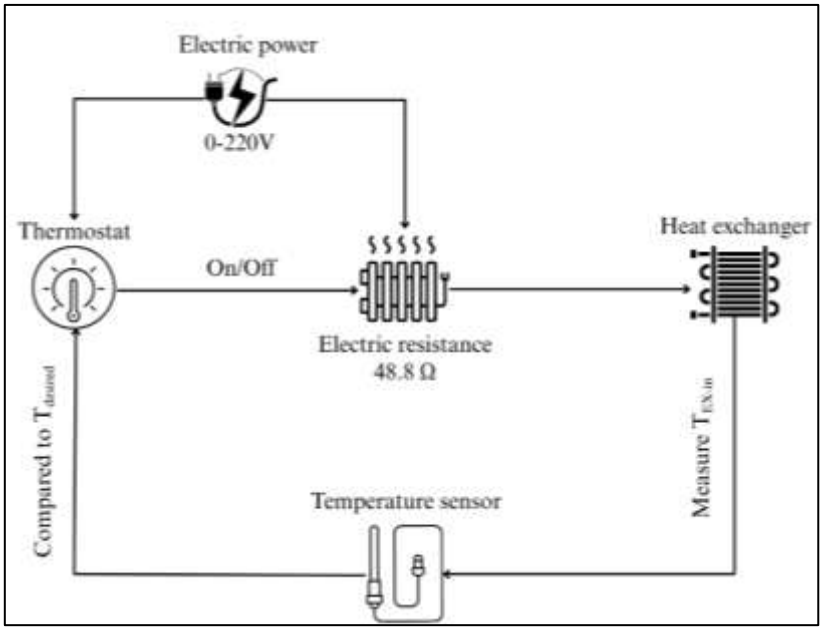


***Figure II.8**. Schematic of the control unit.*

II.4 Phase 3: Integration of the novel wavy fin design and evaluation of auxiliary heater position effects

The third phase of this experimental study focused on optimizing the performance of the HDPSAH system through the integration of five wavy fins, each 100 mm high, mounted at carefully selected angles on the absorber plate and spaced 200 mm apart, as illustrated in Figure II.9. The incorporation of these fins aimed to enhance convective heat transfer and, consequently, improve overall thermal efficiency.

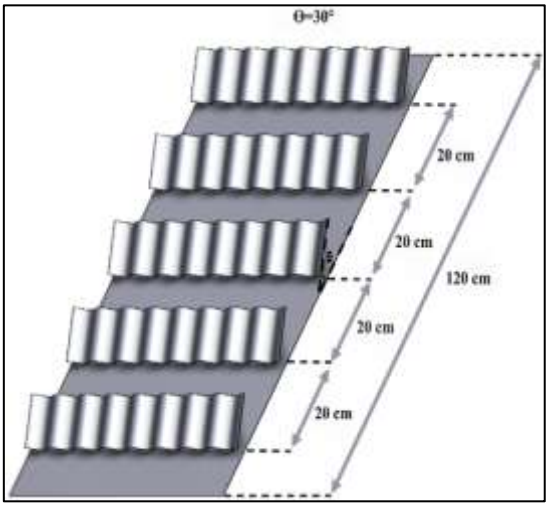


Figure II.9. *Illustrative design of the wavy-fin arrangement*

Moreover, this phase also included an analysis of the influence of the auxiliary heater position, based on experimental testing, by comparing its placement at the U-turn section (position 1) and at the outlet section (position 2). This assessment examined the impact of heater location on electrical energy consumption as well as the overall performance of the system, as shown in Figure II.10.

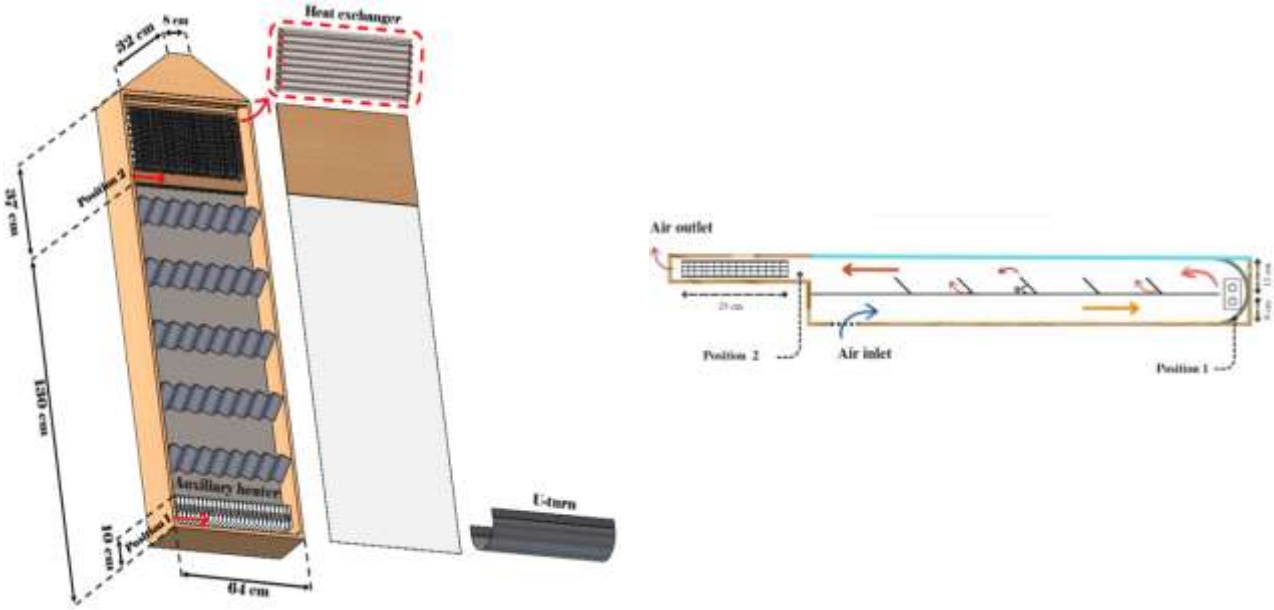


Figure II.10. *Schematic view of the HDPSAH with fins.*

II.4.1 Experimental procedures followed in the third phase

The third phase was carried out in two sequential steps. The first step consisted of preliminary tests conducted under controlled laboratory conditions to identify the optimal fin-inclination configuration in terms of thermal performance, while the second step focused on analyzing the influence of the auxiliary heater position under real outdoor conditions. Figure II.11 provides a detailed schematic of the procedures followed in this phase.

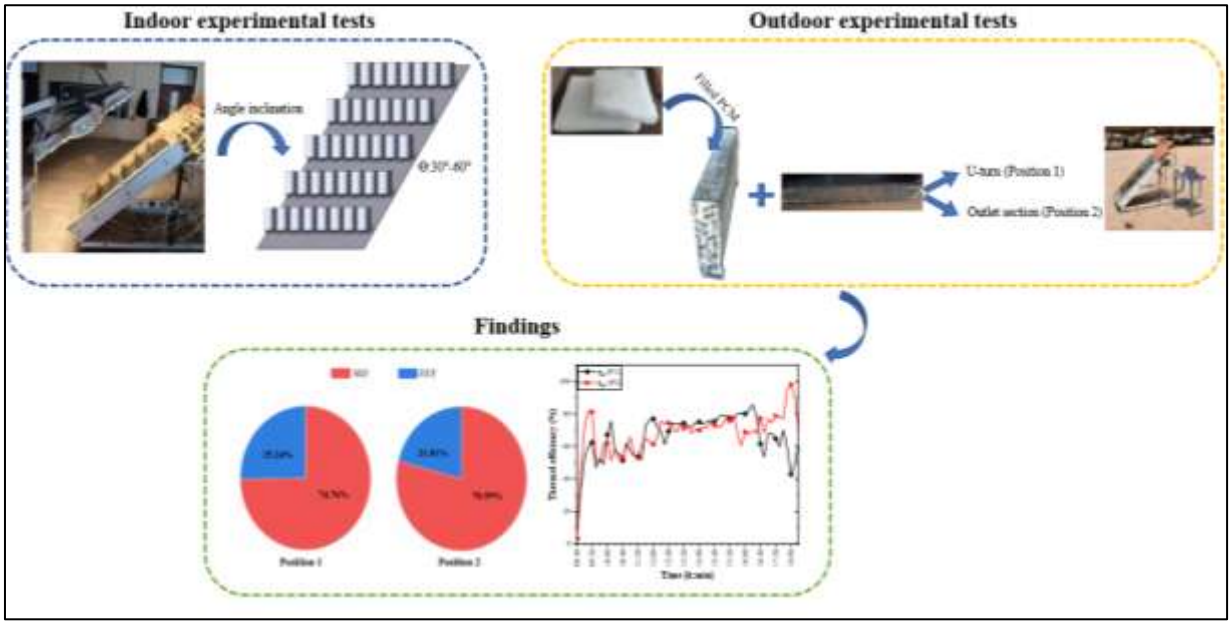
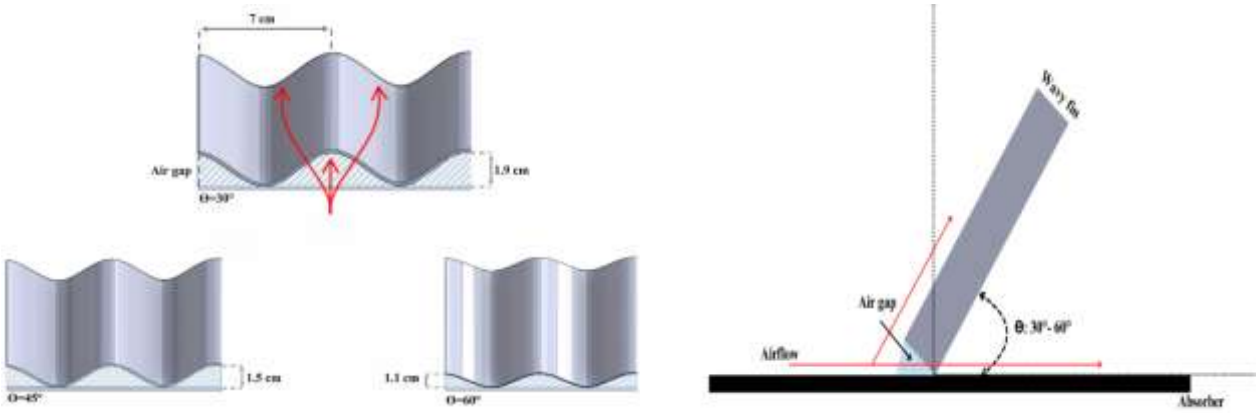


Figure II.11. *Overview of the experimental steps conducted during phase 3.*

II.4.1.1 Indoor experimental tests

The indoor experiments were conducted under controlled laboratory conditions using an artificial solar simulator equipped with halogen lamps, ensuring stable and repeatable operating conditions. The objective of this stage was to identify the most effective fin-inclination angle in terms of thermal performance. Accordingly, three fin inclination angles (30°, 45°, and 60° relative to the absorber plate) were tested and compared against a flat absorber plate, as shown in Figure II.12 (a–b). The solar simulator was positioned perpendicular to the collector at a distance of 400 mm from the glass cover, with the intensity set to 500

W/m², as illustrated in Figure II.13. During these indoor tests, both the LHTSU and the auxiliary heater were intentionally excluded to isolate the effect of fin inclination.



(a) (b)

Figure II.12. *(a-b) Illustration of fin arrangements at different inclination angles (30°, 45°, and 60°)*



Figure II.13. *Laboratory setup*

II.4.1.2 Outdoor experimental tests

In the outdoor experiments, the objective remained consistent with that of Phase 2, which was to maintain a stable outlet-air temperature under variable climatic conditions. In this phase, the focus shifted to examining the influence of the auxiliary heater position on the performance of the HDPSAH. The auxiliary heater was installed first in Position 1 and then in Position 2, with each configuration tested on a separate day under comparable operating conditions during the spring period from April 15 to 28, 2025, as shown in Figure II.14. The control strategy, including thermostat operation, was kept identical to that used in Phase 2. The experiments were conducted daily from 08:40 to 19:40, with the auxiliary heater automatically switching off around 18:20 due to the extended daylight duration characteristic of the spring season.



Figure II.14. *Experimental setup for outdoor testing*

II.5 Experimental measurements and uncertainty evaluation

Before conducting any experimental tests, all measuring devices were inspected and calibrated to ensure the reliability and accuracy of the recorded data. Solar irradiance was measured using SOLAR-100, while ambient wind speed and relative humidity were obtained from a professional AERCUS weather station installed near the test platform.

Airflow characteristics, including air velocity and mass flow rate, were measured using a 6190SI thermo-anemometer. Temperature measurements were performed using K-type thermocouples positioned at well-defined locations of the collector, including the absorber plate, glass cover, inlet and outlet sections, the auxiliary heater, and the TSU. All thermocou-

ple signals were recorded continuously through a DAQ9174 data acquisition module connected to a LabVIEW interface, enabling real-time visualization and storage of temperature data.

During the experimental tests of Phases 2 and 3, the electrical voltage supplied to the auxiliary heater was measured using a Uni-T UT588 digital multimeter, and an electronic balance was also used during the preparation of the paraffin-wax PCM. Table II.2 presents details of the instruments used.

Table II.2. *Instruments used for measurements*

Devices	Accuracy	Image
Solar irradiance meter (SOLAR-100)	±5%	
Data Acquisition System	50 ppm of sample rate	
Thermo-anemometer (6190SI)	±5%	
Power Supply controller (KPS305D)	±0.1%	
Thermocouple type (K)	±0.25 °C	
AERCUS weather station	±5%	

Multimeter (Uni-T UT588)	±0.5%	
Inclined liquid column manometer	±2%	

Figure II.15 shows the LabVIEW interface used for real-time monitoring and recording of experimental data, providing visualization of temperatures, operational parameters, and other measurements. It enables the simultaneous display of multiple signals, data storage for post-processing, and precise control over measurement intervals, ensuring accurate and reliable data collection.

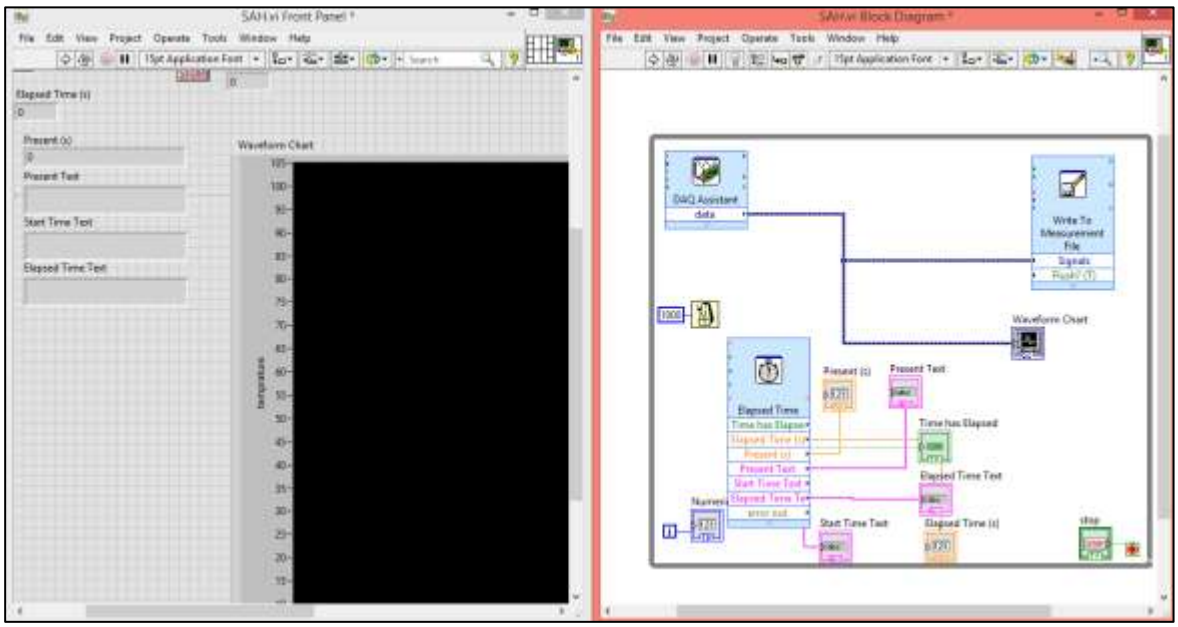


Figure II.15. *LabVIEW Interface with block diagram*

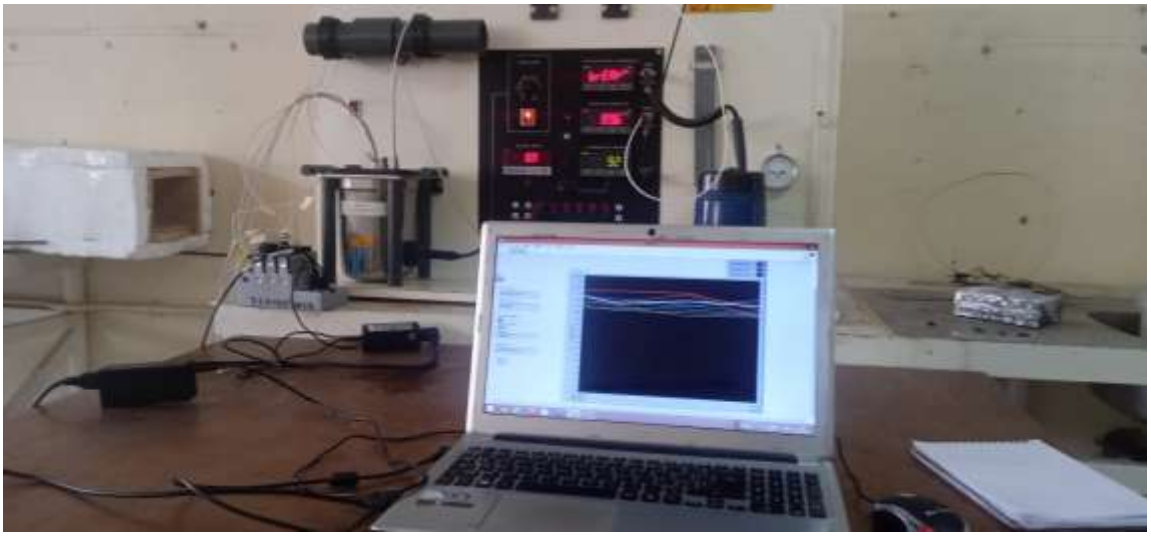
II.5.1 Thermocouple calibration procedure and measurement performance evaluation

To ensure reliable temperature measurements and to select the most suitable thermocouples for the experimental setup, a systematic calibration procedure was adopted. Measurement errors were minimized by using thermocouples of identical quality and sourced from the same manufacturer, which reduces variability related to material composition and fabrication tolerances. The existing Type K thermocouples were calibrated by comparison with a high-accuracy reference thermocouple. A Type T Testo AQ606 thermocouple, recognized for its measurement stability and precision, was used as the calibration reference (Figure II.16 (a)). This comparative calibration approach is widely recommended for improving measurement accuracy in thermal experiments. The calibration was carried out by simultaneously immersing both the test thermocouples and the reference thermocouple in a controlled hot-water bath within the experimental test bench, as illustrated in Figure II.16 (b). The water temperature was allowed to vary gradually, enabling continuous monitoring of the temperature response of each sensor.

The recorded temperature evolution was then analysed to assess and compare the thermocouples' measurement accuracy, response time, and overall reliability. This comparative analysis enabled the identification of the thermocouples exhibiting the most consistent and accurate behavior, which were subsequently selected for use in the experimental measurements.



(a)



(b)

Figure II.16. *Photograph of the calibration setup: (a) reference sensor; (b) experimental test bench.*

The measurement uncertainties were assessed following Eq. (1) [49]:

$$W_R = \left[\left(\frac{\partial R}{\partial x_1} W_1 \right)^2 + \left(\frac{\partial R}{\partial x_2} W_2 \right)^2 + \ldots + \left(\frac{\partial R}{\partial x_n} W_n \right)^2 \right]^{1/2} \quad (1)$$

In this formulation, R denotes the dependent variable, $x_1, x_2, \ldots, x_n$ represent the independent the independent variables, and W corresponds to the uncertainty associated with the depend-

ent variable. The combined measurement uncertainty is then obtained using the following relation:

Temperature:

$$W_T = \left[\left(W_{thermocouple}\right)^2 + \left(W_{connection}\right)^2 + \left(W_{reading}\right)^2 \right]^{1/2} \quad (2)$$

Irradiation:

$$W_I = \left[\left(W_{solarmetre}\right)^2 + \left(W_{reading}\right)^2 \right]^{1/2} \quad (3)$$

Velocity:

$$W_v = \left[\left(W_{anemometer}\right)^2 + \left(W_{reading}\right)^2 \right]^{1/2} \quad (4)$$

Voltage:

$$W_u = \left[\left(W_{multimeter}\right)^2 + \left(W_{reading}\right)^2 \right]^{1/2} \quad (5)$$

The relative uncertainty of the mass flow rate can be written as:

$$\frac{W_{\dot{m}}}{\dot{m}} = \left[\left(\frac{W_v}{v} \right)^2 \right]^{1/2} \quad (6)$$

The relative uncertainty of the useful heat can be written as:

$$\frac{W_{Q_u}}{Q_u} = \left[\left(\frac{W_{\dot{m}}}{\dot{m}} \right)^2 + \left(\frac{W_T}{T} \right)^2 \right]^{1/2} \quad (7)$$

The relative uncertainty of the input solar radiation can be written as:

$$\frac{W_{Q_s}}{Q_s} = \left[\left(\frac{W_I}{I} \right)^2 + \left(\frac{W_{A_{abs}}}{A_{abs}} \right)^2 \right]^{1/2} \quad (8)$$

The relative uncertainty of the thermal efficiency can be expressed as:

$$\frac{W_{\eta_{th}}}{\eta_{th}} = \left[\left(\frac{W_{Q_u}}{Q_u} \right)^2 + \left(\frac{W_{Q_s}}{Q_s} \right)^2 + \left(\frac{W_P}{P} \right)^2 \right]^{1/2} \quad (9)$$

II.6 Data analysis

II.6.1 Analysis of energy performance

The useful thermal energy delivered by the system is calculated according to Eq. (10).

$$Q_u = \dot{m} C_{p,f} (T_{out} - T_{in}) \quad (10)$$

Based on the useful heat gain, the thermal efficiency is evaluated as follows:

$$\eta_{th} = \frac{Q_u}{IA_{abs} + P_{fan} + P_{el}} \quad (11)$$

Where P_{el} denotes the electrical power consumed by the auxiliary heater during phases 2 and 3. When the auxiliary heater is deactivated or excluded, the term P_{el} is eliminated.

During phases 2 and 3, the HDPSAH system operates using three distinct energy sources: solar thermal energy (E_s), electrical energy (E_{el}) consumed by the auxiliary heater and the electric fan, and thermal storage energy (E_{ts}) released from the storage medium. Accordingly, the total energy input to the system can be expressed as:

$$E_{total} = E_s + E_{el} \quad (12)$$

$$E_s = IA_{abs}.t_s \quad ; \quad E_{el} = P_{fan} t_{fan} + P_{el} t_r \quad (13)$$

Here, t_s, t_{fan}, t_r correspond to the time periods (in hours) associated with solar radiation, fan operation, and auxiliary heater activity, respectively. According to Eq. (13), the solar energy fraction (SEF) and the electric energy fraction (EEF) can be expressed as [44]:

$$SEF = E_S / E_{total} \quad ; \quad EEF = E_{el} / E_{total} \quad (14)$$

The top heat loss is calculated using Eq. (15) [18]:

$$Q_{loss} = Q_{conv} + Q_{rad} = Ah_{conv}\left(T_g - T_a\right) + A\sigma\varepsilon_g\left(T_g^4 - T_s^4\right) = Ah_{conv}\left(T_g - T_a\right) + Ah_{rad}\left(T_g - T_a\right) \quad (15)$$

II.6.2 Analysis of exergy performance

Exergy analysis is employed to assess the effectiveness of the HDPSAH in converting thermal energy into useful heat. Based on the second law of thermodynamics, this approach enables the identification and quantification of irreversibility within the system. Accordingly, the exergy balance for the HDPSAH is formulated as follows [22]:

$$\sum \dot{E}x_{in} - \dot{E}x_{out} = \sum \dot{E}x_{dest} \tag{16}$$

Accordingly, the exergy input to the collector can be expressed as follows [40]:

$$\dot{E}x_{in} = I.A_{abs}.\left[1-\frac{4}{3}\frac{T_{amb}}{T_{sun}}+\frac{1}{3}\left(\frac{T_{amb}}{T_{sun}}\right)^{4}\right]+P_{fan}+P_{el} \tag{17}$$

Here, T_{sun} =6000 K [50].

While the exergy gain is expressed by the following equation [18]:

$$\dot{E}x_{out} = \dot{m}C_{p,f}\left[(T_{out}-T_{in})-T_{amb}\ln\left(\frac{T_{out}}{T_{in}}\right)\right] \tag{18}$$

On this basis, the exergy efficiency of the HDPSAH is evaluated as given in [18]:

$$\eta_{ex} = \frac{\dot{E}x_{out}}{\dot{E}x_{in}} \tag{19}$$

II.6.2.1 Sustainability assessment criteria

An understanding of exergy provides a valuable framework for linking energy performance with sustainability considerations, enabling the identification of inefficiencies and the reduction of resource losses and environmental impacts. Within this context, the sustainability index (SI), relative CO_2 reduction potential (RCRP), and improvement potential (IP), are defined as follows [51]:

$$SI = \frac{1}{1-\eta_{ex}} \tag{20}$$

$$RCRP = \frac{\eta th}{1-\psi_R} \tag{21}$$

$$IP = (1-\eta_{ex})\left(\dot{E}x_{in} - \dot{E}x_{out}\right) \tag{22}$$

ψ_R denotes the rational exergy management efficiency, which is defined as follows [51]:

$$\psi_R = \left(\frac{1-\frac{T_{amb}}{T_{out}}}{1-\frac{T_{amb}}{T_{Abs}}}\right) \tag{23}$$

II.6.3 Environmental impact analysis

At both global and national levels, environmental analysis is now widely applied to quantify the environmental impacts of fabricated systems, using metrics such as embodied energy, energy payback time (EPBT), and carbon dioxide emissions. Where embodied energy denotes the cumulative amount of energy consumed during the manufacture or construction of a product, component, or system[52].

The energy payback time (EPBT) indicates the duration, expressed in years, required for the system to offset the energy expended during its manufacturing process, and is defined as follows [49]:

$$EPBT = \frac{Embodied\ energy\ (kWh)}{Annual\ \ thermal\ energy\ output\ (kWh/\ year)} \tag{24}$$

The annual thermal energy output is computed as follows:

$$Annual\ thermal\ energy\ output = Daily\ thermal\ output\ \times N_d \tag{25}$$

N_d corresponds to the total annual number of sunshine days, estimated at 320 days in Algeria [53].

With an average emission factor of 0.98 kg CO_2/kWh for coal-generated electricity, the total annual CO_2 emissions are computed as follows [54]:

$$CO_2 \text{ emission per year} = \frac{Embodied\ energy}{Lifetime} \times \frac{1}{1-L_a} \times \frac{1}{1-L_t} \times 0.98 \quad (26)$$

given that L_a (domestic appliance losses) and L_t (transmission losses).

II.6.4 Economic feasibility analysis

The economic evaluation was conducted by taking into account the specific socioeconomic context of Algeria, including local energy prices and prevailing market conditions. This contextualization ensures that the results of the economic assessment are realistic and representative of the conditions under which the system is expected to operate. The analysis focuses on estimating the key economic parameters of the system, including the investment cost, capital recovery factor (CRF), first annual cost (FAC), annual salvage value, and payback period (PBP). To enhance clarity and transparency, the methodology adopted for the economic assessment is presented through a step-by-step calculation procedure, which can be summarized as follows:

The CRF is calculated using Eq. (26) [18]:

$$CRF = \frac{i(1+i)^n}{(1+i)^n - 1} \quad (27)$$

Here, i denotes the interest rate and n the system lifetime, assumed to be 3[52] and 15 years, respectively.

The First Annual Cost is determined using Eq. (27) [8]:

$$FAC = CRF \times P \tag{28}$$

P is the capital cost

The ASV is determined using Eq. (28) [18]:

$$ASV = SFF \times S \tag{29}$$

in which SFF refers to the sinking fund factor, while S corresponds to the salvage value.

$$SFF = \frac{i}{(1+i)^n - 1} \quad ; \quad S = 0.2 \times P \tag{30}$$

The AMC is assumed 10% of the FAC

where the annual electrical energy cost (Ce) is determined as follows [44]:

$$Ce = E_{el}.Cu.N_d \tag{31}$$

Cu is the unit price of electric energy (5.06 DZD/kWh) [52].

Thus, the total annual cost (TAC) is computed as follows [18]:

$$TAC = FAC + AMC + Ce - ASV \tag{32}$$

The economic cost of useful heat output, expressed per kilowatt-hour (C/kWh) is obtained using the following formulation [8]:

$$C/_{kWh} = \frac{TAC}{annual\ useful\ heat} \tag{33}$$

While the PBP, defined as the minimum time required to recover the initial investment, is calculated as follows [8]:

$$PBP = \frac{TAC}{CUE} \tag{34}$$

CUE denotes the annual cost associated with the useful energy produced by the collector.

II.7 Summary of experimental methodology

This chapter presented the experimental methodology employed to investigate and optimize the performance of the HDPSAH integrated with an LHTSU. The experimental work was structured into three successive phases: the first phase focused on identifying the optimal air gap configuration of the baseline DPSAH under controlled conditions, the second phase examined the integration of an auxiliary electric heater and the LHTSU to enhance temperature regulation and stabilit, and the third phase assessed the influence of auxiliary heater positioning under outdoor operating conditions, together with the integration of a novel wavy-fin design.

The measurement instruments, data acquisition system, and uncertainty analysis were also described to ensure the reliability and accuracy of the experimental data. The experimental procedures and data-processing methods detailed in this chapter provide a solid foundation for the analysis and discussion of the results presented in the subsequent chapter. Figure II.17 illustrates the adopted experimental methodology.

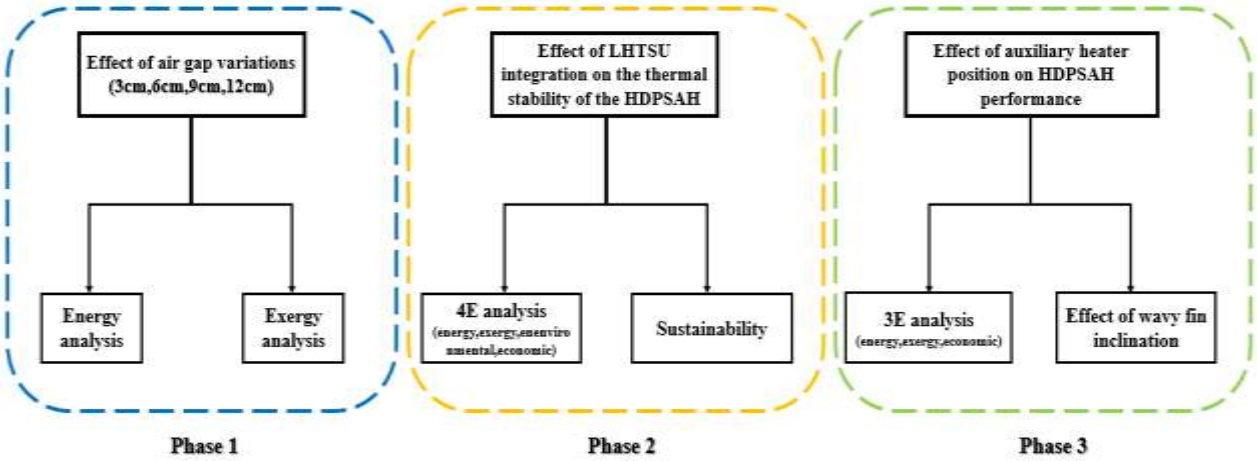


Figure II.17. *Experimental methodology flowchart*

Chapter III: Results and discussion

III.1 Introduction

The HDPSAH system was assessed under different operating conditions, including controlled laboratory conditions and real outdoor environments, through detailed energy, exergy, environmental, and economic analyses. The findings presented in this chapter highlight key thermal behaviors, including the effect of air gap variation on DPSAH performance, the impact of integrating an LHTSU and an auxiliary electric heater on temperature regulation and thermal stability, and the influence of auxiliary heater positioning and wavy-fin integration on the overall system performance.

III.2 Effect of air gap variations on DPSAH Performance

Figure III.1 illustrates the temporal behavior of the absorber and outlet temperatures for the four configurations (3, 6, 9, and 12 cm) under a controlled irradiation of 270 W/m². At the initial stage, when the collector is exposed to uniform irradiation, both the absorber and outlet temperatures in all configurations exhibit a rapid increase. This behavior is primarily attributed to the large temperature gradient between the collector components and the surrounding environment. Subsequently, the temperature rise rate gradually decreases, and the system stabilizes after approximately 2000 s (33 min). A steady-state regime is reached around 4500 s (75 min), indicating that thermal equilibrium has been established throughout all regions of the collector.

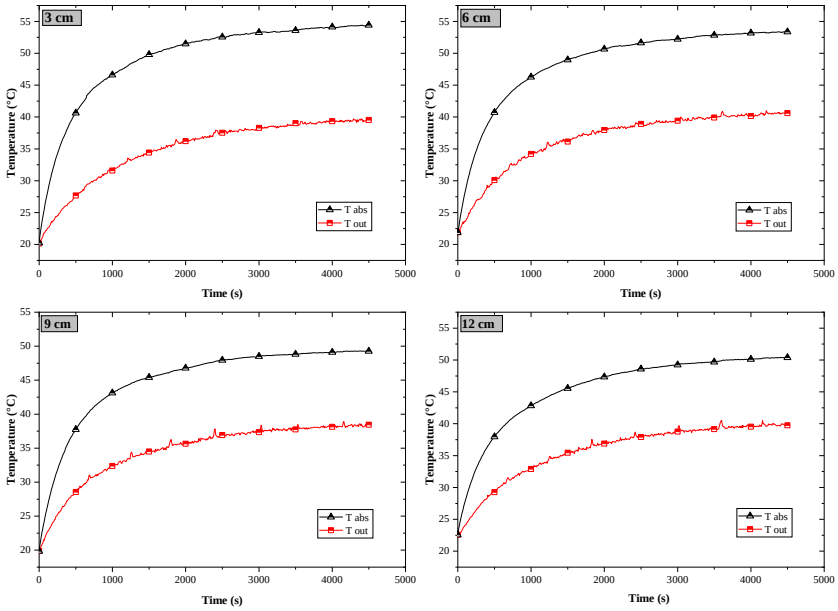


Figure III.1. *Temperature evolution of the absorber and outlet temperatures for 3, 6, 9, and 12 cm Configurations*

As shown in Figure III.2 (a), the thermal efficiency reaches a steady state after approximately 75 minutes, attaining a maximum value of 66.4% for the 12 cm configuration. In comparison, the 9, 6, and 3 cm configurations exhibit reductions in thermal efficiency of 2.4%, 7.8%, and 14.4%, respectively, relative to the optimal configuration. These results indicate that increasing the height of the upper air channel significantly enhances thermal efficiency, owing to improved heat absorption. As illustrated in Figure III.2 (b), the 12 cm configuration delivers the highest useful heat gain, reaching 126.2 W. Furthermore, the present experimental findings are in good agreement with the DPSAH model (7th design) reported by Verma et al. [55], in which a thermal efficiency of approximately 60% was achieved.

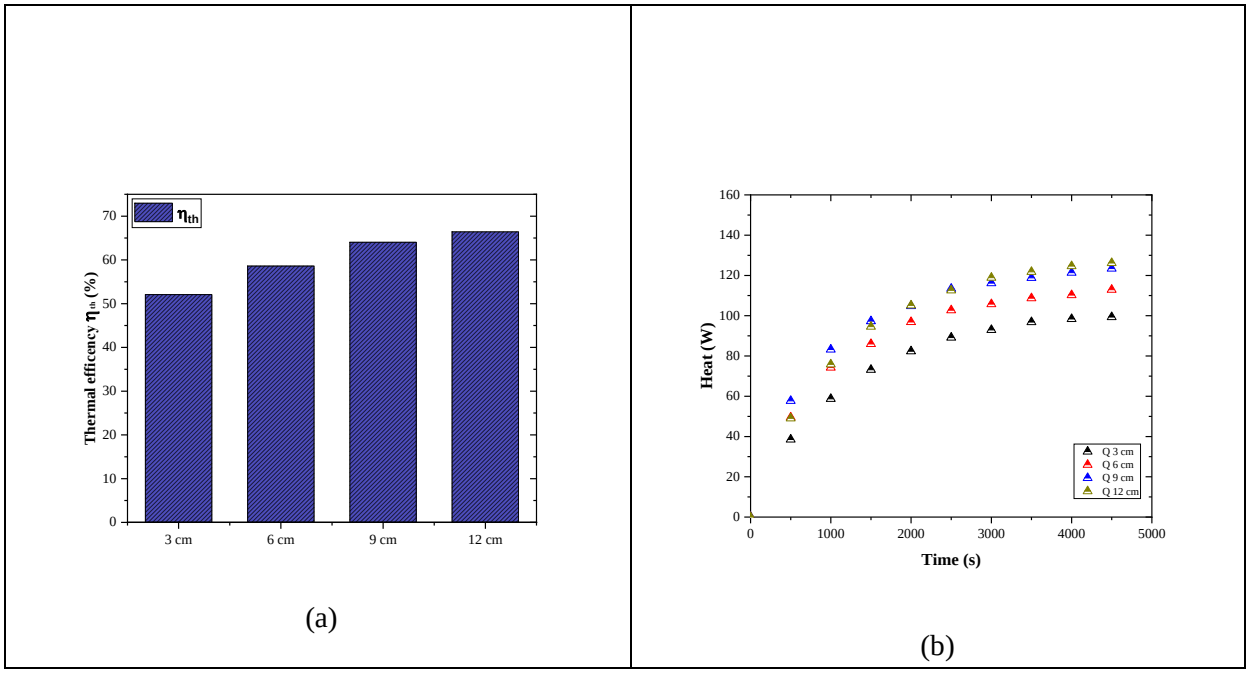


Figure III.2. *Comparison of (a) thermal efficiencies for the 3, 6, 9, and 12 cm configurations and (b) useful heat gain*

In this work, an exergetic assessment is conducted to examine the DPSAH system's capability to convert available thermal energy into useful heat. As illustrated in Figure III.3, the exergy efficiency is evaluated for four different configurations. The lowest exergy efficiency is observed for the 3 cm configuration, at 2.1%. Increasing the height of the upper air channel leads to a gradual enhancement in performance, yielding efficiencies of 2.4%, 2.5%, and 2.6% for the 6, 9, and 12 cm configurations, respectively. This trend is mainly associated with higher exergy destruction occurring at smaller channel heights, particularly in the 3 cm configuration, where irreversibility and thermal losses to the surrounding are more pronounced. The corresponding exergy destruction values are 148.81 W, 148.42 W, 148.29 W, and 148.22 W for the 3, 6, 9, and 12 cm configurations, respectively, which negatively affects the amount of useful heat produced. Overall, the average exergy efficiency across all tested configurations is approximately 2.4%. These findings are in close agreement with the DPSAH model reported by Abo-Elfadl et al. [56], where exergy efficiency values were found to vary

between 1.6% and 3%. Consequently, additional design optimizations are required to further reduce exergy losses and enhance system performance.

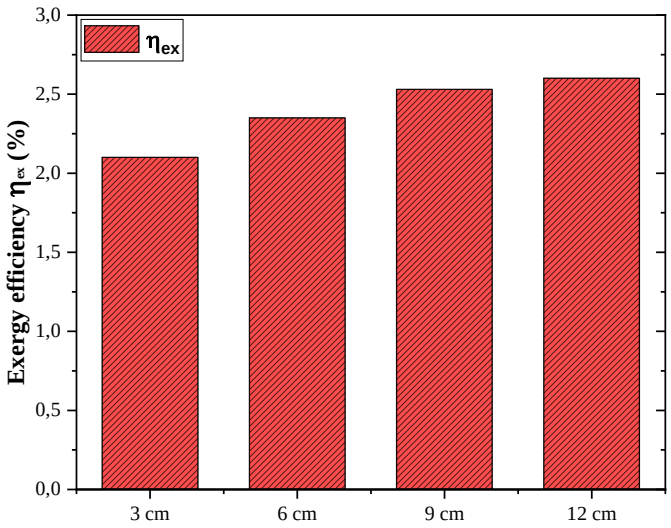


Figure III.3. *Comparison of exergy efficiency for various DPSAH configurations.*

III.3 Effect of LHTSU integration on the thermal stability of the HDPSAH

To ensure continuous operation of the system, an electric finned heater is installed in the U-turn section. In addition, an LHTSU is integrated into the outlet section, as described in the previous chapter. The experimental tests on the HDPSAH were carried out at the University of Tlemcen, Algeria (34.920533° N, 1.301264° W) on 24 November 2024, during the autumn season. The experimental setup was installed at 8:00 a.m, and data collection commenced one hour later. As shown in Figure III.4, the measured solar irradiance during the experimental period ranged from 32 W/m² to a maximum of 1025 W/m², with an average value of 517 W/m². Solar radiation increased gradually during the morning hours, reaching its peak intensity of 1025 W/m² at 13:10, before decreasing in the afternoon. The ambient air temperature varied from a minimum of 17 °C to a maximum of 29.5 °C recorded at 12:30, with a mean value of 24.78 °C. Wind speed, an important parameter in outdoor experiments,

exhibited an average value of 1.5 m/s, which is consistent with ASHRAE recommendations indicating that wind velocity should not exceed 4.5 m/s.

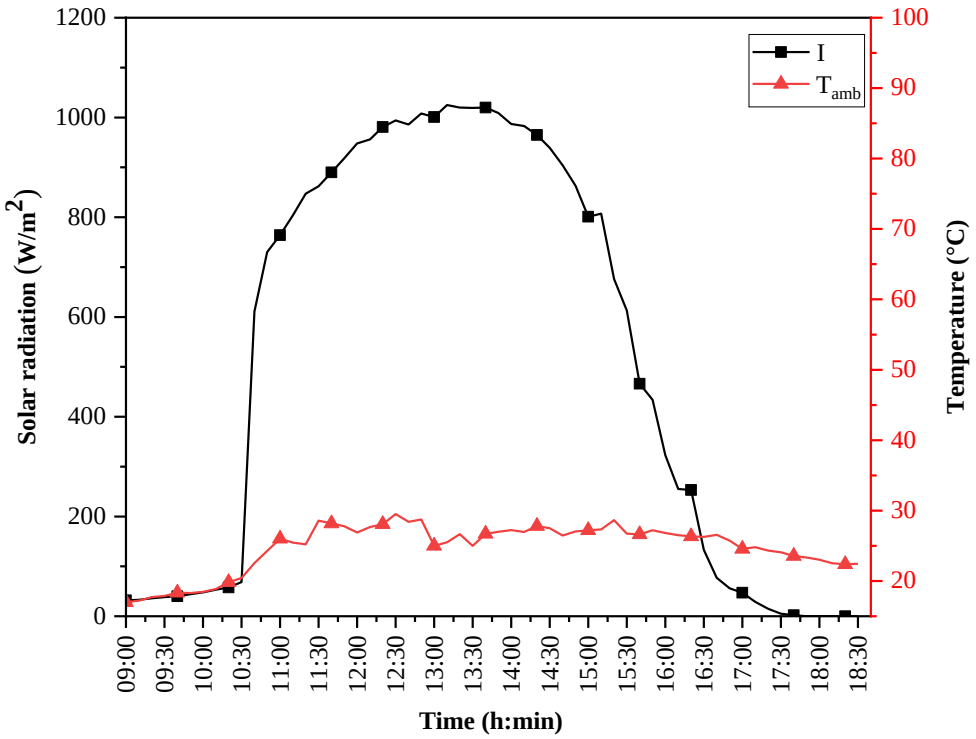


Figure III.4.*Variation of ambient temperature and solar irradiance over time.*

Figure III.5 presents the operating profile of the auxiliary heater over the course of the experimental period. During the early hours of the day, the auxiliary heater was frequently active, delivering an electrical power of 755.41 W, which indicates that the available solar energy was insufficient to sustain the target temperature at the TSU inlet. As the intensity of solar radiation increased, the activation duration of the auxiliary heater progressively declined. Consequently, prolonged periods of inactivity for the electric resistance heater were noted, with a cumulative operating time of 1.68 h recorded during this phase. At 12:04, the resistance heater was deactivated, as solar radiation alone became adequate to maintain the required temperature. The heater remained inactive until 15:02, after which it was reactivated due to the reduction in solar irradiance in order to preserve the desired temperature. The auxil-

iary heater continued operating until it was fully switched off at 17:00, resulting in a total operating duration of 2.2 h for the entire experimental day.

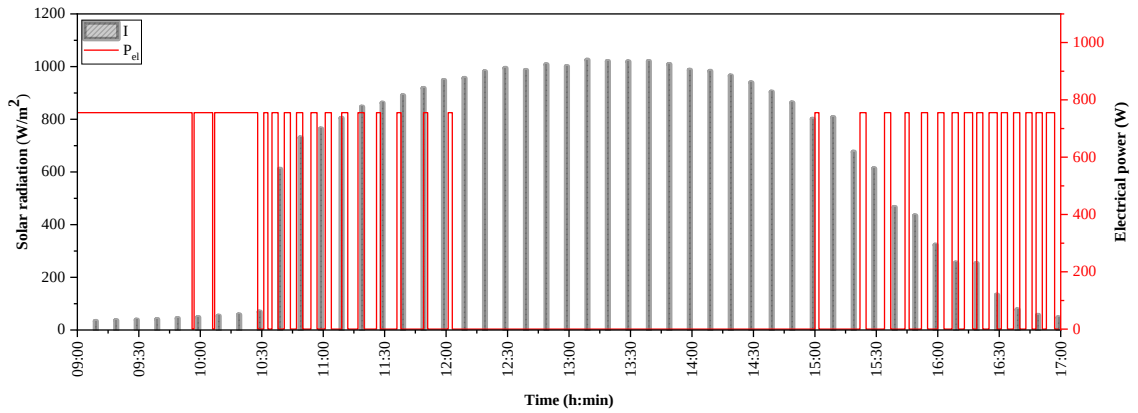


Figure III.5. *Impact of incident solar radiation on auxiliary electrical power usage.*

Figure III.6 illustrates the temperature variations of the system components, including the absorber, ambient, outlet, auxiliary heater, and PCM, measured at 10 min intervals during the experiment at a fixed mass flow rate of 0.024 kg/s. Throughout the morning, temperatures of all components increased progressively, with the auxiliary heater reaching the highest temperature of 102.4 °C. These fluctuations were influenced by the frequent on/off cycling of the resistance heater, highlighting its function in compensating for insufficient solar radiation to maintain the target outlet temperature. As solar radiation intensity increased around 10:20 a.m, the activity of the auxiliary heater decreased, leading to a gradual reduction in its temperature. During midday, the absorber attained the highest temperatures, peaking at 67.8 °C due to its efficient solar energy absorption, with an average temperature of 55 °C, demonstrating its effectiveness in capturing and transferring heat. Concurrently, the PCM began to melt around 10:20, reaching a temperature of 56 °C. Once fully melted, the PCM temperature stabilized at approximately 55 °C, enabling it to regulate and maintain the outlet temperature at 54 °C ± 1.25 °C. As solar radiation declined later in the day, the auxiliary heater resumed operation, increasing in temperature to sustain the desired outlet temperature until 17:00. Simul-

taneously, the PCM released stored thermal energy, helping to maintain the outlet temperature above ambient levels for approximately 1.5 h.

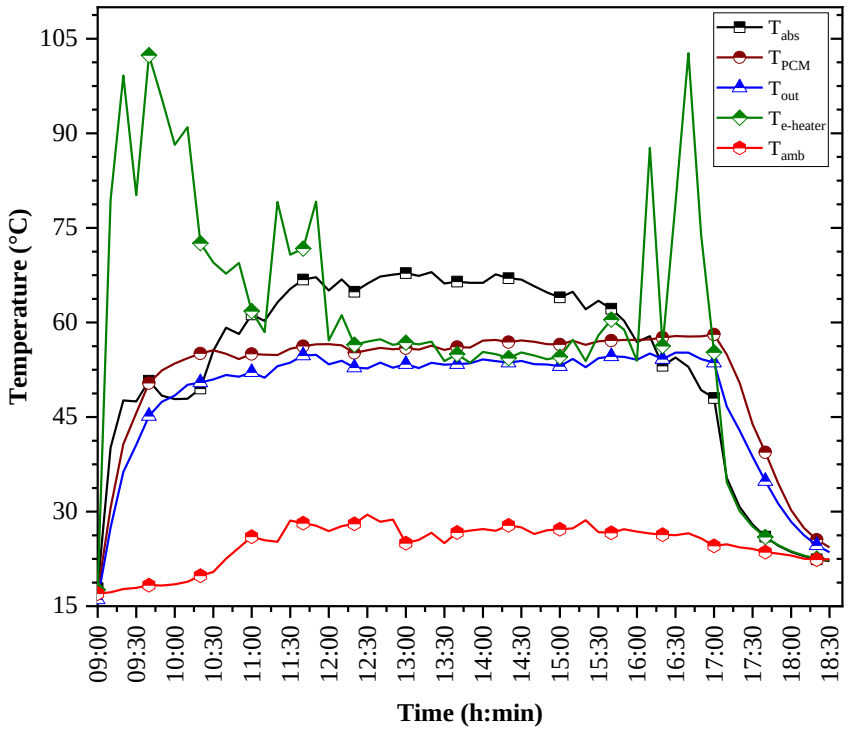


***Figure III**.6. Temporal temperature variations of the HDPSAH components.*

To assess the influence of the LHTSU on the system's thermal performance, two temperature differences were analyzed: Pre-LHTSU (LHTSU inlet temperature - SAH inlet temperature) and Post-LHTSU (LHTSU outlet temperature - SAH inlet temperature). As shown in Figure III.7, the Pre-LHTSU temperature difference exhibited higher values with significant fluctuations, exceeding 15 °C, and reaching a maximum of 48 °C at 09:40 a.m. In contrast, the Post-LHTSU temperature difference remained considerably more stable, varying within a narrower range of 25-30 °C. During the sunset period, the inlet temperature at the heat exchanger dropped rapidly, approaching ambient conditions, whereas the outlet temperature decreased more gradually due to heat release from the PCM. This thermal storage effect extended the system's operational period by approximately 1.5 h. Similarly, Balakrishnan et

al. [30] observed around 1 h of hot air supply after sunset in a modified SAH equipped with rectangular fins containing 0.75 kg of paraffin wax.

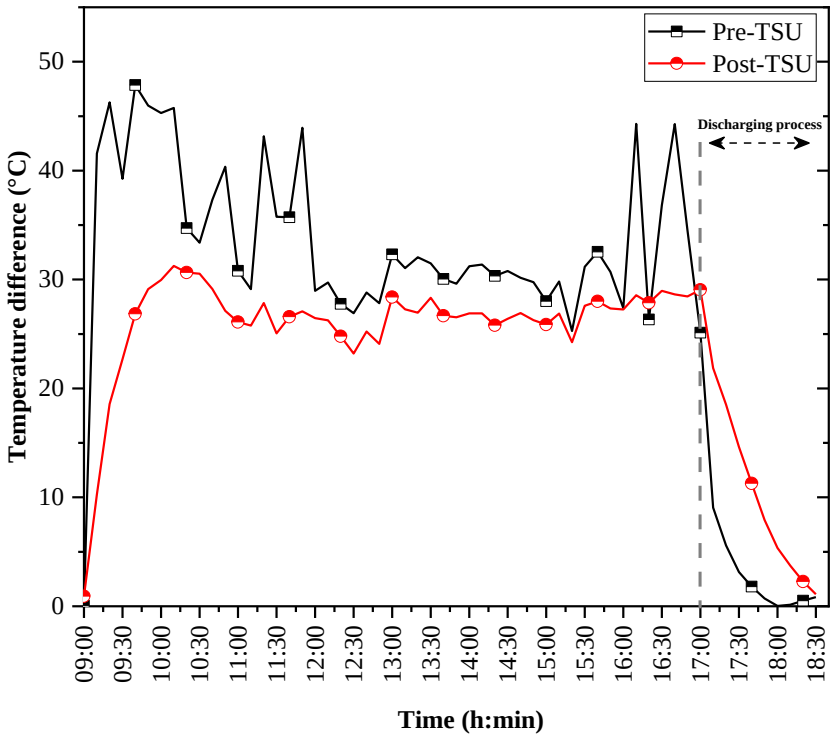


Figure III.7. *Temperature difference evaluation upstream and downstream of the LHTSU.*

Minimizing reliance on electrical energy and conventional fuels, such as natural gas, is a primary objective in hybrid energy systems. This can be accomplished by maximizing the utilization of renewable energy, thereby creating a more sustainable and cost-effective solution. As depicted in Figure III.8, solar energy was the primary contributor, supplying 81.35% of the total energy and substantially reducing dependence on electricity. The remaining energy requirement was met by electricity, which accounted for approximately 18.65% of the total energy supplied. These findings are particularly notable when compared to the results reported by Hadibi et al. [44] for an intermittent solar-electric drying system with a sensible storage medium, where the energy contributions under cloudy conditions were 83% from electrical energy, 14% from solar energy, and 3% from thermal storage.

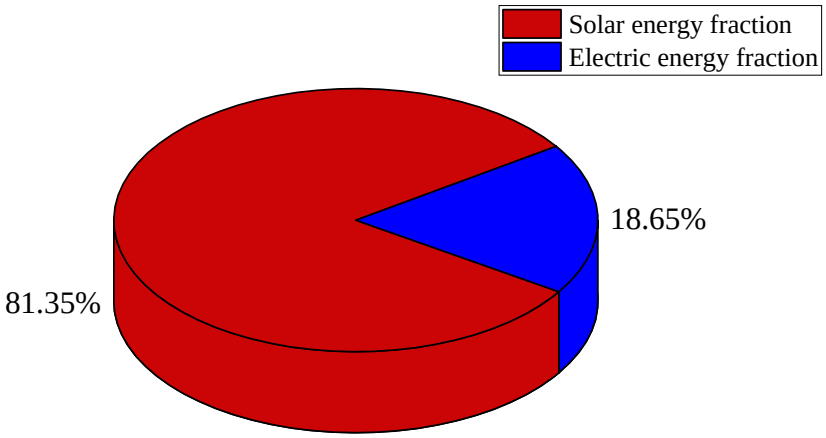


Figure III.8. *Relative contribution of solar and electrical energy to the total system energy.*

Figure III.9 illustrates the temporal variation of thermal efficiency throughout the experimental period. At the initial stage of operation, thermal efficiency increases rapidly, reaching a peak around 10:20 a.m. This behavior is attributed to the combined contribution of solar energy and the auxiliary electric heater, which facilitates rapid system response during startup. Subsequently, thermal efficiency remains relatively stable during the midday period, fluctuating between 67% and 80%. This stable performance is primarily driven by the dominance of solar energy and the melting of the PCM, which absorbs surplus thermal energy and helps maintain consistent efficiency, demonstrating the system's capability to operate effectively under conditions of maximum solar irradiance. In the afternoon, frequent activation of the auxiliary heater influences the efficiency profile, which attains a maximum value of 94% before declining as solar radiation intensity diminishes. Overall, the HDPSAH system achieves an average thermal efficiency of 72.3%. Comparable performance has been reported in the literature, where Sajawal et al. [57] achieved thermal efficiencies ranging from 53.2% to 71.9% using a DPSAH integrated with metallic finned tubes filled with PCMs of different melting temperatures. Similarly, Hedau and Singal [58] reported a thermal efficiency of 61% for a DPSAH–PCM system employing semicircular tubes with perforated ribs at a mass flow rate of 0.025 kg/s.

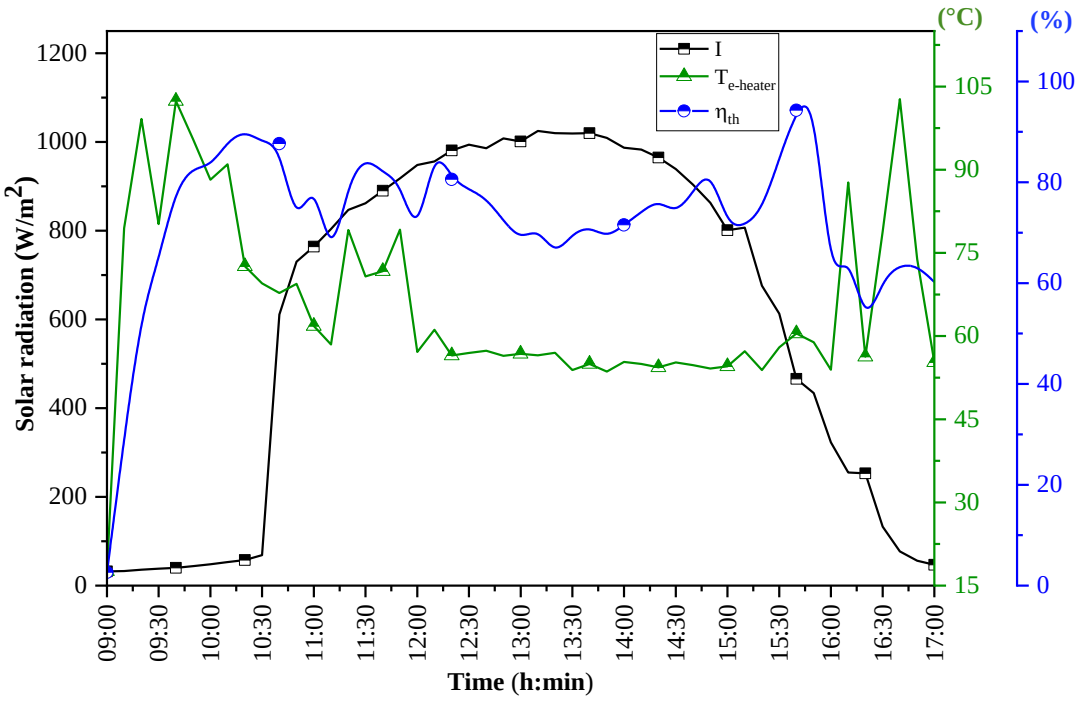


Figure III.9. *Combined impact of solar energy input and auxiliary heater temperature on thermal efficiency.*

In contrast to the first law of thermodynamics, which addresses the conservation of energy without considering its usefulness [59], Exergy analysis, on the other hand, focuses on the quality and work potential of the energy produced. As illustrated in Figure III.10, the exergetic performance of the collector depends on the balance between usable exergy output and exergy destruction. During the initial operating period, the exergy output increases steadily, reaching a maximum value of 37.5 W, driven mainly by the rise in solar irradiance in combination with the contribution of the auxiliary heater. As the operation continues, the influence of the LHTSU becomes increasingly significant, supplying an exergy output in the range of 20.5-31.6 W. Consequently, the exergetic efficiency exhibits temporal variations between 3.02% and 4.08%, with an average value of approximately 3.5%. The relatively low exergetic efficiency is largely associated with substantial exergy destruction, which varies between 778.09 W and 1132 W. This destruction is primarily governed by factors such as the temperature difference between the solar source and the absorber surface, thermal losses to the sur-

roundings, and the temperature gradient between the absorber and the working fluid, as also reported by Abo-Elfadl et al. [56]. In the present study, a noticeable reduction in exergy destruction is observed around midday, reaching a minimum of 550 W as solar radiation intensifies and the absorber temperature increases. Comparable trends have been documented in the literature, Assadeg et al. [38] achieved an exergetic efficiency of 3.2% at a mass flow rate of 0.09 kg/s in a DPSAH incorporating fins and PCM, while Ebadi et al. [60] reported exergetic efficiencies ranging from 1% to 3.5% for a hybrid dryer operating at an air mass flow rate of 0.025 kg/s

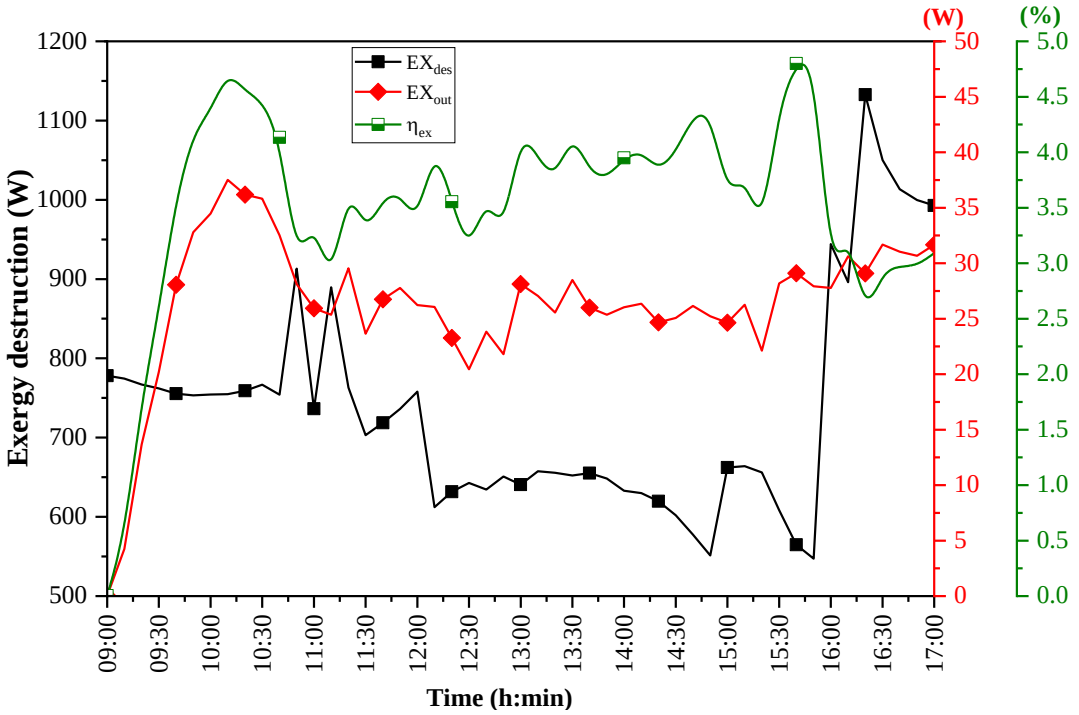


Figure III.10. *Variation of exergy gain and destruction and their impact on exergetic efficiency over time.*

According to Eqs. (19), (20), (21), improving exergetic efficiency while reducing irreversibilities plays a crucial role in enhancing system sustainability. As depicted in ure III.11, the sustainability index (Si) attains an average value of 1.04, indicating efficient resource utilization and environmentally favorable performance. Comparable outcomes were

reported by Albdoor et al. [3], who achieved Si values ranging from 1.007 to 1.015 in a SAH equipped with double triangular fins arranged in various configurations. Furthermore, Nwakuba et al. [61] demonstrated that the Si increases with airflow rate, reporting values between 1.14 and 6.12 for a hybrid solar dryer system. The average improvement potential (IP) of the present HDPSAH was found to be 0.709 kW, representing the theoretical margin for further performance enhancement. In addition, the relative CO_2 reduction potential reached a value of 2.89, highlighting the system's capability to mitigate carbon emissions by nearly threefold when compared to conventional systems. These findings compare favorably with those reported by Fudholi et al. [62], who obtained average IP values ranging from 0.740 to 0.780 kW using a DPSAH collector integrated with longitudinal fins at mass flow rates between 0.03 and 0.1 kg/s.

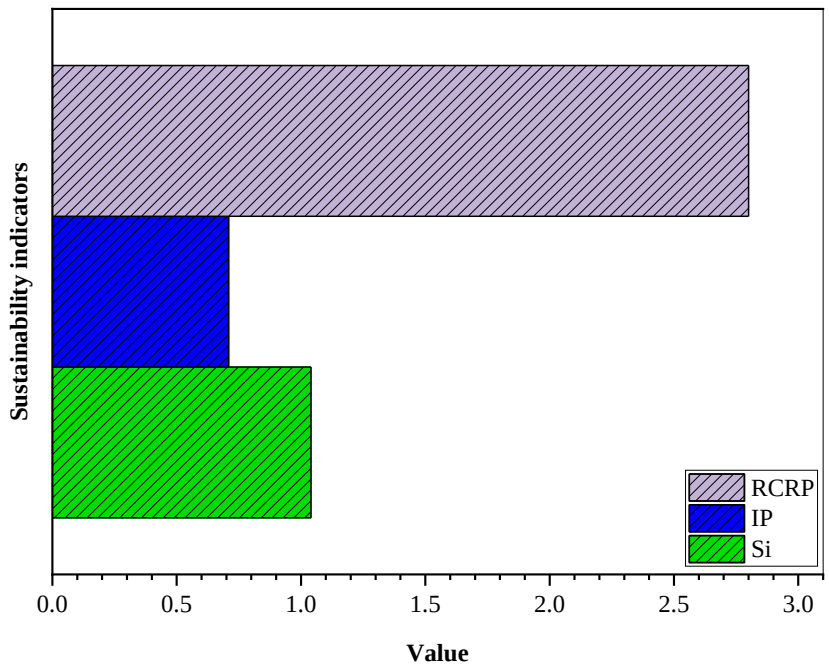


Figure III.11. *Evaluation of sustainability indicators for the system.*

III.3.1 Environmental and economic assessment

As detailed in Table III.1, the HDPSAH is composed of multiple materials, resulting in a total mass of 59.431 kg. The cumulative embodied energy of the system is estimated at 747.63 kWh, with aluminum contributing the largest proportion, accounting for 52.49% of the total embodied energy. The calculated energy payback time is approximately 0.48 years, indicating a rapid recovery of the invested energy when compared to the system's expected operational lifespan of 15 years.

Table III.1. *Distribution of embodied energy among HDPSAH materials*

Materials	Quantity (kg)	Embodied energy coefficient (kWh/kg)	Total (kWh)
Glass	12.631	7.28[52]	91.94
Aluminum	7.1	55.28[52]	392.49
Plywood	16.785	0.44[63]	7.39
Steel	0.48	8.89[53]	4.27
Mild steel	17.17	8.89[64]	152.64
Glass wool	0.3	4.044[54]	1.21
Paraffin wax	0.73	16[63]	11.68
Paint	0.545	25.11[53]	13.68
Plastic	0.2	19.44[53]	3.88
Copper	3.49	19.61[54]	68.44
		Total (kWh)	747.63

Table III.2 shows the system's estimated yearly CO_2 emissions over a projected operational lifespan of 5 to 15 years. The HDPSAH demonstrates relatively low emissions, producing 101.77 kg of CO_2 per year, which is significantly lower than the 182.78 kg/year reported for the DPSAH-PCM system developed by Arun et al.[54] over the same 15-year period. This comparison shows the environmental advantage of the HDPSAH in reducing carbon emissions over its lifetime.

Table III.2*. Variation of CO_2 emissions with operational lifespan.*

Life span (years)	5	10	15
CO_2 emission (kg/year)	305.33	152.66	101.77

Economic evaluation is a crucial factor for stakeholders and industrial developers seeking to determine the practical viability of a system. According to Table III.3, the payback period of the HDPSAH is estimated at 0.65 years, equivalent to roughly 7 months and 27 days, with an associated cost of 3.3 DZD/kWh. This exceptionally short PBP can be attributed to the low cost of raw materials, affordable electricity rates in Algeria, and minimal interest rates, which make the investment very appealing. Beyond the PBP, additional economic indicators further support the system's feasibility. The total annual cost of 5151.41 DZD/year, coupled with an ASV of 322.2 DZD/year, demonstrates that the system maintains low operational expenses while preserving a reasonable residual value at the end of its service life, which shows that it will be economically viable in the long run.

Table III.3. *Economic assessment of the HDPSAH system.*

Parameters	Cost/detail
Capital cost of HSAH	30000 DZD
Capital recovery factor (CRF)	0.0837
The fixed annual cost	2511 DZD/year
The annual maintenance cost	251.1 DZD/year
Salvage value (S)	6000 DZD
Annual salvage value (ASV)	322.2 DZD/year
Electricity cost (Ce=5.06 DZD/kWh)	2711.512 DZD/year
Total annual cost	5151.412 DZD/year
Cost per kWh	3.3 DZD/kWh
Payback period (PBP)	0.65 years

1 USD=133.191 DZD

III.4 Effect of wavy-fin Inclination and auxiliary heater position on HDPSAH Performance

III.4.1 Indoor analysis: effect of wavy-fin inclination

In this phase, the study focuses on optimizing the performance of the HDPSAH through the integration of wavy fins. A parametric investigation was conducted to identify the optimal fin inclination angle. The experiments were carried out under controlled laboratory conditions, where the solar radiation intensity was maintained at a constant value of 500

W/m² and the air mass flow rate was fixed at ṁ = 0.0114 kg/s. Figure III.12 illustrates the temporal evolution of the temperature difference between the outlet and inlet air for various fin inclination angles (30°, 45°, and 60°), in comparison with a flat plate absorber. In all arrangements, the temperature difference increases progressively over time before reaching a stable regime after approximately 103 min. The results demonstrate that the incorporation of inclined wavy fins leads to a significantly higher temperature rise than that obtained with the flat plate absorber. This improvement can be attributed to the increased heat transfer surface area and the extended residence time of air within the collector. Among the investigated configurations, the 45° fin inclination produces the highest temperature difference, reaching 22.83 °C, which corresponds to an increase of about 5 °C relative to the flat plate absorber. The 30° inclination follows closely with a temperature difference of 21.5 °C, whereas the 60° configuration results in a lower value of 19.7 °C, representing only a 1.7 °C enhancement compared to the reference case. These findings indicate that fin inclinations of 30° and 45° favor the development of stronger secondary flow structures. This behavior is associated with the larger air gaps between the fins and the glass cover, as well as between the wavy fins and the absorber, which are approximately 19 mm and 15 mm, respectively, as reported in Table III.4. Such geometrical features promote improved air circulation and more effective convective heat transfer. Conversely, increasing the fin inclination to 60° significantly reduces these gaps, particularly the distance between the fins and the absorber, which decreases to about 11 mm, thereby restricting airflow recirculation and weakening air mixing.

Table III.4. *Variation of air gap spacing with inclination angle.*

Inclination angle (°)	Air gap size (mm)
30	19
45	15
60	11

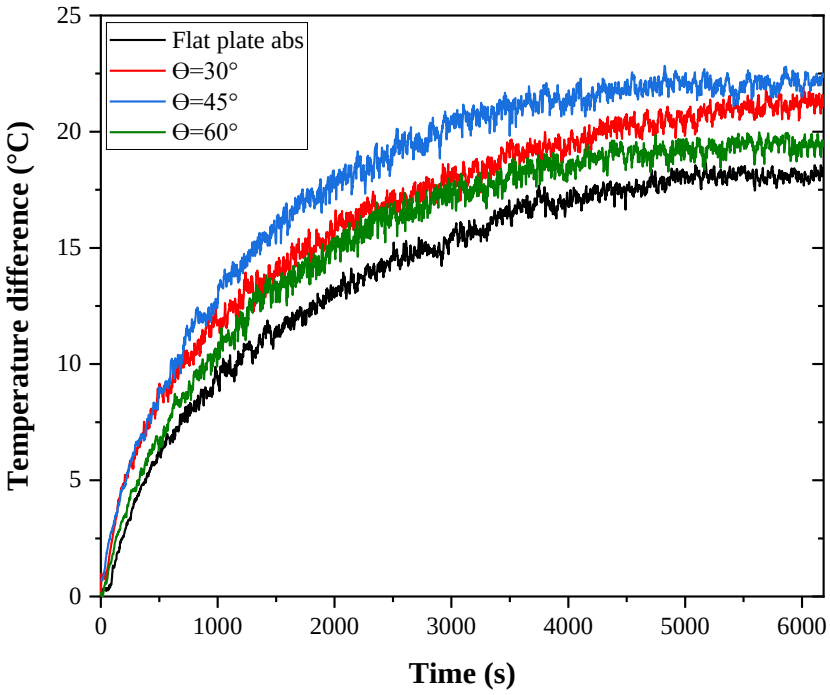


Figure III.12. *Comparison of temperature difference for different configurations.*

Figure III.13 shows that the change in thermal efficiency follows a pattern similar to that of the temperature difference, which indicates that thermal efficiency increases with rising outlet air temperature. Among the examined configurations, the 45° yields the highest thermal efficiency, reaching a value of 73.3%. In contrast, configurations with fin inclination angles of 30° and 60°, as well as the flat plate arrangement, show reductions in thermal efficiency of approximately 3.8%, 9.3%, and 13.8%, respectively, when compared to the optimal configuration. Based on these findings, the 45° fin inclination was identified as the most effective and was therefore selected for subsequent outdoor experimental investigations.

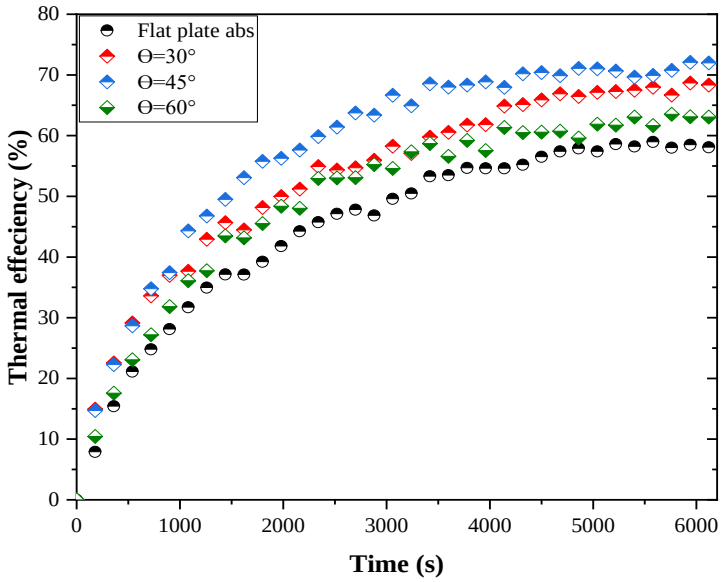


Figure III.13. *Comparison of thermal efficiency for different configurations*

III.4.2 Outdoor analysis: effect of auxiliary heater position

The outdoor experimental investigation was designed to examine the impact of the electric auxiliary heater's placement on the thermal response and overall performance of the HDPSAH system. Figure III.14 presents the daily evolution of ambient temperature and solar irradiance measured during two distinct experimental days in April. Tests conducted on April 23, corresponding to auxiliary heater position 1, and on April 27, corresponding to position 2, exhibited comparable meteorological conditions. In both cases, solar irradiance increased progressively during the morning hours, reaching peak values of 1066 W/m² and 1050 W/m² around midday, before decreasing gradually in the afternoon. The average daily solar radiation was recorded at 660 W/m² and 630 W/m², respectively. Ambient temperature followed a similar diurnal pattern on both days, with maximum values of 28.8 °C and 27.5 °C, and mean temperatures of 23.26 °C and 24.01 °C, respectively. Additionally, the average wind velocity remained relatively stable, with measured values of 1.38 m/s and 1.42 m/s. The close correspondence of these environmental parameters ensures comparable operating conditions,

thereby enabling a reliable assessment of the effect of auxiliary heater positioning on the system's outdoor thermal performance.

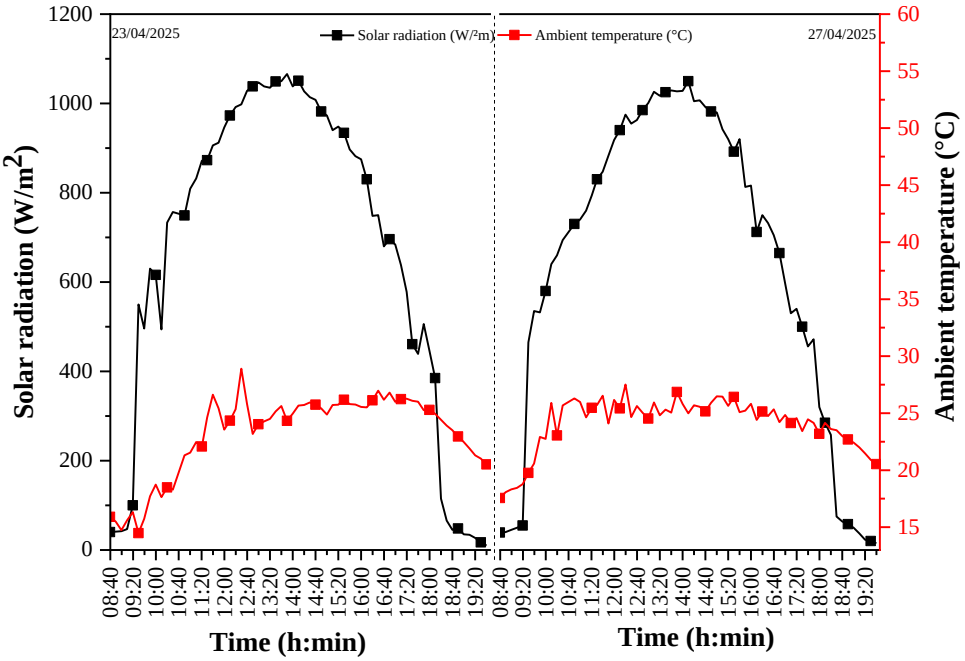


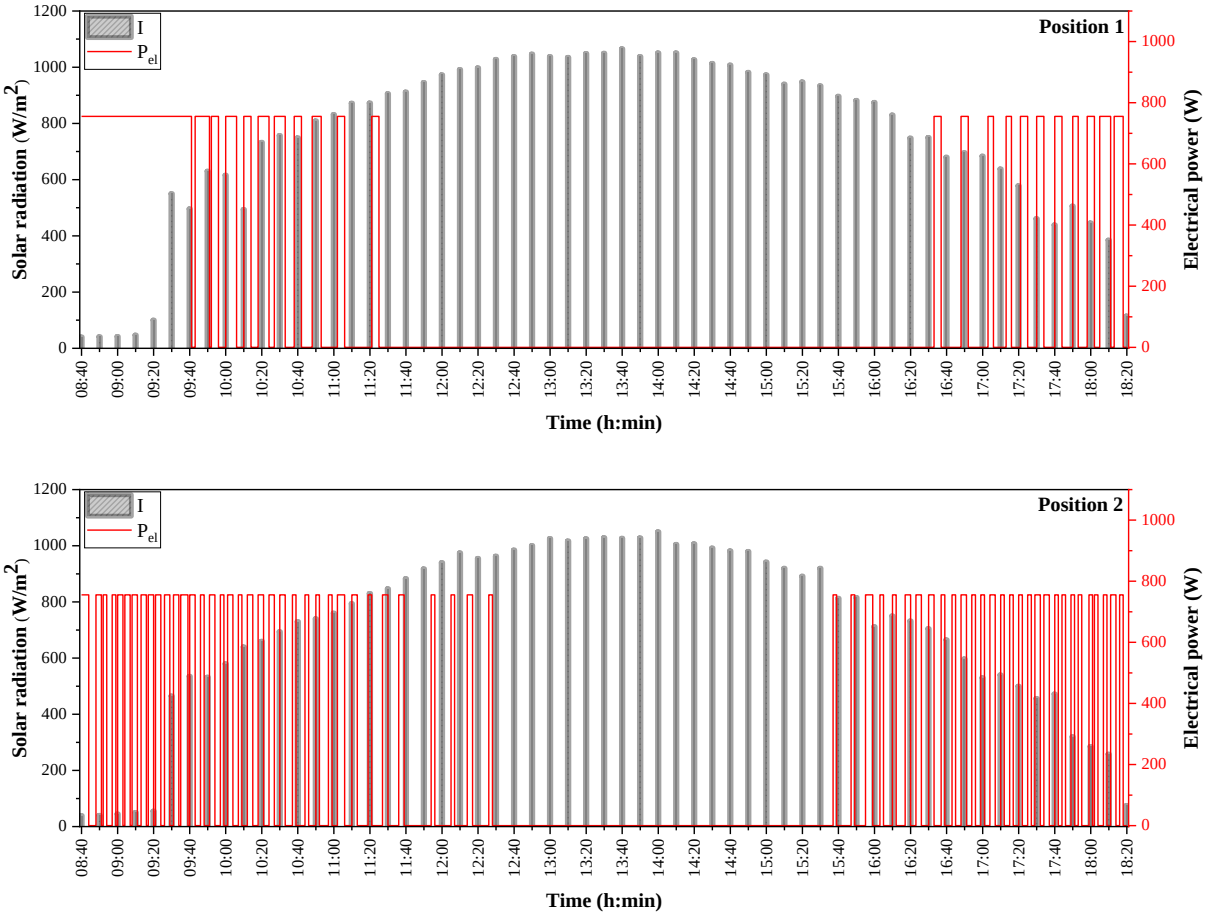
Figure III.14.*Temporal variation of ambient temperature and solar irradiance*.

Figure III.15 (a) illustrates the operating duration of the electric auxiliary heater during the experimental tests conducted for two different installation configurations, referred to as position 1 and position 2. In both configurations, the auxiliary heater was intermittently activated, delivering a maximum electrical power of 755.41 W, which indicates that solar energy alone was insufficient to maintain the desired outlet air temperature throughout the experimental period. As solar irradiance increased during the day, a corresponding decrease in the operating duration of the auxiliary heater was observed.

When the auxiliary heater was installed in position 1, longer activation periods were recorded, particularly during the morning hours and toward the end of the test. In contrast, positioning the auxiliary heater in position 2 resulted in shorter and more frequent on/off cycles, with some activation intervals limited to approximately one minute. The total operating time of the auxiliary heater reached 135 min for configuration 1, compared to 102 min for

configuration 2, corresponding to a reduction of 33 min.

Solar energy remained the dominant energy source in both configurations. As shown in Figure III.5 (b), solar energy contributions accounted for 74.76% and 78.99% of the total energy input in configurations 1 and 2, respectively. However, configuration 1 exhibited a higher dependence on electrical energy, which represented 25.24% of the total input, compared to 21.01% for configuration 2. These results demonstrate improved solar energy utilization in configuration 2 and are consistent with previously reported findings, such as those of Koşan [39], who reported a solar energy contribution of 69% and an electrical share of 31% for a DPSAH system equipped with an infrared heating film.



(a)



(b)

Figure III.15. *(a) Operating profile of the auxiliary heater under variable solar irradiance; (b) distribution of energy contributions for the two configurations.*

Figure III.16 illustrates the diurnal evolution of the absorber and outlet air temperatures for the two investigated configurations. When the auxiliary heater was mounted in position 1, the absorber temperature remained consistently higher, reaching a peak value of 73 °C, compared with 69 °C for position 2. Over the entire experimental duration, an average temperature difference of approximately 6.5 °C was observed between the two configurations. This behavior is attributed to the heater placement at the U-turn section, which enhances absorber heating through combined convective and radiative heat transfer, in addition to the energy supplied by solar irradiation. In contrast, when the auxiliary heater was located in position 2, its contribution to absorber heating was limited, and the absorber temperature was predominantly governed by solar energy input. for the outlet air temperature, configuration 2 exhibited a more stable thermal response, with an average value of 54 ± 1.3 °C. On the other hand, configuration 1 showed larger fluctuations in the outlet temperature, indicating a slower thermal response and less effective temperature regulation. Furthermore, during the late afternoon period, the outlet temperature in configuration 2 exceeded that of configuration 1 by

approximately 2 °C, which can be attributed to the efficient thermal energy release from the LHTSU.

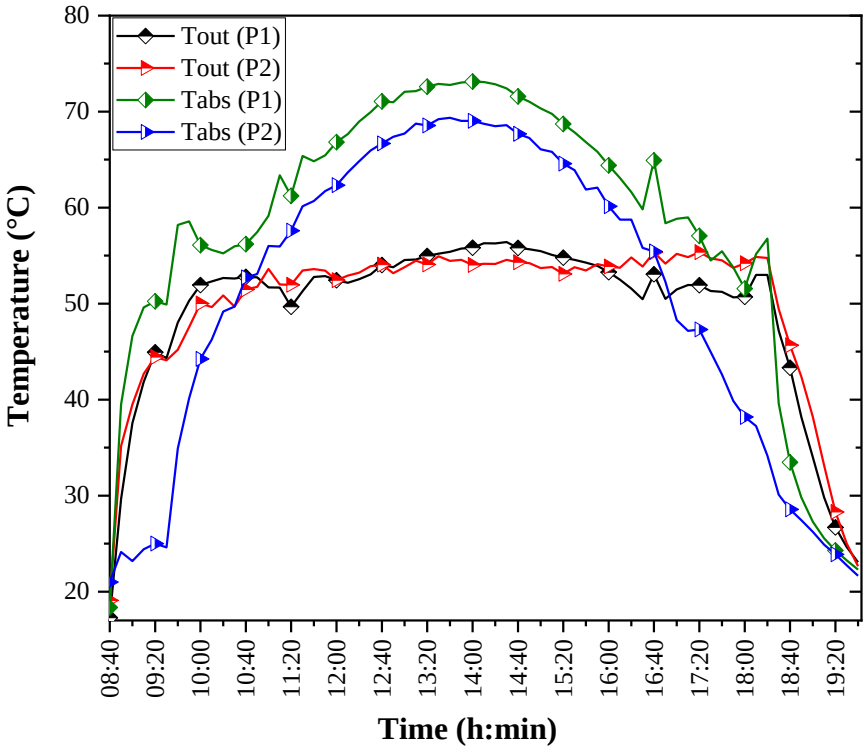


Figure III.16. *Evolution of absorber and outlet air temperatures for two configurations*

To further elucidate these trends, Figure III.17 presents the variation of the temperature difference between outlet and inlet air for both configurations. In configuration 1, higher temperature differences were recorded, reaching a maximum of 34.6 °C, accompanied by pronounced fluctuations exceeding 11 °C. By contrast, configuration 2 demonstrated a more uniform thermal behavior, with the temperature difference varying within a narrower range of 24-32 °C, reflecting improved thermal stability.

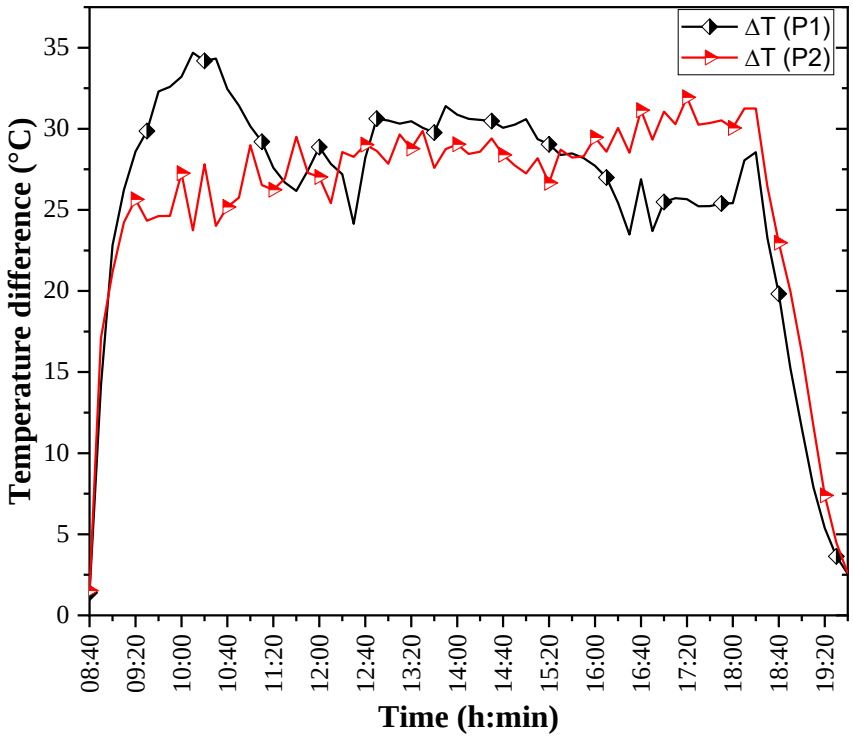


Figure III.17. *Comparison of the temperature differences.*

Figure III.18 depicts the time-dependent variation of the PCM temperature inside the heat exchanger for both examined configurations. The results indicate that, in configuration 2, the PCM reaches its melting temperature at an earlier stage compared to configuration 1, signifying an earlier onset of the charging process. Throughout the operational period, the PCM temperature remains consistently higher in configuration 2, suggesting that heat is supplied to the PCM more directly and in a more concentrated manner when the auxiliary heater is installed near the outlet section. By contrast, when the auxiliary heater is positioned in the U-turn section (configuration 1), the heated airflow travels a longer distance and undergoes greater mixing before entering the heat exchanger. This flow behavior leads to a comparatively lower and more uniform PCM temperature. Nevertheless, placing the auxiliary heater closer to the heat exchanger in configuration 2 induces more frequent temperature oscillations in the PCM, which are associated with the intermittent on/off operation of the heater. These oscillations become more pronounced during the late afternoon period, particularly when the

PCM temperature exceeds 70 °C, as longer heater activation intervals are required to compensate for the reduction in solar irradiance. During the discharging phase, the PCM temperature in configuration 2 remains higher than that observed in configuration 1, confirming a greater thermal energy storage capacity in this configuration. This enhanced energy storage contributes to sustaining a higher outlet air temperature, in agreement with the thermal performance trends discussed previously.

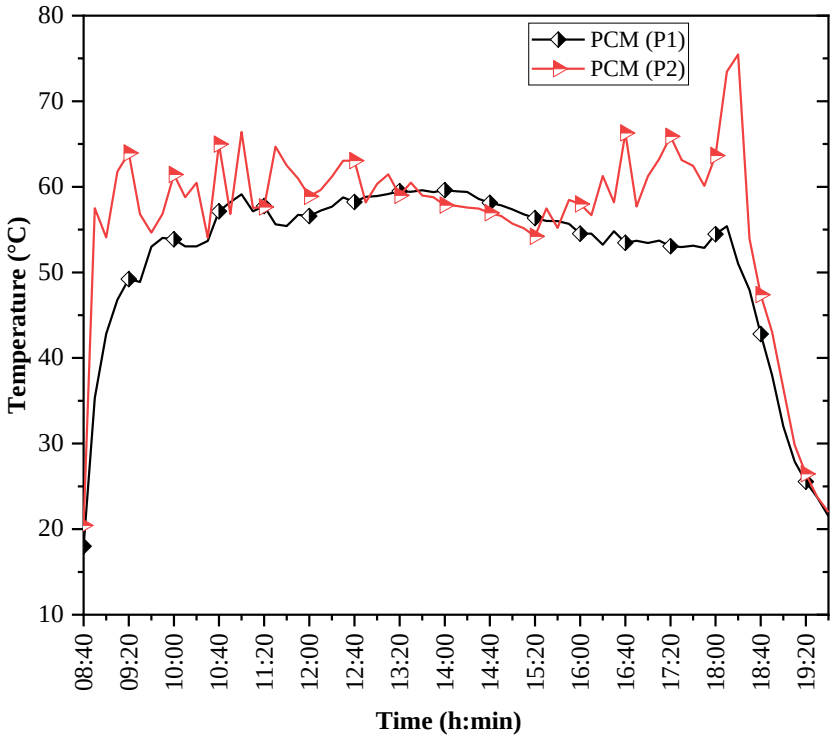


Figure III.18. *Comparison of PCM temperature evolution under different configurations.*

Figure III.19 illustrates the temporal variation of top heat losses for the two investigated configurations. The results indicate that configuration one has consistently larger heat losses, especially in the morning and late afternoon, with a maximum value approaching 341 W and an average loss of 241.66 W over the whole operating period. This behavior is mainly related to the installation of the auxiliary heater in the U-turn section, which leads to an increase in absorber temperature. As a result, enhanced convective and radiative heat transfer occurs between the absorber and the glass cover, causing substantial thermal losses to the sur-

rounding environment. On the other hand, configuration 2 exhibits significantly lower top heat losses, with an average value of 164.43 W. The reduction in heat dissipation can be attributed to the relocation of the auxiliary heater to the outlet section, which limits the temperature difference across the absorber and consequently reduces heat transfer to the glass cover.

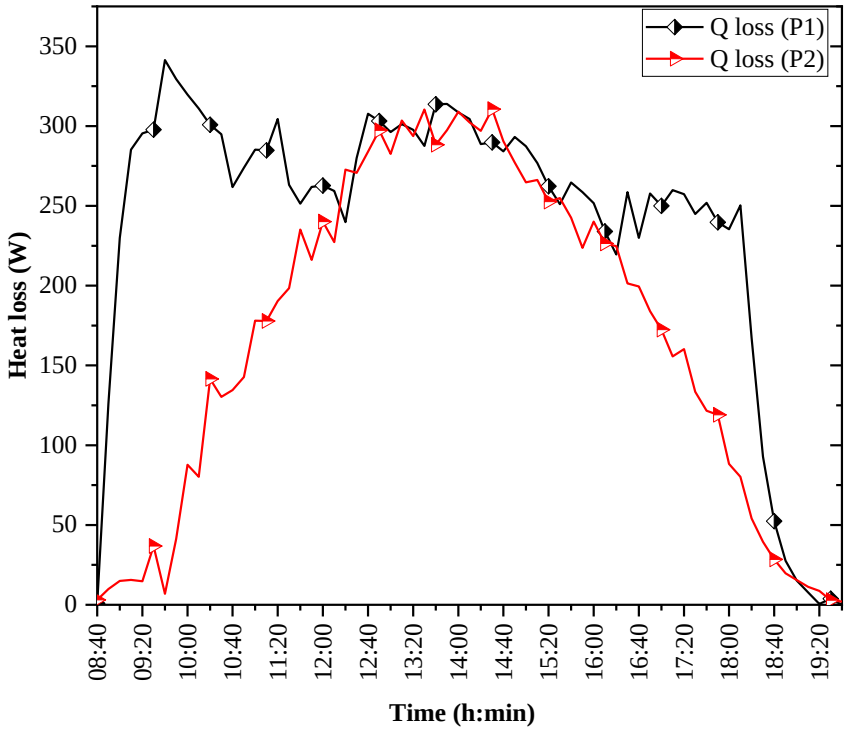


Figure III.19. *Temporal variation of top heat losses.*

Figure III.20 illustrates the evolution of thermal efficiency throughout the day for both configurations. Configuration 2 exhibits higher thermal efficiency during the early morning and late afternoon periods compared to configuration 1. This improvement is mainly attributed to the lower electrical energy demand of the auxiliary heater during these intervals. Around midday, both configurations maintain similarly high thermal efficiency values, ranging from approximately 70% to 79%, due to the dominant contribution of solar energy as the primary heat source. Over the entire operating period, the DPSAH achieves average thermal efficiencies of 65.62% and 68.14% for configurations 1 and 2, respectively. These results compare favorably with those reported for similar system designs, as summarized in Table III.5.

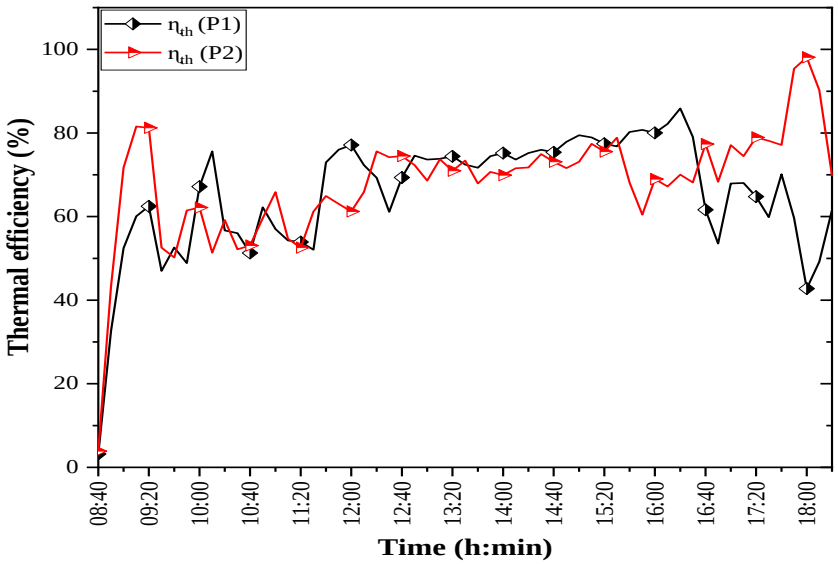


Figure III.20. *Variation of thermal efficiency during the operating period*

Table III.5. *Comparison between the present study and previously reported works.*

Details	Thermal efficiency (%)	PCM type	Auxiliary Heater	Ref.
HDPSAH Integrated with Rectangular Fins	76.4		Infrared film	[39]
Recycled HSAH with LHTSU	53	Paraffin wax (RT38)	Electrical heater (2000 W)	[42]
Hybrid SAH integrated with vertical baffles	58.5		Electrical heater (1000 W)	[40]
DPSAH with Cylindrical Tubes Filled with PCM	65%	paraffin wax		[8]
DPSAH integrated with semi-circular finned tubes filled with PCM	71.9%	RT44HC and RT18HC		[57]
DPSAH Integrated with Perforated Ribs and PCM	61%	Paraffin wax		[58]
SAH with V-corrugated absorber comprising PCM	57.02%	Paraffin wax+ MWCNT		[63]
Present study	65.6-68.1	Paraffin wax	electric finned	electric finned

	heater	heater

Table III.6 summarizes the measurement accuracy associated with the experimental instruments and apparatus employed in this study.

Table III.6. *Accuracy characteristics of the experimental equipment.*

Measured and computed parameters	Uncertainty (Phase 2 and Phase 3)	
Irradiation	±10	±10
Temperature	±0.27	±0.27
Velocity	±0.2	±0.22
Voltage	±0.97	±0.97
mass flow rate	±5%	±11.5%
useful heat	±5.1%	±11.6%
input solar radiation	±1.9%	±1.6%
thermal efficiency	±5.5%	±14.2%

III.5 Conclusion

This chapter presented a comprehensive experimental analysis of a hybrid double-pass solar air heater integrated with a latent heat thermal storage unit, based on energy, exergy, economic, and environmental evaluations. The experimental work was divided into three main phases: parametric and dimensional analysis, assessment of the impact of latent heat thermal storage on system performance, and optimization of the HDPSAH through fin integration and auxiliary heater positioning. The reliability of the experimental results was ensured through uncertainty analysis, confirming the accuracy of the measurements. The findings demonstrate that the proposed configurations significantly influence the thermal behavior and performance of the hybrid system, highlighting the effectiveness of the implemented enhancements. Over-

all, the results provide valuable insight into performance improvement strategies for hybrid solar air heater systems.

General Conclusion

This thesis presented a comprehensive experimental investigation of a hybrid double-pass solar air heater (HDPSAH) integrated with a latent heat thermal storage unit, with the objective of developing a reliable system suitable for all-weather operation in space heating and drying applications. A multi-criteria evaluation framework was adopted, incorporating energy, exergy, economic, and environmental analyses to provide a holistic assessment of the proposed system's performance and sustainability.

The experimental work was systematically structured into three main phases. The first phase focused on parametric and dimensional investigations to establish baseline performance characteristics and to evaluate the influence of key geometric and operational parameters. The second phase examined the integration of the latent heat thermal storage unit (LHTSU) and assessed its impact on thermal stability, energy efficiency, and system reliability. The third phase addressed further system optimization through the integration of wavy fins and the evaluation of the optimal position of the auxiliary electric heater. Throughout the experimental campaign, particular emphasis was placed on the accuracy and reliability of the measured data. A detailed uncertainty analysis was conducted to account for instrumental accuracy and measurement errors, thereby ensuring the validity of the experimental results and enabling meaningful comparison with existing studies reported in the literature. The experimental work yielded the following key findings:

Phase 1- Effect of air gap variation

- Increasing the height of the upper air channel was found to significantly enhance thermal performance. The maximum thermal efficiency of 66.4% was achieved for the

12 cm configuration, while reductions of 2.4%, 7.8%, and 14.4 % were observed for the 9, 6, and 3 cm configurations, respectively.

- Smaller upper channel heights resulted in higher exergy destruction, indicating increased irreversibility and heat losses under these configurations.

Phase 2- Integration of latent heat thermal storage

- The integration of the LHTSU enabled stable outlet air temperatures of 54 ± 1.25 °C, with a temperature difference ranging between 25 °C and 30 °C, and extended the system's operating period by approximately 1.5 hours after sunset.
- The use of latent heat storage significantly reduced reliance on electrical energy, resulting in a daily electricity consumption of 1674.6 Wh, corresponding to only 18.65% of the total energy supplied.
- At an air mass flow rate of $\dot{m}$ = 0.024 kg/s, the HDPSAH achieved an average thermal efficiency of 72.3% and an average exergetic efficiency of 3.5%. The sustainability indicators: sustainability index (SI), improvement potential (IP), and renewable contribution ratio potential (RCRP), were found to be 1.04, 0.709 kW, and 2.89, respectively.
- From an environmental and economic perspective, the system reduced CO_2 emissions from 305.33 kg/year to 101.77 kg/year over a lifespan of 15 years. Additionally, the energy payback time and investment payback period were determined to be 0.48 years and 0.65 years, respectively, demonstrating the cost-effectiveness of the proposed system.

Phase 3- Heat transfer enhancement and auxiliary heater optimization

- The integration of wavy fins with an inclination angle of 45° enhanced the collector's thermal efficiency by 13.8% compared to a conventional flat absorber.

- Positioning the auxiliary electric heater at the outlet section (configuration 2) provided improved thermal regulation, minimized temperature fluctuations, and maintained a stable outlet air temperature of 54 ± 1.3 °C under outdoor operating conditions. This configuration required 4.23% less electrical energy than configuration 1 due to reduced auxiliary heater activation time and more effective utilization of the thermal energy stored in the PCM.

Overall, the results show that the proposed design modifications significantly influence the thermal behavior and overall performance of the hybrid system. The combined integration of latent heat thermal storage and heat transfer enhancement techniques improved energy utilization, enhanced thermal stability, and reduced dependence on auxiliary electrical heating under variable operating conditions. The energy, exergy, economic, and environmental analyses collectively confirm the advantages of the optimized HDPSAH–LHTSU configurations in terms of efficiency, sustainability, and practical applicability.

Despite these promising results, certain limitations were identified. The current heat exchanger design restricts the integration of larger PCM quantities, thereby limiting the system's heat storage capacity. Future design modifications could enhance the discharging duration and further improve overall thermal efficiency. In addition, future work should consider testing the system under different seasonal conditions and airflow rates, integrating photovoltaic modules to power auxiliary components, and conducting detailed CFD simulations to gain deeper insight into the system's thermal and flow behavior

References

[1] L. Pérez-Lombard, J. Ortiz, C. Pout, A review on buildings energy consumption information, Energy Build. 40 (2008) 394–398. https://doi.org/10.1016/j.enbuild.2007.03.007.

[2] A. Atia, M. Teggar, A. Laouer, Performance of various solar dryer types integrating latent heat storage for drying agricultural products: An up-to-date review, J. Energy Storage 102 (2024) 114048. https://doi.org/10.1016/j.est.2024.114048.

[3] A.K. Albdoor, Z.A.H. Obaid, M.S. Kamel, I.D.J. Azzawi, Energy, exergy, economic and environmental analysis of a solar air heater integrated with double triangular fins: Experimental investigation, Int. J. Thermofluids 24 (2024) 100979. https://doi.org/10.1016/j.ijft.2024.100979.

[4] A. Sachdeva, C. M., A. Yadav, Development and thermodynamic analysis of a novel heat pipe vacuum tube solar collector with sensible heat storage, Energy Sources Part Recovery Util. Environ. Eff. 45 (2023) 1511–1532. https://doi.org/10.1080/15567036.2023.2178552.

[5] M. Akhbari, A. Rahimi, M.S. Hatamipour, Modeling and experimental study of a triangular channel solar air heater, Appl. Therm. Eng. 170 (2020) 114902. https://doi.org/10.1016/j.applthermaleng.2020.114902.

[6] N. Kalita, P. Muthukumar, A. Dalal, Performance investigation of a hybrid solar dryer with electric and biogas backup air heaters for chilli drying, Therm. Sci. Eng. Prog. 52 (2024) 102646. https://doi.org/10.1016/j.tsep.2024.102646.

[7] A. Biçer, A.G. Devecioğlu, V. Oruç, Z. Tuncer, Experimental investigation of a solar air heater with copper wool on the absorber plate, Int. J. Green Energy 17 (2020) 979–989. https://doi.org/10.1080/15435075.2020.1818245.

[8] E. Vengadesan, V. Dhinakaran, S. Senthil, P. Renugadevi, R. Senthil, Performance augmentation of solar air heater using absorber with multi-functional encapsulated PCM tubes, J. Energy Storage 72 (2023) 108296. https://doi.org/10.1016/j.est.2023.108296.

[9] H. Hassan, S. Abo-Elfadl, Experimental study on the performance of double pass and two inlet ports solar air heater (SAH) at different configurations of the absorber plate, Renew. Energy 116 (2018) 728–740. https://doi.org/10.1016/j.renene.2017.09.047.

[10] N.E. Wijeysundera, L.L. Ah, L.E. Tjioe, Thermal performance study of two-pass solar air heaters, Sol. Energy 28 (1982) 363–370. https://doi.org/10.1016/0038-092X(82)90253-5.

[11] A.J. Mahmood, L.B.Y. Aldabbagh, F. Egelioglu, Investigation of single and double pass solar air heater with transverse fins and a package wire mesh layer, Energy Convers. Manag. 89 (2015) 599–607. https://doi.org/10.1016/j.enconman.2014.10.028.

[12] A.E.A. Abdulmejeed, A.D. Tuncer, A. Khanlari, A. Gungor, Investigation of combined parallel and triple-pass v-corrugated solar air heater: A numerical and experimental study, Process Saf. Environ. Prot. 185 (2024) 1385–1398. https://doi.org/10.1016/j.psep.2024.03.107.

[13] P.P. Borah, K.K. Pathak, A. Gupta, S. Roy, B. Das, Experimental study of a solar air heater with modified absorber plate through square obstacles with threaded pin fins, Appl. Therm. Eng. 228 (2023) 120544. https://doi.org/10.1016/j.applthermaleng.2023.120544.

[14] O. Elakrout, O. Ghriss, A. Bouabidi, H. Garcia Castellanos, S. Mohtaram, A. Keçebaş, Y. Aryanfar, Investigative analysis of the influence of diverse fin configurations on the performance of a dual pass solar air collector, Therm. Sci. Eng. Prog. 50 (2024) 102545. https://doi.org/10.1016/j.tsep.2024.102545.

[15] A. Kumar, Akshayveer, A.P. Singh, O.P. Singh, Efficient designs of double-pass curved solar air heaters, Renew. Energy 160 (2020) 1105–1118. https://doi.org/10.1016/j.renene.2020.06.115.

[16] R. Pandey, M. Kumar, Efficiencies assessment of an indoor designed solar air heater characterized by V baffle blocks having staggered racetrack-shaped perforation geometry, Sustain. Energy Technol. Assess. 47 (2021) 101362. https://doi.org/10.1016/j.seta.2021.101362.

[17] R. Fattoum, A. Hidouri, M. El Hadi Attia, M. Arıcı, M. Ammar Abbassi, Optimization of solar air heaters performance using parallel porous wire mesh: energy, exergy, and enviro-economic analyses, Therm. Sci. Eng. Prog. 48 (2024) 102385. https://doi.org/10.1016/j.tsep.2024.102385.

[18] S. Abo-Elfadl, M. S. Yousef, M.F. El-Dosoky, H. Hassan, Energy, exergy, and economic analysis of tubular solar air heater with porous material: An experimental study, Appl. Therm. Eng. 196 (2021) 117294. https://doi.org/10.1016/j.applthermaleng.2021.117294.

[19] V. Madadi Avargani, S. Zendehboudi, A. Rahimi, S. Soltani, Comprehensive energy, exergy, enviro-exergy, and thermo-hydraulic performance assessment of a flat plate solar air heater with different obstacles, Appl. Therm. Eng. 203 (2022) 117907. https://doi.org/10.1016/j.applthermaleng.2021.117907.

[20] S.K. Yadav, A. Lanjewar, Experimental analysis of solar air heater duct with discrete arc-pattern combined staggered element roughness on absorber plate, Environ. Dev. Sustain. 25 (2023) 8651–8675. https://doi.org/10.1007/s10668-022-02417-0.

[21] S. Singh, S.K. Chaurasiya, B.S. Negi, S. Chander, M. Nemś, S. Negi, Utilizing circular jet impingement to enhance thermal performance of solar air heater, Renew. Energy 154 (2020) 1327–1345. https://doi.org/10.1016/j.renene.2020.03.095.

[22] F. Bayrak, H.F. Oztop, A. Hepbasli, Energy and exergy analyses of porous baffles inserted solar air heaters for building applications, Energy Build. 57 (2013) 338–345. https://doi.org/10.1016/j.enbuild.2012.10.055.

[23] S.I.U. Din, A. Ibrahim, R.K. Ajeel, A. Fazlizan, A.A. Ishak, A.B. Al-Aasam, Thermal performance analysis of a double-pass solar air heater with lava rock as porous and sensible heat storage material, J. Energy Storage 95 (2024) 112564. https://doi.org/10.1016/j.est.2024.112564.

[24] S. Algarni, V. Tirth, A. Saxena, P. Gupta, A comparative study of different low-cost sensible heat storage materials for solar air heating: an experimental approach, Energy Sources Part Recovery Util. Environ. Eff. 44 (2022) 912–933. https://doi.org/10.1080/15567036.2022.2050854.

[25] A. Sachdeva, M. Chandrashekara, A. Yadav, Experimental investigation of a novel solar air heater based on heat pipe vacuum tube collector integrated with finned-tube heat exchanger, J. Therm. Anal. Calorim. 148 (2023) 10917–10936. https://doi.org/10.1007/s10973-023-12413-9.

[26] A. Tiwari, A. Kumar, Solar air heater based on double-ends open evacuated tube with & without phase change material: An experimental investigation, J. Energy Storage 72 (2023) 108265. https://doi.org/10.1016/j.est.2023.108265.

[27] R.A. Kumar, B.G. Babu, M. Mohanraj, Experimental investigations on a forced convection solar air heater using packed bed absorber plates with phase change materials, Int. J. Green Energy 14 (2017) 1238–1255. https://doi.org/10.1080/15435075.2017.1330753.

[28] S.I.U. Din, A. Ibrahim, A. Fazlizan, H.A. Kazem, K. Sopian, Anwer.B. Al-Aasam, M.A.A. Rahmat, Performance analysis of a photovoltaic double-pass solar air heater with

staggered-Sandwich PCM cylinders as dual cooling and latent heat storage, J. Energy Storage 132 (2025) 117739. https://doi.org/10.1016/j.est.2025.117739.

[29] B. Brahma, A.K. Shukla, D.C. Baruah, Design and performance analysis of solar air heater with phase change materials, J. Energy Storage 61 (2023) 106809. https://doi.org/10.1016/j.est.2023.106809.

[30] P. Balakrishnan, S.K. Vishnu, J. Muthukumaran, R. Senthil, Experimental thermal performance of a solar air heater with rectangular fins and phase change material, J. Energy Storage 84 (2024) 110781. https://doi.org/10.1016/j.est.2024.110781.

[31] P. Sudhakar, M. Cheralathan, Encapsulated PCM based double pass solar air heater: A comparative experimental study, Chem. Eng. Commun. 208 (2021) 788–800. https://doi.org/10.1080/00986445.2019.1641701.

[32] H.S. Dheyab, M.S.M. Al-Jethelah, M. Baccar, Closed collector –storage solar air heating system thermal performance: an experimental study, Energy Sources Part Recovery Util. Environ. Eff. 44 (2022) 10006–10023. https://doi.org/10.1080/15567036.2022.2144965.

[33] A. Saxena, A.A. Sagade, D.B. Singh, S.K. Joshi, A. Suryavanshi, P. Gupta, M. Sethi, Thermal performance of an economical air heater for space heating using composite energy storage materials, Energy Sources Part Recovery Util. Environ. Eff. 46 (2024) 8297–8319. https://doi.org/10.1080/15567036.2024.2370337.

[34] J. Muthukumaran, R. Senthil, Experimental performance of a solar air heater using straight and spiral absorber tubes with thermal energy storage, J. Energy Storage 45 (2022) 103796. https://doi.org/10.1016/j.est.2021.103796.

[35] D. Chaatouf, B. Raillani, M. Salhi, S. Amraqui, A. Mezrhab, Experimental and numerical study of a natural convection indirect solar dryer with PCM tubes: Dynamic, thermal and nutritional quality analysis, Sol. Energy 264 (2023) 111975. https://doi.org/10.1016/j.solener.2023.111975.

[36] A. El Khadraoui, S. Bouadila, S. Kooli, A. Guizani, A. Farhat, Solar air heater with phase change material: An energy analysis and a comparative study, Appl. Therm. Eng. 107 (2016) 1057–1064. https://doi.org/10.1016/j.applthermaleng.2016.07.004.

[37] S. Bouadila, S. Kooli, M. Lazaar, S. Skouri, A. Farhat, Performance of a new solar air heater with packed-bed latent storage energy for nocturnal use, Appl. Energy 110 (2013) 267–275. https://doi.org/10.1016/j.apenergy.2013.04.062.

[38] J. Assadeg, A.H.A. Al-Waeli, A. Fudholi, K. Sopian, Energetic and exergetic analysis of a new double pass solar air collector with fins and phase change material, Sol. Energy 226 (2021) 260–271. https://doi.org/10.1016/j.solener.2021.08.056.

[39] M. Koşan, Performance analysis of an infrared film assisted solar air heater for drying applications, Energy Sources Part Recovery Util. Environ. Eff. 44 (2022) 8146–8160. https://doi.org/10.1080/15567036.2022.2120577.

[40] A. Heydari, Experimental analysis of hybrid dryer combined with spiral solar air heater and auxiliary heating system: Energy, exergy and economic analysis, Renew. Energy 198 (2022) 1162–1175. https://doi.org/10.1016/j.renene.2022.08.110.

[41] N. Nwakuba, V.C. Okafor, O.O. Okorafor, Techno-economic analysis of a hybrid solar-electric dryer, Energy Sources Part Recovery Util. Environ. Eff. 46 (2024) 10289–10313. https://doi.org/10.1080/15567036.2020.1782537.

[42] S. Singh, R. Chauhan, V. Kumar, N. Kumar, S.K. Chaurasiya, Experimental Thermal Performance Investigation of a Commercial Recyclic Thermal Energy Storage Integrated Solar Air Heater, (2024). https://doi.org/10.2139/ssrn.5070372.

[43] A. Hassan, A.M. Nikbahkt, Z. Welsh, P. Yarlagadda, S. Fawzia, A. Karim, Experimental and thermodynamic analysis of solar air dryer equipped with V-groove double pass collector: Techno-economic and exergetic measures, Energy Convers. Manag. X 16 (2022) 100296. https://doi.org/10.1016/j.ecmx.2022.100296.

[44] T. Hadibi, S. Mengjie, R. Jiangtao, Y. Wang, A. Benseddik, L. Ming, R.H.E. Hassanien, T.K. Abdelkader, Comprehensive analysis and experimental study on the novel intermittent solar-electric onion drying technology, Renew. Energy 238 (2025) 121949. https://doi.org/10.1016/j.renene.2024.121949.

[45] N. Embarek, I. Sulimieh, A.N. Korti, H. Guellil, Effect of Air Gap Variations on a Double-Pass Solar Air Heater Performance: A Combined Experimental and Numerical Approach, Appl. Sol. Energy 61 (2025) 21–34. https://doi.org/10.3103/S0003701X24603454.

[46] M. Owureku-Asare, I. Oduro, F.K. Saalia, C. Tortoe, J. Ampah, K. Ambrose, Drying Characteristics and Microbiological Quality Assessment of Solar-Dried Tomato, Int. J. Food Sci. 2022 (2022) 1–13. https://doi.org/10.1155/2022/2352327.

[47] M.A. Leon, S. Kumar, S.C. Bhattacharya, A comprehensive procedure for performance evaluation of solar food dryers, Renew. Sustain. Energy Rev. 6 (2002) 367–393.

[48] J.A. Duffie, W.A. Beckman, Solar engineering of thermal processes, photovoltaics and wind, Fifth edition, Wiley, Hoboken, New Jersey, 2020.

[49] R.J. Moffat, Describing the uncertainties in experimental results, Exp. Therm. Fluid Sci. 1 (1988) 3–17. https://doi.org/10.1016/0894-1777(88)90043-X.

[50] S.M. Parsa, A. Rahbar, D. Javadi Y, M.H. Koleini, M. Afrand, M. Amidpour, Energy-matrices, exergy, economic, environmental, exergoeconomic, enviroeconomic, and heat transfer (6E/HT) analysis of two passive/active solar still water desalination nearly 4000m: Altitude concept, J. Clean. Prod. 261 (2020) 121243. https://doi.org/10.1016/j.jclepro.2020.121243.

[51] A.K. Hegde, Raghuvir Pai, K.V. Karanth, Performance augmentation of solar air heaters: A comprehensive analysis, Sol. Energy 253 (2023) 527–553. https://doi.org/10.1016/j.solener.2023.01.031.

[52] T. Hadibi, A. Boubekri, D. Mennouche, A. Benhamza, N. Abdenouri, 3E analysis and mathematical modelling of garlic drying process in a hybrid solar-electric dryer, Renew. Energy 170 (2021) 1052–1069. https://doi.org/10.1016/j.renene.2021.02.029.

[53] M.A. Kherrafi, A. Benseddik, R. Saim, S. Bahaz, T. Messeguem, Experimental and numerical study of performance enhancement in a direct solar dryer integrated with obstacles, Appl. Therm. Eng. 259 (2025) 124942. https://doi.org/10.1016/j.applthermaleng.2024.124942.

[54] K.R. Arun, M. Srinivas, C.A. Saleel, S. Jayaraj, Influence of the location of discrete macro-encapsulated thermal energy storage on the performance of a double pass solar plate collector system, Renew. Energy 146 (2020) 675–686. https://doi.org/10.1016/j.renene.2019.07.036.

[55] R. Verma, R. Chandra, H.P. Garg, Optimization of solar air heaters of different designs, Renew. Energy 2 (1992) 521–531. https://doi.org/10.1016/0960-1481(92)90091-G.

[56] S. Abo-Elfadl, M.S. Yousef, H. Hassan, Energy, exergy, and enviroeconomic assessment of double and single pass solar air heaters having a new design absorber, Process Saf. Environ. Prot. 149 (2021) 451–464. https://doi.org/10.1016/j.psep.2020.11.020.

[57] M. Sajawal, T. Rehman, H.M. Ali, U. Sajjad, A. Raza, M.S. Bhatti, Experimental thermal performance analysis of finned tube-phase change material based double pass solar air heater, Case Stud. Therm. Eng. 15 (2019) 100543. https://doi.org/10.1016/j.csite.2019.100543.

[58] A. Hedau, S.K. Singal, Study on the thermal performance of double pass solar air heater with PCM-based thermal energy storage system, J. Energy Storage 73 (2023) 109018. https://doi.org/10.1016/j.est.2023.109018.

[59] M.C. Ndukwu, M. Simo-Tagne, F.I. Abam, O.S. Onwuka, S. Prince, L. Bennamoun, Exergetic sustainability and economic analysis of hybrid solar-biomass dryer integrated with copper tubing as heat exchanger, Heliyon 6 (2020) e03401. https://doi.org/10.1016/j.heliyon.2020.e03401.

[60] H. Ebadi, D. Zare, M. Ahmadi, G. Chen, Performance of a hybrid compound parabolic concentrator solar dryer for tomato slices drying, Sol. Energy 215 (2021) 44–63. https://doi.org/10.1016/j.solener.2020.12.026.

[61] N.R. Nwakuba, M.C. Ndukwu, G.U. Asonye, S.N. Asoegwu, G.I. Nwandikom, Environmental Sustainability Analysis of a Hybrid Heat Source Dryer, Polytechnica 3 (2020) 99–114. https://doi.org/10.1007/s41050-020-00026-2.

[62] A. Fudholi, K. Sopian, M.Y. Othman, M.H. Ruslan, B. Bakhtyar, Energy analysis and improvement potential of finned double-pass solar collector, Energy Convers. Manag. 75 (2013) 234–240. https://doi.org/10.1016/j.enconman.2013.06.021.

[63] P. GaneshKumar, V.S. Vigneswaran, P. Murugan, M. Cheralathan, R. Velraj, S.C. Kim, V. Ramkumar, Exploring the thermal performance of a solar air heater with a V-corrugated and shot-blasted absorber plate comprising nano-enhanced phase change materials, J. Energy Storage 77 (2024) 109955. https://doi.org/10.1016/j.est.2023.109955.

[64] B. Brahma, A.K. Shukla, D.C. Baruah, Energy, exergy, economic and environmental analysis of phase change material based solar dryer (PCMSD), J. Energy Storage 88 (2024) 111490. https://doi.org/10.1016/j.est.2024.111490.